

COAL BED METHANE – CONCENTRATED SOLAR POWER HYBRID
SYSTEM POTENTIAL IN ZIMBABWE

A THESIS SUBMITTED TO
THE BOARD OF GRADUATE PROGRAMS
OF
MIDDLE EAST TECHNICAL UNIVERSITY, NORTHERN CYPRUS CAMPUS

BY

BRUCE MUTUME

IN PARTIAL FULFILLMENT OF THE REQUIREMENTS
FOR
THE DEGREE OF MASTER OF SCIENCE
IN
SUSTAINABLE ENVIRONMENT AND ENERGY SYSTEMS PROGRAM

JANUARY 2023

Approval of the Board of Graduate Programs

Prof. Dr. Cumali Sabah

Chairperson

I certify that this thesis satisfies all the requirements as a thesis for the degree of Master of Science

Assoc. Prof. Dr. Ceren Ince

Program Coordinator

This is to certify that we have read this thesis and that in our opinion it is fully adequate, in scope and quality, as a thesis for the degree of Master of Science.

Prof. Dr. Murat Fahrioglu

Co-Supervisor

Asst. Prof. Dr. Doruk Alp

Supervisor

Examining Committee Members

Prof. Dr. Serkan Abbasoğlu

CIU/
Energy Systems Eng.

Asst. Prof. Dr. Canras Batunlu

METU-NCC/
EEE

Asst. Prof. Dr. Doruk Alp

METU-NCC/
PNGE

I hereby declare that all information in this document has been obtained and presented in accordance with academic rules and ethical conduct. I also declare that, as required by these rules and conduct, I have fully cited and referenced all material and results that are not original to this work.

Name, Last name: Bruce Mutume

Signature:

ABSTRACT

COAL BED METHANE – CONCENTRATED SOLAR POWER HYBRID SYSTEM POTENTIAL IN ZIMBABWE

Mutume, Bruce

Master of Science, Sustainable Environment and Energy Systems Program

Supervisor: Asst. Prof. Dr. Doruk Alp

Co-Supervisor: Prof. Dr. Murat Fahrioglu

January 2023, 147 pages

Despite the adverse environmental effects of fossil fuels, developing nations with inexpensive coal resources have difficulty switching to green energy. To ease the transition, natural gas is considered as the bridging fuel. Integrating conventional power plants (PP) with concentrated solar power (CSP) represents a more innovative strategy. To evaluate the feasibility of a gas-CSP hybrid, the North-Western region of Zimbabwe is chosen as the research area. The assessment's success is dependent on the following four essential aspects: (1) selecting a suitable location for both coal bed methane (CBM) and CSP; (2) CBM in-place volume and production estimation; (3) feasibility of CSP for an integrated solar combined cycle (ISCC) power plant; and (4) conducting a techno-economic and environmental analysis of the ISCC system.

Using Monte-Carlo Simulation (MCS), the North-Western region OGIP estimated to range from 706 Bm³ to 5 699 Bm³. The Hwange-Lupane area was identified from the North-Western region as the zone with the most preferred conditions for CBM exploration. The Hwange-Lupane region's potential for CSP was investigated using a combination of the Geographic Information System and Analytic Hierarchy Process (GIS-AHP). Theoretically, Lupane's and Hwange's CSP potentials range from 1 207 to 1 613 TWh/year and 529 to 696 TWh/year, respectively. Zimbabwe has enough solar resources to switch to clean energy, as shown by the CSP potential found in this study.

The Lupane region (the study area) was found to be the ideal location for the ISCC system by the GIS-AHP analysis. Accordingly, the CBM resources specific to Lupane are estimated and found to range from 250 to 1 400 Bm³.

A Techno-economic and environmental analysis of a standalone CSP, Combined Cycle Gas Turbine (CCGT), and ISCC systems was carried out to validate the proposal. According to the results, the proposed ISCC PP only technically competes with the CCGT PP, where the latter generates electricity 7 % higher than the former, proving to be more sustainable than the use of standalone CCGT, CSP and coal-fueled PP.

Regarding average cost (\$) per kWh, comparable CSP, CCGT, and ISCC PPs have Levelized Cost of Electricity (LCOE) values of 0.178 \$/kWh, 0.063 \$/kWh, and 0.0581 \$/kWh, respectively. Because its LCOE is the lowest, and it is also technically efficient and environmentally friendly, ISCC is proposed for transition to green energy. The feasibility of custom ISCC system was established by a resultant LCOE of 0.0728 \$/kWh, less than Zimbabwe's retail cost of electricity (0.12 \$/kWh) and cost of electricity generation (0.095 \$/kWh).

Keywords: Coal bed methane, Concentrated solar power, Sustainability, Power poverty, Zimbabwe

ÖZ

ZİMBABVE'DE KÖMÜR YATAĞI METANI - KONSANTRE GÜNEŞ ENERJİSİ HİBRİT SİSTEM POTANSİYELİ

Mutume, Bruce
Yüksek Lisans, Sürdürülebilir Çevre ve Enerji Sistemleri
Tez Yöneticisi: Asst. Prof. Dr. Doruk Alp
Ortak Tez Yöneticisi: Prof. Dr. Murat Fahrioglu

Ocak 2023, 147 sayfa

Fosil yakıtların olumsuz çevresel etkilerine rağmen, ucuz kömür kaynaklarına sahip gelişmekte olan ülkeler yeşil enerjiye geçişte geri kalmaktadır. Bu geçişi kolaylaştırmak için doğal gaz ara yakıt olarak kabul bulmuştur. Ancak, konsantre güneş enerjisi (CSP) ile geleneksel enerji santrallerinin entegre edilmesi daha yenilikçi bir yaklaşımdır. Bu çalışmada, bir gaz-CSP hibrit santralin fizibilitesini değerlendirmek için Zimbabve'nin Kuzey-Batı bölgesi araştırma alanı olarak seçilmiştir. Hibrit santralin başarısı aşağıdaki dört temel hususta incelenmiştir: (1) hem kömür yatağı metanı (CBM) hem de CSP için uygun yer seçimi; (2) CBM miktarı (OGIP) ve üretimi tahmini; (3) entegre güneş kombin çevrim santrali (ISCC) için CSP fizibilitesi; ve (4) ISCC sisteminin tekno-ekonomik ve çevresel analiz sonucu.

Bu çalışmada, Monte-Carlo Simülasyonu (MCS) kullanılarak, Kuzey-Batı bölgesinin CBM miktarı 706 Bm³ ile 5 699 Bm³ arasında hesaplanmıştır. Ardından, Zimbabve'nin Kuzey-Batısındaki Hwange-Lupane bölgesi CBM keşfi için en uygun koşullara sahip bölge olarak saptanmıştır. Hwange-Lupane bölgesinin CSP potansiyeli, Coğrafi Bilgi Sistemi ve Analitik Hiyerarşi Süreci (GIS-AHP) kombinasyonu kullanılarak araştırılmıştır. Teorik olarak hesaplanan Lupane ve Hwange CSP potansiyelleri sırasıyla 1 207 ila 1 613 TWh/yıl ve 529 ila 696 TWh/yıl arasında değişmektedir. CSP potansiyelinin gösterdiği üzere, Zimbabve, temiz enerjiye geçmek için yeterince güneş ışığı almaktadır.

GIS-AHP analizi ile ISCC sistemi için en ideal yer olarak Lupane bölgesi (nihai çalışma alanı olarak) belirlenmiştir. Lupane için CBM miktarının 250 ila 1400 Bm³ arasında değiştiği saptanmıştır.

ISCC sistemin geçerliliğini teyit etmek için CSP, Kombine çevrim enerji santrali (CCGT) ve ISCC sistemlerin tek başlarına bağımsız teknolojik-ekonomik ve çevresel analizi yapılmıştır. Buradan alınan sonuçlara göre, ISCC santralin teknik olarak tek rakibi, ISCC santrale göre % 7 daha çok elektrik üreteceği hesaplandığı için, sadece CCGT santraldir. Bu sonuç, ISCC santralin tek başına kıyaslandığında CCGT, CSP ve kömür yakıtlı termik santrallerin herbirinden daha sürdürülebilir olduğunu göstermektedir.

KWh başına maliyetler göz önüne alındığında ise, CSP, CCGT ve ISCC santrallerin seviyelendirilmiş elektrik maliyeti (LCOE) sırasıyla 0.178 \$/kWh, 0.063 \$/kWh ve 0.0581 \$/kWh olarak hesaplanmıştır. Buna göre, ISCC sistem tekno-ekonomik olarak verimli ve çevre dostu olduğu için yeşil enerjiye geçişte tercih edilmesi gereken sistem olarak önerilmektedir. Güncel ISCC sistemin 0.0728 \$/kWh olarak hesaplanan LCOE'nin, Zimbabwe'nin hem perakende elektrik maliyeti (0.12 \$/kWh) hem de elektrik üretim maliyetinden (0.095 \$/kWh) düşük olması, ISCC sistemin fizibilitesini teyit etmektedir.

Anahtar Kelimeler: Kömür yatağı metanı, Konsantre güneş enerjisi, Sürdürülebilirlik, Güç yoksulluğu, Zimbabwe

Dedicated To My Parents (Simon & Ruth Mutume)

ACKNOWLEDGMENTS

I want to express my most profound appreciation to my supervisor Asst. Prof. Dr. Doruk Alp for his guidance, patience, support, and an understanding heart all through my studies. I would like too to show appreciation to my co-supervisor Assoc. Prof. Dr. Murat Fahrioglu for his expertise and counsel.

I would like to show appreciation to METU NCC and the METU family for presenting me with the opportunity to complete one of my life goals. In addition, I would like to give my special gratitude to my companions and family for standing with me all the way. Last but not least, I would want to thank God for everything.

TABLE OF CONTENTS

ABSTRACT.....	v
ÖZ.....	vii
ACKNOWLEDGMENTS	x
TABLE OF CONTENTS.....	xi
LIST OF TABLES	xvii
LIST OF FIGURES	xxi
1. INTRODUCTION	1
1.1 Impact of Greenhouse Gases	2
1.2 Power Generating Technologies	4
1.2.1 Hybrid Power Systems	6
1.3 Motivation for Study.....	7
1.4 Research Gap	8
1.5 Research Questions and Objectives	8
1.6 Thesis Organization	10
2. THERMAL POWER PLANTS	11
2.1 The Brayton Cycle (GT cycle).....	11
2.2 The Rankine Cycle (ST cycle).....	12
2.3 Combined Cycle Gas Turbine Power Plants.....	13
2.3.1 CCGT Working Principle.....	14
2.3.2 Heat Recovery Steam Generator – HRSG	15
2.3.3 CCGT PP Supplementary Firing.....	17
2.3.4 CCGT Configuration.....	18

2.4	Power Plant Performance Parameters	19
2.4.1	Heat Rate.....	19
2.4.2	Thermal efficiency	20
2.4.3	Energetic Efficiency	20
2.4.4	Operational Efficiency	21
2.4.5	The Load Factor.....	21
2.4.6	Capacity Factor	21
2.4.7	Economic Efficiency.....	22
2.4.8	Levelized Cost of Electricity (LCOE)	22
2.4.9	Specific Fuel Consumption.....	23
2.5	CBM-CCGT Design Considerations	26
3.	SOLAR AND HYBRID POWER PLANTS	29
3.1	Solar Photovoltaics	30
3.2	Concentrated Solar Power – CSP	33
3.3	Energy Storage	36
3.4	Power Generation Potential	38
3.4.1	Plant Location and Multi-criteria Decision-Making (MCDM)	39
4.	HYBRID POWER PLANTS.....	45
4.1	Integrated Solar Combined Cycle (ISCC) Systems.....	45
4.1.1	Technology, System Design and Equipment	46
4.1.2	Solar Integration	47
4.1.3	Assessment of Integrated Solar Combined Cycle Power Plant	49
5.	COAL BED METHANE.....	51
5.1	Natural Gas	51

5.2	Coal Bed Methane.....	52
5.3	Origin of Coal	53
5.4	Origin of Coal Bed Methane.....	53
5.5	Adsorption Capacity and the Langmuir Isotherm.....	55
5.6	Coal Bed Methane Deposition	56
5.7	Coal Bed Methane Resources and Reserves	57
5.8	CBM Reserve Estimation	59
5.8.1	Uncertainty in OGIP and Probabilistic Methods.....	61
5.8.2	Recovery Factor and Uncertainty in Reserves	62
5.9	Coal Bed Methane Production	62
5.9.1	Temperature Effect on Adsorption.....	64
5.9.2	Coal Bed Methane Production Analysis	65
5.9.3	Decline Curve Analysis for Gas Wells	67
5.10	Enhanced CBM Production	69
5.11	Productivity Enhancement by Hydraulic Fracturing	69
6.	ZIMBABWE AND THE STUDY AREA	71
6.1	Zimbabwe: Country Overview	72
6.2	Zimbabwe Energy Sector.....	74
6.2.1	Current Acts and Policies.....	75
6.2.2	Ongoing Plans of the Zimbabwean Government	76
6.3	Power Generation in Zimbabwe	77
6.4	Past Studies on Power Generation in Zimbabwe	78
6.5	Zimbabwe’s Coal Reserves.....	79
6.6	Coal Bed Methane Potential in Zimbabwe	81

6.7	Zimbabwe: Study Area.....	82
6.8	Study Area: Climate	83
7.	PROBLEM STATEMENT	85
8.	METHODOLOGY	87
8.1	Assessment of Coal Bed Methane Generated Power	88
8.1.1	Site Selection for Coal Bed Methane.....	88
8.1.2	Resource Density	89
8.2	Original Gas in Place Estimation	89
8.2.1	Monte Carlo Simulation.....	90
8.2.2	Field Data and Analysis	91
8.2.3	Parameter Distribution.....	96
8.3	Site Selection for Concentrated Solar Power	97
8.3.1	Criteria Definition.....	98
8.3.2	Data Collection	99
8.3.3	Solar Irradiance.....	99
8.3.4	Orography	100
8.3.5	Location	100
8.3.6	Water resources.....	100
8.3.7	Restrictive Area Processing	101
8.4	Assessment of Concentrated Solar Power	102
8.5	Evaluation of the ISCC PP	102
8.6	Modeling the ISCC PP	106
9.	RESULTS.....	109
9.1	Zimbabwe Coal Bed Methane Evaluation.....	109

9.1.1	Sensitivity Analysis	111
9.1.2	Resource Density Comparison	113
9.1.3	Coal Bed Methane site Evaluation	113
9.2	Concentrating Solar Power Evaluation	115
9.2.1	Exclusion Zones	116
9.2.2	Criteria for the Hwange-Lupane Region	117
9.2.3	Analytic Hierarchy Process	119
9.2.4	Power Potential of Land Suitable for CSP	122
9.3	Lupane coal bed methane Evaluation	124
9.4	Technical Analysis	126
9.4.1	Capacity Factor for the CSP	127
9.4.2	Capacity Factor for CCGT and ISCC	128
9.4.3	Overall Efficiency as a Function of Total Plant Capacity	130
9.5	Economic Analysis	131
9.6	Environmental Analysis	135
9.7	Economic Analysis - Updated	136
9.8	Finalized CBM-ISCC PP Evaluation	138
9.8.1	Well Count and Production Rates without HF Application	140
9.8.2	Well Count and Production Rates with HF Application	142
10.	CONCLUSIONS	145
10.1	Recommendations	147
	REFERENCES	149
	APPENDICES	165
A.	Standalone CCGT vs. CCGT derived from ISCC	165

B. CSP LCOE vs. Plant Capacity.....	166
-------------------------------------	-----

LIST OF TABLES

TABLES

Table 1.1. World CO ₂ emissions by fuel type from 1750 to 2020 [6].....	2
Table 1.2. Power generation and equivalent emission by source, (+) [14].....	5
Table 1.3. Worldwide integrated solar-gas systems using parabolic trough technology [17]	6
Table 1.4. Research questions and objectives of current study	9
Table 1.5. Thesis organization	10
Table 2.1. Some of the world’s largest Combined Cycle Gas Turbine Power Plants [25].....	14
Table 2.2. Power plant specifications	23
Table 3.1. Typical features of solar thermal technologies [72]	36
Table 3.2. Feasibility of concentrating solar power literature review	40
Table 3.3. AHP importance scale [87].....	41
Table 3.4. Random consistency indexes [87]	42
Table 4.1. Integrated Solar Combined Cycle (ISCC) applications	47
Table 4.2. Assessment of ISCC PP	49
Table 5.1. CBM resources in major APEC economies [109].....	52
Table 5.2. Resource/reserve estimation literature review	59
Table 5.3. The overall proportion of CBM expected to be recovered from total resources (ordered according to increasing RFs).....	62
Table 5.4. Specific gas production for CBM seams in United States [150]	67
Table 6.1. GHG emission by sector, Zimbabwe [158]	71
Table 6.2. Acts governing Zimbabwe’s energy sector [157].....	75
Table 6.3. Policies governing Zimbabwe’s energy sector [157].....	75
Table 6.4. RE targets by the Zimbabwean energy sector [157].....	76
Table 6.5. Non-renewable energy targets by the Zimbabwean energy sector[170]	76
Table 6.6. Zimbabwe’s power plants and generation statistics[163].....	77

Table 6.7. Metallurgical coal qualities for Zimbabwe [181].....	81
Table 8.1. Site selection criteria	88
Table 8.2. Karoo basin CBM data for the study area of Zimbabwe.....	91
Table 8.3. Hydrogeology of the study area of Zimbabwe.....	92
Table 8.4. Histogram of target area	93
Table 8.5. Histogram of coal density data [202]	94
Table 8.6. Thickness data [180] [198] [203]	95
Table 8.7. Histogram of gas content data [199]	96
Table 8.8. Summary of parameter distributions	97
Table 8.9. Data sources for Concentrated Solar Power site selection.....	99
Table 8.10. Solar resource and site selection [208].....	100
Table 8.11. Exclusion criteria and averaged values adopted for current study	101
Table 8.12. Input parameters	105
Table 9.1. CBM OGIP and reserve estimates.....	111
Table 9.2. Sensitivity of OGIP to input parameters	112
Table 9.3. CBM resource densities for the study area of Zimbabwe	113
Table 9.4. CBM site evaluation	114
Table 9.5. AHP pairwise comparison matrix [X].....	120
Table 9.6. Normalized matrix [w].....	120
Table 9.7. Coordinates of the suitable land for CSP	121
Table 9.8. Summary of parameters used in MCS for the power potential of Hwange	122
Table 9.9. Summary of parameters used in MCS for the power potential of Lupane	123
Table 9.10. Range of TPSE in percentiles.....	124
Table 9.11. MCS inputs for Lupane	125
Table 9.12. CBM OGIP and reserve estimates for Lupane.....	126
Table 9.13. The technical results of the Rankine cycle.....	126
Table 9.14. LCOE by technology for Zimbabwe [223]	131
Table 9.15. LCOE for an ISCC system for different CCGT + CSP combinations.....	138

Table 9.16 The ISCC _{600MW} power plant properties determined by EBSILON.....	139
Table 9.17. CBM production rate and well count parameters	140
Table 9.18. Arps CBM results for Lupane without HF	141
Table 9.19. Arps CBM results for Lupane with HF	142

LIST OF FIGURES

FIGURES

Figure 1.1. Share of the population with access to electricity [18].....	8
Figure 2.1. (b) Brayton cycle and the (a) gas turbine schematic	12
Figure 2.2. Temperature vs. Specific enthalpy diagram for the Brayton and Rankine cycles.....	13
Figure 2.3. Combined Cycle Gas Turbine power plant scheme (Adopted from [27])	15
Figure 2.4. Multistage high-pressure modular HRSG Series [32].....	17
Figure 2.5. Multi shaft T.H. Wharton CCGT PP [36]	19
Figure 2.6. Specific fuel consumption as a function of power [46].....	24
Figure 2.7. SFC vs. generated power output for a simple cycle gas turbine.....	25
Figure 2.8. Gas turbine performance	26
Figure 2.9. Coal bed methane production and power plant lifetime.....	27
Figure 3.1. Positive and negative-type junctions regulating current flow in a circuit [61].....	31
Figure 3.2. Photovoltaic conversion in a solar cell [56]	31
Figure 3.3. Presentation of a solar cell, module, and array [63]	32
Figure 3.4. World's largest solar farm located in India [65]	33
Figure 3.5. Types of solar thermal technologies [70]	35
Figure 3.6. Schematic of a large-scale parabolic trough solar power plant [73]	36
Figure 3.7. Typical variation of irradiance (supply), and consumption (demand) for a day of variable cloud (Adopted from [51]).....	37
Figure 4.1. Integrated Solar Combined Cycle [91].....	46
Figure 5.1. Global CBM market share, by application [108]	52
Figure 5.2. Hydrocarbon generation during coalification (Adopted from [114] and [115]).....	54
Figure 5.3. CBM operating conditions are shown on a typical Langmuir Isotherm. (Adopted from [121]).....	55
Figure 5.4. Adsorbed and free gas on a coal surface [123].....	56

Figure 5.5. Resource classification (Adopted from [124]).....	58
Figure 5.6. Schematic of CBM extraction process [144]	63
Figure 5.7. Production stages of CBM [145]	64
Figure 5.8. Methane adsorption content curves for bituminous coal [146].....	65
Figure 5.9. Stages in gas production [149].....	66
Figure 5.10. Production decline curves used in oil and gas [149].....	68
Figure 5.11. Coal bed methane decline curve b value range.....	69
Figure 6.1. The landlocked country of Zimbabwe	73
Figure 6.2. The structure of the power sector in Zimbabwe [157].....	74
Figure 6.3. Coal-occurrences and location of coalfields in Zimbabwe [180]	80
Figure 6.4. Geological location of study area.....	82
Figure 6.5. Geographical distribution of the Karoo Supergroup formation in South- Central Africa [188]	83
Figure 6.6. Yearly average temperature map of the study area (adopted from [166])	84
Figure 8.1. Methodology for choosing ISCC site.....	87
Figure 8.2. Flow chart of MCS methodology used in this study.....	91
Figure 8.3. Target area.....	93
Figure 8.4. Gas content values from desorption testing (Adopted from [199])	95
Figure 8.5. Methodology for Concentrated Solar Power potential analysis.....	98
Figure 8.6. Steps to modelling RES in SAM [211].....	103
Figure 8.7. EBSILON’s ISCC SGT 4 000 F [217].....	107
Figure 8.8. EBSILON’s CCGT Siemens SGT5-4000F [217].....	107
Figure 9.1. Histogram of OGIP values calculated by MCS	110
Figure 9.2. CDF of OGIP values obtained for different combinations	110
Figure 9.3. Sensitivity plot of OGIP to the input parameters	112
Figure 9.4. Geographical location of Hwange and Lupane regions of Zimbabwe	115
Figure 9.5. Land cover of Region 1: Hwange-Lupane area	116
Figure 9.6. Protected area of Region 1: Hwange-Lupane area.....	117
Figure 9.7. Direct normal irradiance of Region 1: Hwange-Lupane area	118

Figure 9.8. Slope data of the Region 1: Hwange-Lupane area	118
Figure 9.9. Electricity grid, road distribution, and river distribution data of Region 1: Hwang-Lupane area	119
Figure 9.10. Land suitability for concentrating solar power.....	121
Figure 9.11. CDF of TPSE values for Hwange obtained from different combinations, P50 =611 TWh/year	123
Figure 9.12. Cumulative distribution function of TPSE values for Lupane obtained from different combinations, P50 = 1 403 TWh/year	124
Figure 9.13. CDF of OGIP for Lupane	125
Figure 9.14. Monthly plots of solar hours vs Irradiance for Lupane region	127
Figure 9.15. Total electric power to grid for Lupane from a CSP plant	128
Figure 9.16. Actual power Output from ISCC systems at different theoretical capacities.....	129
Figure 9.17. Actual power Output from CSP, CCGT and ISCC plants at different theoretical capacities	130
Figure 9.18. Efficiency of the gas turbine and solar cycle.....	130
Figure 9.19. LCOE from SAM	133
Figure 9.20. ISCC_87 and ISCC_81.09 LCOE difference	134
Figure 9.21. Levelized cost of electricity for different technologies	134
Figure 9.22. Payback period	134
Figure 9.23. KgCO ₂ eq from CSP capacities	135
Figure 9.24. KgCO ₂ eq from different capacities of CCGT and ISCC processes.	135
Figure 9.25. LCOE considering cost of CO ₂ emissions.....	136
Figure 9.26. (a) Well's production rate with time, (b) A well's cumulative production, (c) Demand from GT vs. supply from the wells.....	142
Figure 9.27. Well's production rate with time, (b) A well's cumulative production, (c) Demand from GT vs. supply from the wells	143
Figure 10.1. CCGT_ISCC and CCGT LCOE difference.....	165
Figure 10.2. CSP plants in USA [211].....	166
Figure 10.3. Effect of solar multiple on LCOE [224].....	167

CHAPTER 1

INTRODUCTION

After the industrial revolution of 1750, the emission of Greenhouse Gases (GHGs) fueled by human activities increased astonishingly [1]. GHGs contribute to the greenhouse effect¹ by absorbing radiation from the sun. These gases include carbon dioxide (CO₂), methane (CH₄), nitrous oxide (N₂O), and water vapor (H₂O). CO₂ and CH₄ are the most crucial of the earth's troubling GHGs. During the industrial revolution, GHG concentrations increased mainly due to deforestation (chiefly for agricultural purposes) and other land-use activities [3]. The discovery of fossil fuels in the 1790s led to increased anthropogenic emissions to the atmosphere, resulting in global warming. Groupe d'experts et al. (2007) [4] classify and describe the effects of global climate change in three categories:

1. Cryosphere impacts: Include glacial isostasy², landscape destruction, and regional hydrological changes.
2. Coastal system impacts: Include erosion, flooding, and rising sea levels.
3. Terrestrial impacts: Include desertification and changes in the carbon cycle.

The above-mentioned geological consequences are irreversible and have long and short-term challenges threatening all life. The culprits of GHG emissions from human activities include the combustion of fossil fuels (mainly coal and oil) for electricity, heating, and transportation (US EPA Table 1.1 shows cumulative CO₂ world emissions from 1750 to 2020 by fuel type).

¹ Greenhouse effect: The retaining of heat on the surface of the earth by absorbing radiations from the sun leaving the surface of the earth, acting like a blanket over the earth's surface [2].

² Glacial isostasy: Refers to the feedback of the earth to changes in the ice sheets [5].

Table 1.1. World CO₂ emissions by fuel type from 1750 to 2020 [6]

Source	CO ₂ emissions from 1750 to 2020, [MMts]
Coal	13 980
Oil	11 070
Gas	7 400
Cement	1 630
Flaring	435.03
Other industries	297.75

In 1950, the world emitted 6 billion tonnes (MMMs) of fossil based CO₂, and by 1990 the emissions grew to 22 MMMts. Presently, the world emits over 34 MMMts of fossil CO₂ per annum [6]. There are several sectors responsible for GHG emissions, including power generation and heating, transport, manufacturing and construction, agriculture, aviation, etc. Power generation and heating is the highest contributor, contributing over 31 % of CO₂ emissions from 1990 to 2018 [6]. According to EPA (2022) [7], the largest sources of GHG emissions from human activities are burning fuels for electricity, heat, and transportation. So, methods that can reduce GHG emissions from generating electricity, transportation, and heating must be implemented for a sustainable environment. Due to the concerning contribution by the energy sector, the United Nations General Assembly (UNGA) set the Sustainable Development Goal 7 (SDG7). SDG7 ensures [8]:

- Universal access to affordable, reliable, and modern energy services.
- Increase in renewable energy share.
- Improvement in energy efficiency.

Also, to avoid climate catastrophe, UNGA set SDG13, which takes urgent action to combat climate change and its impacts.

1.1 Impact of Greenhouse Gases

Over the past decades, the world has recorded some of the highest temperatures, lowest precipitations, and increased droughts. The discovery of fossil fuels led to the use and abuse of resources, endangering the environment and fuel supply. Presently, the world faces the

threat of increased GHG emissions causing global warming. Burning of fossil fuels for the generation of electricity and heating, among other causes, has led to drastic climate change effects. These include the threat to all life, higher temperatures, frequent storms, increased droughts, and floods, to mention a few. In general, climate change affects the normal biogeochemical cycle, threatens biodiversity, food security, health, and quality of life.

Irrespective of where GHGs are emitted, the effects disturb the globe. For example, Africa is the most miniature GHG emitting continent, so its emissions are less than some individual countries. For instance, more than what Africa emits, China, and the United States emit approximately 8 and 3 times more emissions, respectively [6]. Yet, Africa suffers the consequences of global warming. An analysis of the nationally determined contributions (NDCs) of 53 countries of Africa by the World Meteorological Organisation reveals that Africa is exceptionally endangered compared with other continents [9]. Of the 53 African countries, 36 to 40 are affected by floods, droughts, temperature increases, and changes in precipitation patterns, rise in sea level, storms, wildfires, and landslides. In contrast, 3 to 25 are affected by dust storms [9].

A study by Eckstein et al. (2019) [10] to determine the most affected countries by extreme weather events related to climate change highlights that Sri Lanka, Dominica, Puerto Rico, Nepal, Peru, Madagascar, Bangladesh, and Thailand, among others, have suffered the effects. The countries mentioned above are not among the top GHG-emitting countries and yet suffer many global warming-related challenges. It is then every country's responsibility to ensure the sustainable use of fossil fuels for a better environment and the well-being of future generations.

The growth and development of Renewable Energy Systems (RES) has brought some hope to the GHG emission-related problems. The UNGA provided 17 goals to obtain a sustainable environment, among which is the global goal on energy, known as SDG-7 (see introduction). SDG-7 has encouraged the adoption of RES. The growth of wind and solar has contributed 10 % to the 38 % of the global clean power share [11]. Besides RES's ability to decarbonize the power sector, RES still have many drawbacks, including power availability, cost, and limited storage capacities. Failure to deal with RES's challenges may result in a lack of reliability of RES. For example, in 2021, though there was an increase in the global share of wind and solar, there was also a 5 % increase in electricity demand [11]. The 5 % increase

led to a rise in the use of coal power and, consequently, GHG emissions. Coal is readily used because the source and technology provide dispatchable generation,³ unlike RES.

1.2 Power Generating Technologies

Electricity generation (EG) is producing electric power from energy sources. Electricity is typically generated at power stations or power plants (PPs) facilities. These PPs input energy sources to generate an electric output. The most common sources include coal, hydrocarbon (oil and natural gas), the hydro, nuclear, wind, and solar. Various methods are used to convert energy sources to electrical energy, including the application of generators, electrochemistry, and photovoltaic effect. Generators are used in thermal PPs. These generators consume fuel to generate electricity, and almost all PPs used in centralized generation are thermal plants [13]. Approximately all fossil fuel-fired PPs, nuclear, geothermal, and solar thermal, are thermal power plants. Fossil fuel thermal PPs convert heat energy from the combustion of sources to electricity by turning turbines through the widely used thermodynamic cycles. Whereas nuclear, geothermal, and solar thermal PPs directly transfer heat from its source to a steam cycle. Renewable energy is generated from some of the following methods:

- Hydro, by direct use of turbines.
- Solar from concentrating solar power and photoelectric effect by the indirect use of turbines.
- Wind, by direct use of turbines.
- Biomass, by the indirect use of steam turbines after combustion.

The global installed capacity share of renewable energy is approximately 38 %, leaving 62 % generated from non-renewable energy [11].

³ Dispatchable generation: The type of electricity generation from either fossil fuels or hydropower that can be controlled to balance electricity supply and demand [12].

Table 1.2. Power generation and equivalent emission by source, (+) [14]

(*) [15] [16]

Source	Since ⁺	PP type	Share [*]	Emissions [*]
Coal	1884	Thermal	36	820
Gas	1903	Thermal	22	490
Hydro	1880s	Water turbine	15	24
Nuclear	1942	Thermal	10	12
Solar	1882	Photovoltaic cells and Solar thermal	4	48
Wind	1941	Turbines	6.6	11
Bioenergy		Thermal	2	230
Non-renewable, others	n.a.	Thermal	4	700
Renewable, other	n.a.	n.a.	0.4	38

There has been growth in power-generating technologies after the growing worldwide demand for energy. Here are some of the energy-related challenges the world is facing:

- Fossil fuel depletion-There has been a notable compromise in the future availability of fossil fuels because of the unsustainable extraction by humans.
- Increased GHG emissions- In the past decades, warming effects have been recorded as a result of GHG increase in the atmosphere, resulting in frequent global warming-related challenges. These challenges include frequent droughts, storms, melting ice, heat waves, etc.
- Challenges in the reliability of RES.
- Challenges in hybridization- Hybridization is a promising technology, but there are only a few studies, especially on the hybridization of solar and thermal PPs. This is supported by the small number of operating integrated solar-gas systems in Table 1.3.

- Lack of electricity accessibility- Irrespective of the increased GHG emissions from generating electricity, some countries are yet to provide power for their entire population.

1.2.1 Hybrid Power Systems

As of 2022, fossil fuel (coal, to be precise) thermal PPs are most readily available because the technology has matured over time through implementation, research, and development.

Hybrid Power Systems (HPSs) have provided better energy security through the combination of power and energy storage systems. HPSs popularly generate electricity from more than one energy source, from several possible combinations. However, this study focuses on the combination of a thermal PP (fired with natural gas) and solar thermal for the following reasons:

- Natural gas is the cleanest fossil fuel (see Table 1.1).
- Natural gas can be used as a fuel in an efficient Combined Cycle Gas Turbine (CCGT) PP (discussed in Chapter 2).
- The CCGT PP can be combined with other technologies in its bottoming cycle.
- Solar is abundant in many regions of the earth.
- Solar thermal can be coupled with other technologies to form a hybrid.

Table 1.3 lists some of worldwide solar-gas PPs, which reduce both natural gas consumption and CO₂ emissions

Table 1.3. Worldwide integrated solar-gas systems using parabolic trough technology [17]

Location	Solar capacity, [MW]	Gas capacity, [MW]	Status
USA	75	1 150	Operational
Mexico	12	464	Under construction
Morocco	20	450	Operational
Algeria	25	130	Operational
Italy	5	130	Operational
Egypt	22	104	Operational

1.3 Motivation for Study

The following points summarize the motivation of this study:

- High share of GHG emissions from fossil fuels, namely coal and oil.
- Drastic changes in the global climate.
- Low electricity accessibility and frequent power outages in some parts of the world.
- Availability of sustainable technologies- With technological advancements in energy efficiency and sustainability, electricity can be generated from fossil fuels and renewables in sustainable ways.
- Growth in RESs- There have been improvements in solar and wind energy in the past decade to combat global climate change. The advances in technology, and economies of scale, reduce renewable power generation costs.

The combination of the points mentioned above can be summarized into two significant motivations for the study:

1. To reduce the impact of GHG emissions (SDG13), that is, the drastic catastrophes such as droughts, floods, and cyclones birthed by climate change.
2. To provide affordable and sustainable energy aligned with Sustainable Development Goal 7 (SDG7), promoting EG in a reasonable, reliable, modern, and sustainable manner [8].

Figure 1.1 shows the share of people with/without access to electricity. Africa and some parts of Asia have the lowest percentage of the population with access to electricity. Africa is abundant in resources compared to the rest of the world: if utilized efficiently, these resources can change the economies and improve living standards.

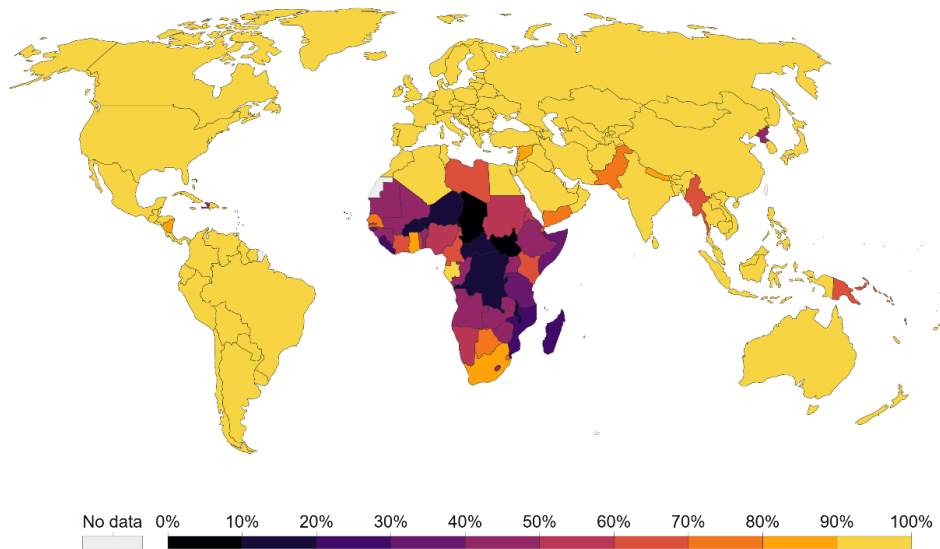


Figure 1.1. Share of the population with access to electricity [18]

1.4 Research Gap

Hybrid PPs offer the potential for uninterrupted power generation, such that if one fails, the other source/technology supports power generation. As can be seen in Table 1.3, there are only a few operating hybrid PPs. There is a need for additional studies on the feasibility of HPSs in different regions of the world.

1.5 Research Questions and Objectives

The main objective of this study is to assess the potential of generating electricity from a solar-gas hybrid. Solar is chosen as a RE source because it is the most abundant energy resource on earth, while natural gas is considered the cleanest non-renewable fuel. Therefore, the solar-gas hybrid is expected to solve the aforementioned energy challenges. Table 1.4 lists the research questions and the corresponding objectives step-by-step, leading to the completion of this study. For the feasibility analysis of generating electricity from an HPS, a study area is chosen as a reference location for the proposed solar-gas system.

Table 1.4. Research questions and objectives of current study

Research Question	Objective
Since coal and oil are the biggest contributors of GHG emissions, what other alternatives can be used, and are they sufficient?	Natural gas in-place estimation for the chosen study area.
How much gas can be extracted from the region, and is it preferable to replace coal and oil with gas?	Techno-economic and environmental analysis for gas production and electricity generation in the chosen study area.
Is it feasible to concentrate solar power in the chosen study area?	Feasibility study of concentrating solar power in the study area.
Is it feasible to generate electricity from a solar-gas hybrid?	To model solar-gas hybrid power generation. Techno-economic, and environmental impact assessment in the study area.
What is the suitable optimum solar energy share that can be integrated into the ISCC?	Assessment of power-generating options.

1.6 Thesis Organization

Table 1.5 gives a detailed description of major parts of the thesis.

Table 1.5. Thesis organization

Chapter	Description
2- Thermal power plants	Gives an overview of power plants, describes the principles, and performances of CCGTPPs, and ISCCPPs.
3- Solar power plants	Describes solar photovoltaics, solar thermal and solar energy storage systems.
4- Hybrid power plants	Describes hybrid power systems focusing on the Integrated Solar Combined Cycle hybrid of solar thermal and natural gas.
5- Coal bed methane	Explains the origin, storage, resource, reserve, production and simulation of CBM.
6- Zimbabwe and study area	The chapter gives an overview of Zimbabwe's energy sector, acts, policies, natural resources, and introduces the study area.
7- Problem statement	Given the study area in Chapter 6, this chapter provides an overview of the power and power related challenges, including its background and the affected.
8- Methodology	Describes the OGIP estimation of CBM, and how it can be used to fuel PPs. Also, the methodology of concentrating solar power, as well as the coupling of CSP and CCGT is described. An assessment of the solar-gas system is given.
9- Results and conclusion	Objectively reports the findings and gives an interpretation of the results.

CHAPTER 2

THERMAL POWER PLANTS

In thermodynamics, power cycles are a series of work-energy-related processes which convert heat input into mechanical work output. There are many PP technologies (using different power cycles), but per the objective of the current study, this chapter outlines Combined Cycle Gas Turbine (CCGT) PPs. The CCGT PP couples the Brayton and Rankine cycles in the gas turbine (GT) and steam-turbine (ST) cycles, respectively.

2.1 The Brayton Cycle (GT cycle)

The Brayton cycle or the GT cycle incorporates a compressor, combustion chamber, GT, and a generator as shown by Figure 2.1 (a), where [19]:

- Air enters the compressor through inlet 1 and is compressed at exit (outlet 1).
- The compressed air at high temperatures and pressure enters the combustion chamber at inlet 2.
- Natural gas is injected through inlet 3 and ignites at constant pressure.
- The air-fuel mixture exits the combustor through outlet 2 into the turbine through inlet 4 and rotates the turbines generating electricity.
- The exhaust is released at outlet 3.

In general, the actual GT cycle is made up of four processes, as shown in Figure 2.1 (b),

- 1-2 Adiabatic process (in the compressor)
- 2-3 Isobaric process (combustion)
- 3-4 Adiabatic process (through turbine and nozzle)
- 4-1 Isobaric (constant pressure heat rejection)

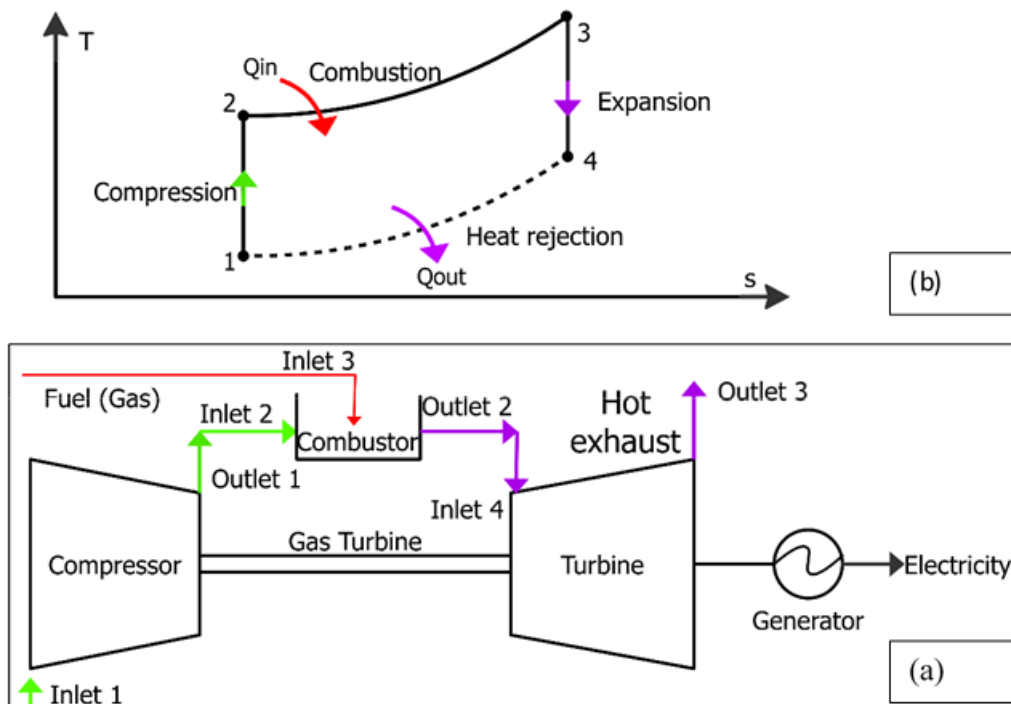


Figure 2.1. (b) Brayton cycle and the (a) gas turbine schematic

2.2 The Rankine Cycle (ST cycle)

The Rankine cycle or the ST cycle describes a process by which STs allow mechanical work to be extracted from the exhaust gas (outlet 3) moving from the heat source to the heat sink⁴. The Rankine cycle is an enclosed cycle that uses water and steam as the working fluid, and consists of a water pump, Heat Recovery Steam Generator (HRSG), ST, and a condenser [21].

- After the Brayton cycle, the exhaust gas (outlet 3) transfers heat to water fed by the pump.
- Water is converted to steam and is sent to the ST.
- Additional electricity is generated in the ST.

⁴ Heat Sink: A passive heat exchanger that transfers the heat generated by a mechanical device to a fluid medium, often air or a liquid [20].

- The exhaust is condensed and sent to the cooling tower, and returned back to the water pump for steam regeneration.

Figure 2.2 shows the T-s diagram for a combined Brayton-Rankine cycle, where the Rankine cycle is made up of four processes namely:

- A-B – Isentropic compression in the pump
- B-C – Heat addition in the boiler
- C-D – Isentropic expansion in the turbine
- D-A – Heat rejection in the condenser

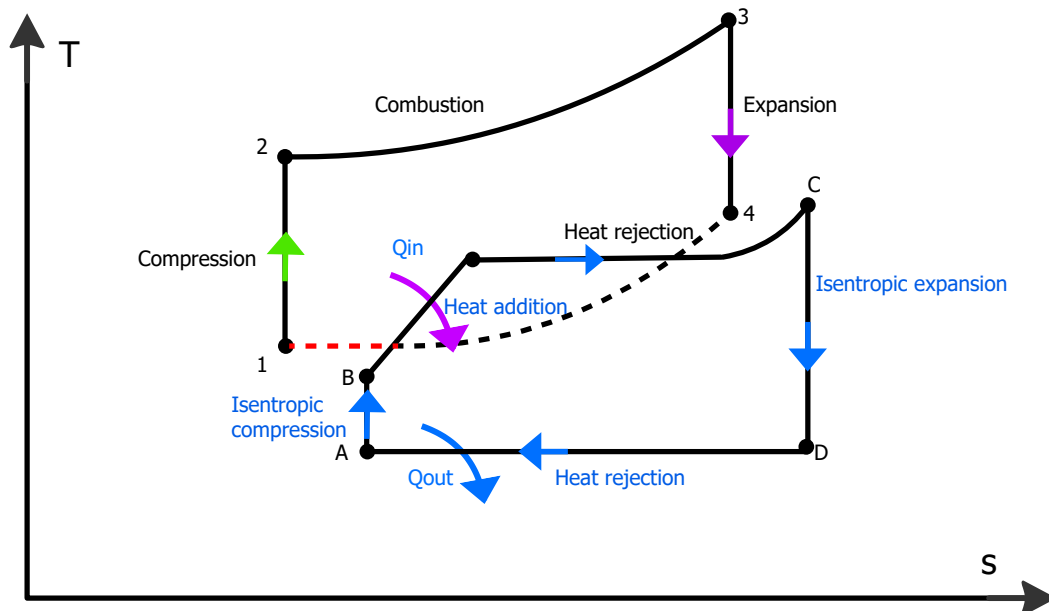


Figure 2.2. Temperature vs. Specific enthalpy diagram for the Brayton and Rankine cycles

2.3 Combined Cycle Gas Turbine Power Plants

A Combined Cycle Gas Turbine (CCGT) is a complex interconnection of a Gas Turbine (GT) and a Steam Turbine (ST), among other components, to achieve higher efficiencies. Due to the higher efficiencies the CCGT PP can achieve, the system has been adopted in most countries. Table 2.1 shows some of the world's largest CCGT PPs exceeding a design capacity of 3 000 MWe. Globally, CCGT PPs amount to about 22 % of the total electricity produced and over 33.33 % of the UK's electricity production [22].

The CCGT process delivers up to 60 % thermal efficiencies, while old coal-fired power stations provide efficiencies between 38 % and 45 %, emitting much higher levels of CO₂, NO_x, and SO_x [23] [24]. The increased efficiencies result from combining two or more thermodynamic cycles to generate more power at the same PP site.

Table 2.1. Some of the world’s largest Combined Cycle Gas Turbine Power Plants [25]

Name	Design capacity [MWe]	Country
Jebel Ali	8 695	United Arab Emirates
Surgut 2	5 657	Russia
Futtsu	5 040	Japan
Burullus	4 800	Egypt
Volta	3 600	Italy
Yokohama	3 325	Japan

2.3.1 CCGT Working Principle

The CCGT system generates electricity from both the GT and ST, as shown in Figure 2.1. The power is generated through following steps:

1. Initially, air is channeled into the compressor, where it is compressed and fed to the combustor.
2. In the combustor, the compressed air is mixed with the fuel (natural gas), and heated at high temperatures.
3. The resulting hot gas expands through the GT.
4. In the GT, burnt gas passes through the blades which start to rotate.
5. The kinetics in the GT generate electricity by the help of generators, which is sent to consumers.
6. In the GT, not all input is converted to electrical energy, but some is lost as heat energy. For instance, Siemens Energy’s SCC5-8000H GT has an efficiency of 41.2 %, meaning 58.8 % of the energy is lost as heat exhaust in a simple GT PP [26].

7. In a CCGT PP, the hot exhaust from the GT is sent to the HRSG.
8. The hot exhaust is passed through the HRSG and sent to the ST, where additional electricity is generated.
9. ST converts mechanical and thermal energy of steam into electrical energy.
10. The exhaust vapor from the ST is condensed in a condenser and is sent to the cooling tower.

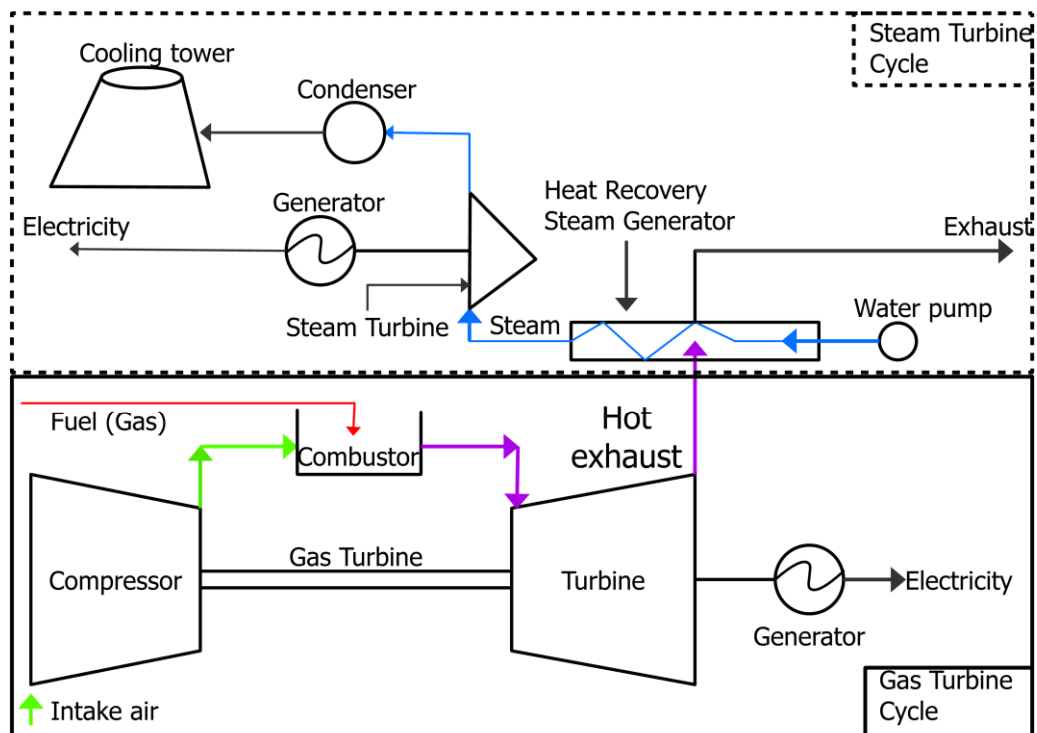


Figure 2.3. Combined Cycle Gas Turbine power plant scheme (Adopted from [27])

2.3.2 Heat Recovery Steam Generator – HRSG

The heat recovery steam generator (HRSG) is a significant component of CCGT PPs used to generate steam from exhaust gas leaving the GTs [28]. The steam generated in the HRSG is used to generate electricity in the ST by the Rankine cycle, and this is why CCGT PPs are efficient power-generating technologies. The HRSG is comprised of three heat exchanger sections, namely:

1. Economizer
2. Evaporator
3. Superheater

The above three works conjointly feeding water into the economizer inlets using pumps. In the economizer, water is heated until it reaches temperatures close to its saturation point and is sent to the evaporator. In the evaporator, the saturated water is turned into saturated steam. Typically, a drum is used to split the saturated water and the saturated steam, and when separated, the saturated steam is superheated into dry superheated steam in the superheater [29]. The dry superheated steam is channeled and expanded in the ST for power generation. Ganapathy (2002) [30] described that HRSGs could be classified into different classes according to:

- Pressure level- The most commonly used pressure levels are single-pressure HRSG, dual-pressure HRSG, and triple-pressure HRSG. Dual and triple-pressure HRSGs extract more heat from the GT exhaust, while single-pressure HRSGs extract less and have high steam temperatures [29].
- Circulation type- There are natural and forced circulations (NC, FC), where water steam mixtures pass evaporators by natural density and pumps, respectively [31].
- Heat input type (whether fired or unfired) - Supplementary firing can be applied to HRSGs to achieve desired temperatures. Ganapathy (2002) [27] describes that fired HRSGs are more efficient than unfired HRSGs because the oxygen in the exhaust gas is enough for supplementary firing.

Figure 2.4 shows a multistage high-pressure modular HRSG Series from Cleaver-Brooks with major integrated components of flue gas bypass systems, evaporators, economizers, duct burners, air firings, and control systems. The Cleaver-Brook's HRSGs produce steam at a rate, pressure, and temperature of 500 000 + lbs./hr., 2 300 psig, and 1 050 °F, respectively [32]

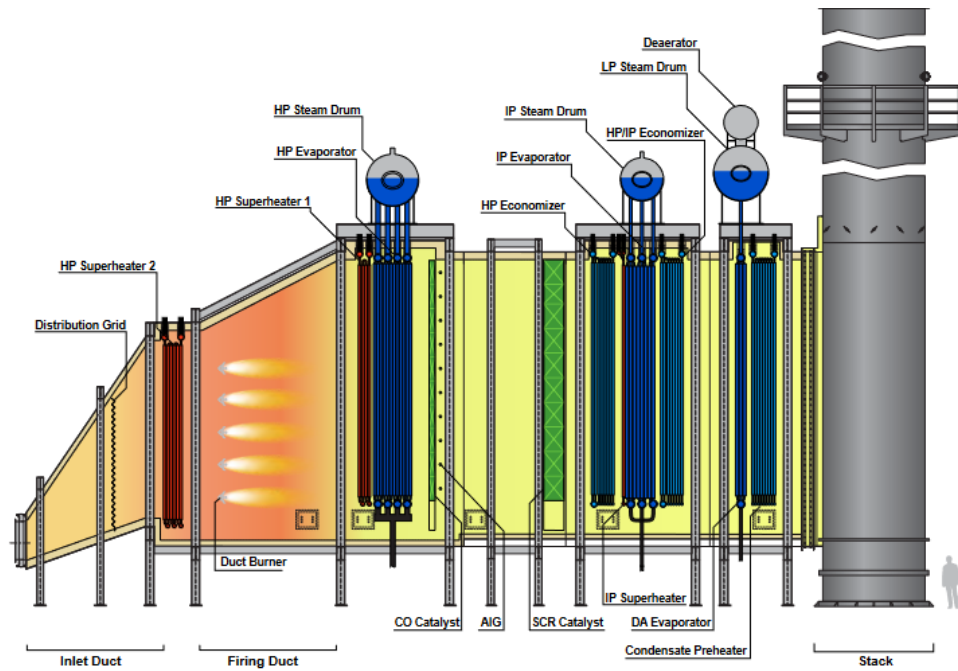


Figure 2.4. Multistage high-pressure modular HRSG Series [32]

2.3.3 CCGT PP Supplementary Firing

To increase the bottoming cycle temperature, supplementary firing can be achieved by adding fuel for combustion in the HRSG. Supplementary firing uses excess oxygen (contained in exhaust gases) to combust the fuel supplement [33]. During fuel combustion in the combustion chamber, the GT uses approximately 25 % - 35 % of the oxygen in the chamber, leaving the rest to exit along with exhaust gases [34]. There are two mechanisms used to burn the fuel supplement in the HRSG, namely [33]:

- Combined cycle with limited supplementary firing - the burner's fuel rate is adjusted to suit the existing oxygen.
- Combined cycle with maximum supplementary firing - a combustion stage is required in the bottoming cycle, though this reduces the PP efficiency.

Supplementary firing can as much as double exhaust gas temperatures. Yet, in most cases, the mechanism reduces energy and exergy efficiency of combined cycle [33].

2.3.4 CCGT Configuration

The CCGT system can be grouped into single-shaft and multi-shaft configurations, where a single shaft consists of one GT, one ST, one generator, and one HRSG [27]. In single-shaft configurations, the GT and the ST are coupled to a generator on a single shaft. Single-shaft CCGT designs have been confirmed to be an extremely efficient and cost-saving option over multi-shaft systems for PP owners and operators seeking to make the most of the value of their assets [35].

Multi-shaft systems have multiple GT generators, and HRSGs. They are beneficial in some areas, such as when reliability and flexibility are needed [35]. Multi-shaft configurations reduce the costs of operating and maintaining the PP, while increasing capital costs by approximately 5 %, and improving the efficiency of the bottoming cycle [33]. Figure 2.5 shows the multi-shaft configuration of the T. H. Wharton electric generating station before the capacity was increased. The T. H. Wharton CCGT PP generates $49 \text{ MWe} \times 4$ from the four GTs, and 102.5 MWe from a single ST.

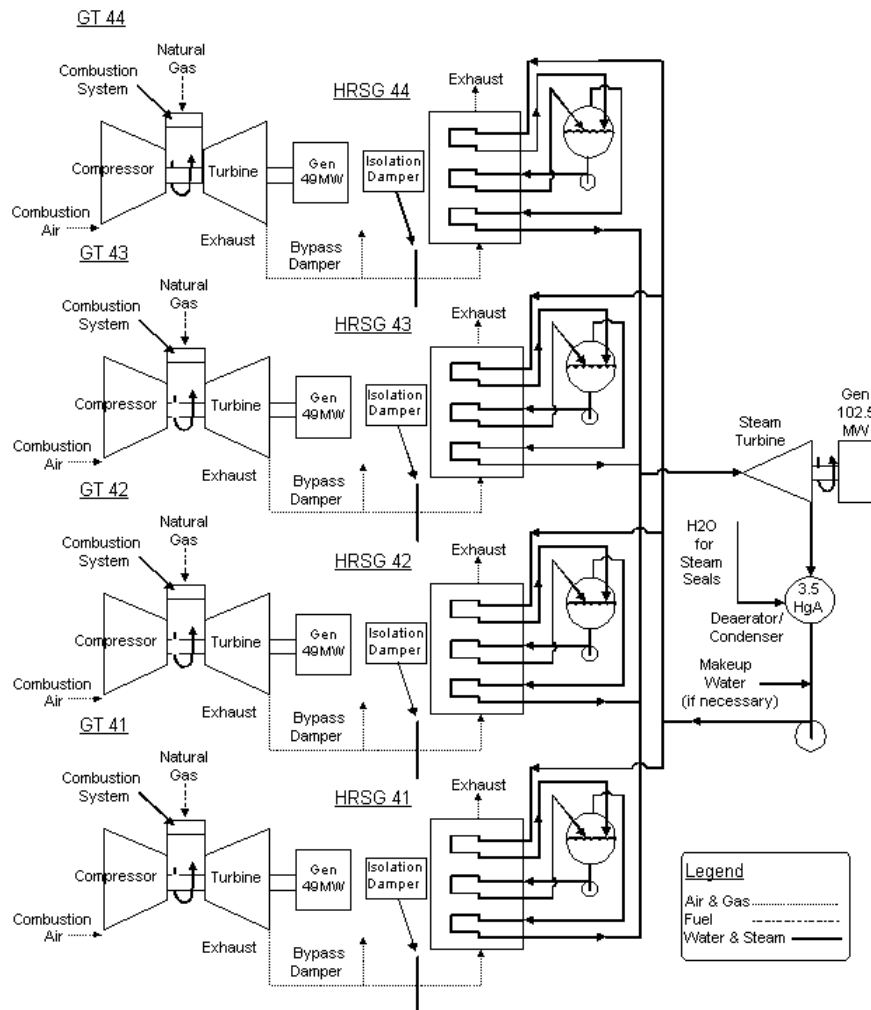


Figure 2.5. Multi shaft T.H. Wharton CCGT PP [36]

2.4 Power Plant Performance Parameters

The performance of a PP can be expressed through various performance factors [39] as explained next.

2.4.1 Heat Rate

Heat rate is the thermal performance of a PP, also known as energy efficiency. It is the measure of energy consumed by a PP to generate 1 kilowatt-hour (kWh) of electricity

expressed in BTUs/kWh⁵. Heat rate represents the efficiency of converting fuel into heat, then electricity [37].

$$\varphi_{hr} = \frac{H}{E} \quad (2.1)$$

Where H, [BTU] is heat supplied to the PP, and E, [kWh] is PP energy output.

Natural gas is the cleanest fossil fuel and has the highest heat rate. The average operating heat rates for coal, hydrocarbon and natural gas are 10 655 BTUs/kWh, 11 259 BTUs/kWh, and 7 732 BTUs/kWh, respectively [38].

2.4.2 Thermal efficiency

In PP technology, generators can be compared accordingly to their thermal efficiencies. To calculate or express the efficiency of a PP as a percentage, we divide the equivalent BTU content of kWh of electricity by the heat rate. Hence, the thermal efficiency of a heat engine is given by:

$$\mu_{te} = \frac{100 \left(3\,412.75 \frac{[BTU]}{[kWh]} \right)}{\varphi} \quad (2.2)$$

Where μ_{te} , [%] is the thermal efficiency, and 1 kWh = 3 412.75 BTU.

2.4.3 Energetic Efficiency

The GT energetic efficiency for Brayton cycle is:

$$\varphi_{GT} = \frac{E_{GT}}{Q_{GT}} = \frac{BTU_{eq}}{heat\ rate} \quad (2.3)$$

Where E_{GT} is the GT power output, Q_{GT} is the GT fuel energy, BTU_{eq} is the equivalent BTU content of a kWh of electricity (3 412 BTUs).

⁵ BTU: British Thermal Units.

The ST energetic efficiency for Rankine cycle is:

$$\varphi_{ST} = \frac{E_{ST}}{Q_{ST} + Q_{exh}} \quad (2.4)$$

Where E_{ST} is the ST power output, Q_{ST} is the ST fuel energy, and Q_{exh} is the exhaust energy output.

The Combined cycle energetic efficiency is:

$$\varphi_{CC} = \frac{E_{GT} + E_{ST}}{Q_{GT} + Q_{ST}} \quad (2.5)$$

2.4.4 Operational Efficiency

Operational efficiency- The ratio of total electricity generated to total potential if the PP were to operate at full capacity, and is given by:

$$\mu_{oe} = \frac{(100)E}{E_{100\%}} \quad (2.6)$$

Where μ_{oe} [%] is the operational efficiency, and $E_{100\%}$ [kWh] potential output if the PP was operating at a 100 % load.

2.4.5 The Load Factor

The ratio of average load to peak load, and is expressed as:

$$\mu_{lf} = \frac{100 (P_{al})}{P_{pl}} \quad (2.7)$$

Where μ_{lf} [%] is the load factor, P_{pl} [kW] is the peak load for the PP in period.

2.4.6 Capacity Factor

Capacity factor is the ratio of actual energy output over a theoretical maximum output. It is used to scrutinize the reliability of different PPs. The capacity factor is expressed as [39]:

$$\mu_{cf} = \frac{100 (P_{al})}{P_{rl}} \quad (2.8)$$

Where μ_{cf} [%] is the capacity factor: P_{al} [kW] is the average load for a PP in a specified period: and P_{rl} [kW] is the rated load capacity for the PP.

2.4.7 Economic Efficiency

Economic efficiency is the ratio of production costs for a period to energy output in that same period. Economic efficiency is given by:

$$\varphi_{ee} = \frac{C}{E} \quad (2.9)$$

Where φ_{ee} [$\frac{cents}{kW}$] is the economic efficiency, C [cents] is the EG cost, E [kWh] is the energy output from the PP.

2.4.8 Levelized Cost of Electricity (LCOE)

PPs can also be compared by the price at which electricity is generated, and generated electricity should be sold at a price that breaks even before the PP's lifetime. Levelized Cost of Electricity (LCOE) or Levelized Energy Cost (LEC) is the term used to compare PPs by the average net present value (NPV) of EG. For LCOE calculations a specific cost in \$/MW or \$/kW for capital cost and \$/kWh for Operations and maintenance is used. Thus, a specific constant cost is used, which is why it would be economic to opt for a huge plant than a small facility. This is the widely used method to estimate cost of electricity and is adopted by the famous LAZARD and EIA [42] [226].

It can be observed from Table 2.2 that the use of natural gas in a CCGT PP is sustainable⁶ considering economics (LCOE), the technical aspect (Capacity factor) and the environment (Emissions data). Generally, 1 MWe from a conventional generator such as coal or natural gas fired PP generates electricity that can power 400 to 900 homes in a year, depending on

⁶ Sustainable: Providing energy from other sources maintaining current operations without sabotaging energy demands or climate of future generations.

the capacity factor [40]. RESs have lower capacity factors than non-renewable energy systems so that the equivalent will power fewer homes. Table 2.2 shows some of power plant specifications belonging to different technologies.

Table 2.2. Power plant specifications

Plant type	LCOE, [\$/MWh] ¹	LCOE, [\$/MWh] ²	Capacity factor ¹	Emissions, [gCO ₂ eq/kWh] ³	Plant eff. [%] ⁴
Thermal- coal	82.61	65 – 152	85	820	38 – 45
CCGT	39.94	45 – 74	87	420	50 – 60
Wind	40 – 105.4	26 – 50	41 – 44	11	34
Solar	33.8 – 49.0	28 – 41	28 – 29	48	18 – 20
Hydroelectric	64.27		54	24	90 – 94
Nuclear			90	12	30 – 33

¹ [41], ² [42], ³ [16], ⁴ [24] [43]

2.4.9 Specific Fuel Consumption

The Specific Fuel Consumption (SFC) is a crucial metric in PP technology because it measures how efficiently a PP converts stored chemical energy in a fuel to mechanical energy [44]. Figure 2.6 shows typical GT SFC as a function of output power. Since PPs consume fuel to generate electricity, SFC is used as a measure of fuel consumed by a PP per kWh of electricity it generates, and is given by:

$$F_{spec} = \frac{F_{tot}}{E_{gen}} \quad (2.10)$$

Where,

F_{spec} – Specific fuel consumption, [m³/kWh]

F_{tot} – Total annual fuel consumed by the PP, [m³/yr.]

E_{gen} – Total annual electricity generated by the PP, [kWh/yr]

Total annual electricity generated by the PP E_{gen} is given by [45]:

$$E_{gen} = PC \times d \times hr \times \varphi \quad (2.11)$$

Where,

PC – Plant capacity, [kW]

d – Days of PP operation

hr – Hours of PP operation

φ – PP efficiency

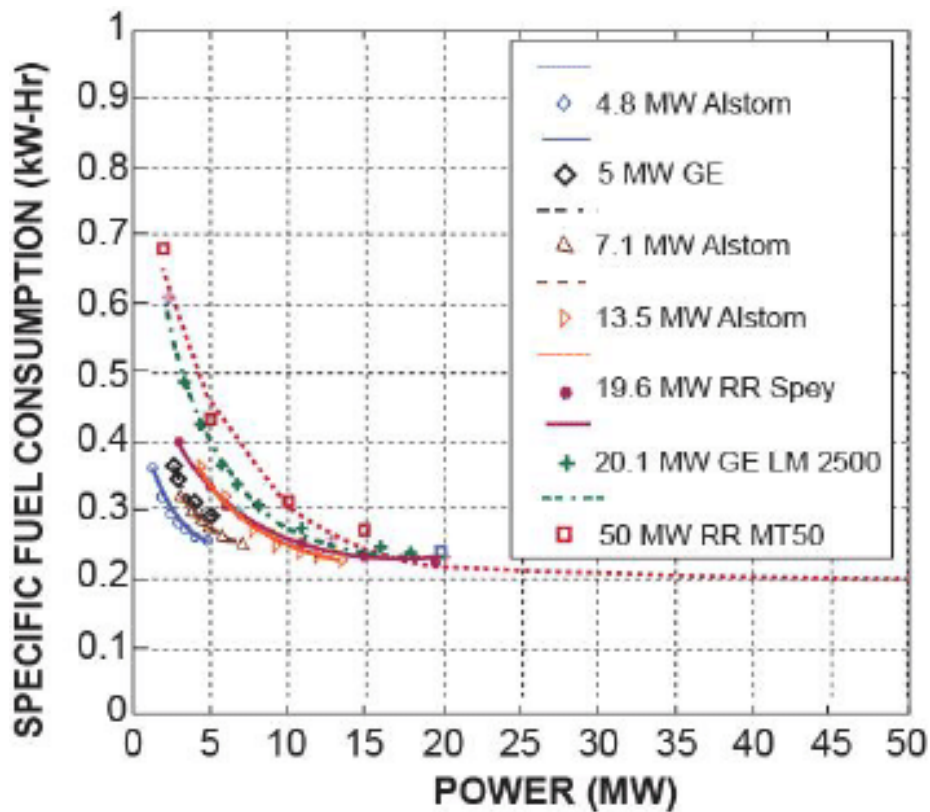


Figure 2.6. Specific fuel consumption as a function of power [46]

Figure 2.6 shows 7 GTs of different capacities, and it can be observed that the fuel efficiency decreases with decreasing power. For instance, the 50 MW RR MT50 would have an SFC of approximately 3.4 times the rated SFC (0.2) when generating only 2 MW of electricity from the rated 50 MW. Of the 7 GTs, the 50 MW turbine is most fuel-efficient when generating 50 MW of electricity. It is more profitable to consider economies of scale when selecting a PP, as it is more advantageous to allow demand to catch up to the supply than

vice-versa. Further, there are disadvantages to operating PPs at partial load (i.e., not total capacity) as it reduces efficiency.

Consider the typical SFC vs. power output plot for a simple cycle GT in Figure 2.7. The horizontal axis shows the load, such that 1 represents a load of 100 % of the PP’s rated power. The vertical axis shows SFC change proportional to load change. Using Figure 2.7, let us consider a Siemens Energy GT operating at different labeled capacities for 30 years. Siemens Energy’s SCC5-8000H simple cycle power generation GT type has a gross capacity of 450 MW, a heat rate of 8 284 BTUs/kWh, and an efficiency of 41.2 % [26].

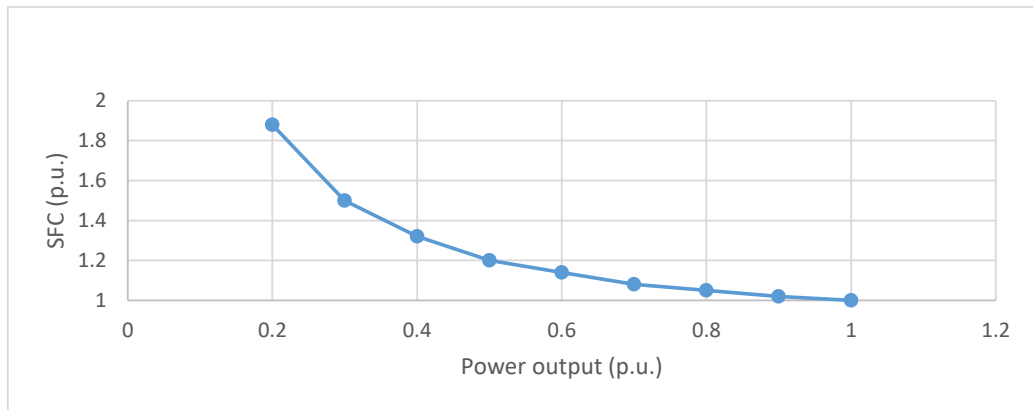


Figure 2.7. SFC vs. generated power output for a simple cycle gas turbine

Employing the electric efficiency vs. relative power relationship of Ruf et al. (2015) [47]:

$$Eff_{Electric} [\%] = 29.674 \cdot \ln(Relative\ power\ [MW]) - 35.38 \quad (2.12)$$

It can be observed from Figure 2.8 that the relative electric efficiency of the GT reduces with a reduction in the load factor. From Figure 2.8, as the load factor of the 450 MW, SCC5-8000H GT reduces from 450 to 90 MW, the electricity generated reduces from 1 179 14 to 126 21 MWh, while the SFC increases from 8 284 to 15 740 BTUs/kWh. If both GTs operate for 30 years, the 90 MW and 450 MW turbines will consume 2.285E+09 m³ and 1.124E+10 m³ of natural gas, respectively. Due to the reduced efficiency and increased SFC, the 90 MW GT consumes 37.35E+06 m³ more natural gas than it would if the 90 MWs were generated within the 100 % load capacity.

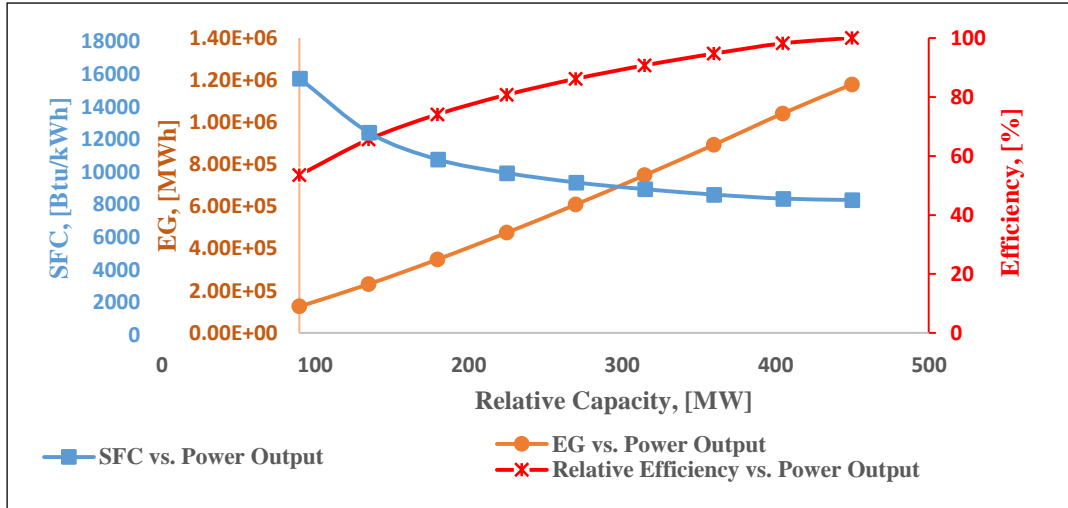


Figure 2.8. Gas turbine performance

The introduction of CCGT/solar hybrids offers many advantages, including reduced GHG emissions and boosted efficiency [48].

2.5 CBM-CCGT Design Considerations

For coal bed methane⁷ (CBM)-CCGT PP there are 3 major design considerations (or constraints):

- PP fuel consumption,
- CBM field production rate
- CBM well count and well rate estimation

Because produced CBM is almost pure methane, it can be fed directly to the PP facilities, requiring no purification processes. Daily field production can be estimated based on the gas

⁷ Coal bed methane: An unconventional natural gas resource.

needed to fire the PP per day (see Chapter 5). Typical gas production rates can be obtained from analogs, i.e., fields of similar characteristics. The CBM-CCGT fuel consumption relationship, summarized in Figure 2.9, is explained next.

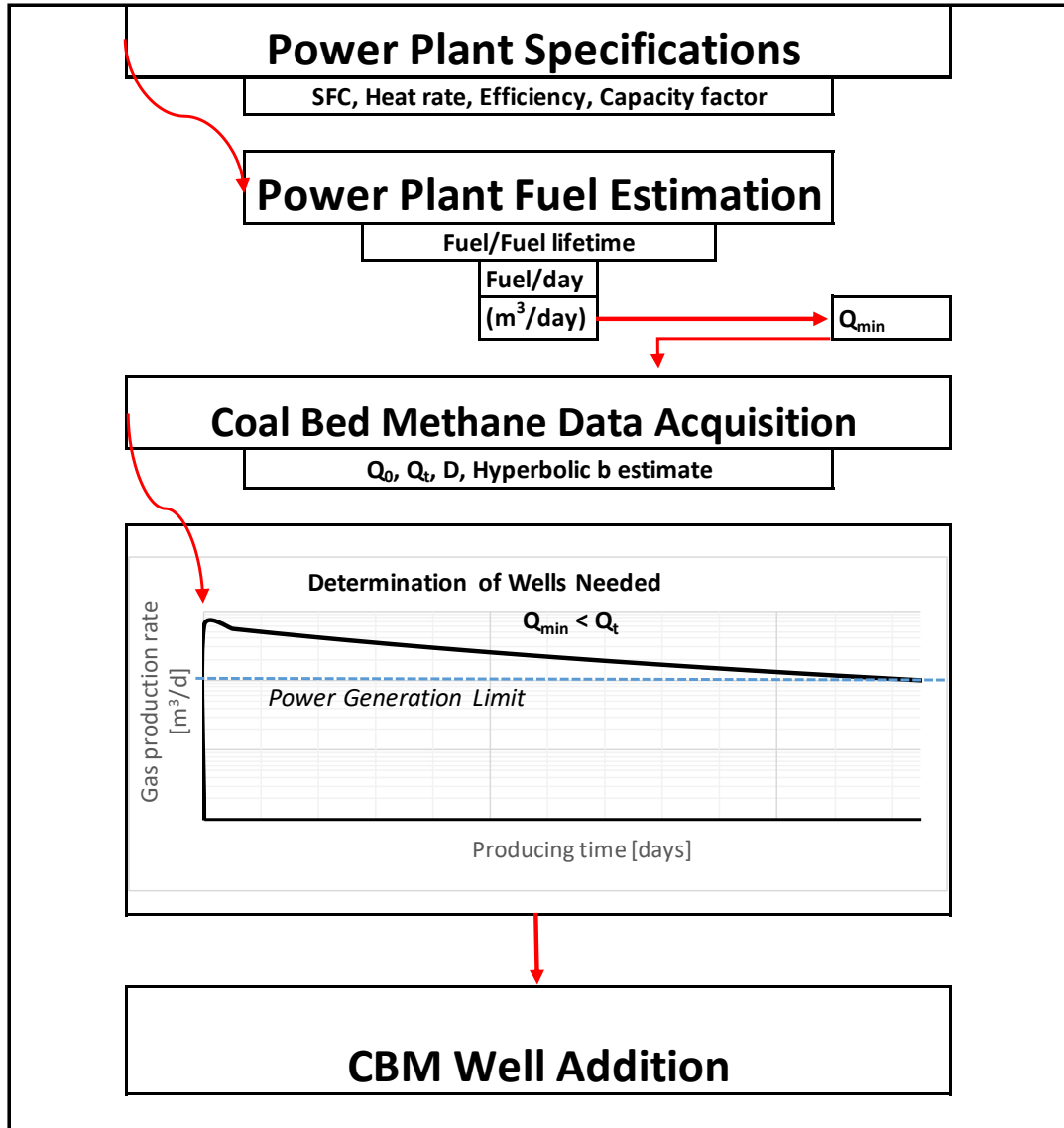


Figure 2.9. Coal bed methane production and power plant lifetime

Considering the 450 MW SCC5-8000H GT mentioned above:

- The GT specifications are obtained from the manufacturer, where in this case the capacity is 450 MW, heat rate is 8 284 BTUs/kWh, and the efficiency is 41.2 %.

- Per above specifications, fuel consumption is calculated for plant lifetime (in this case $1.124 \times 10^{10} \text{ m}^3$), and then per day ($1.026 \times 10^6 \text{ m}^3$).
- The obtained fuel consumption per day value is set to be the total minimum gas flowrate Q_{min} from the producing wells.
- To estimate well flowrate Q_t at a time t after its first production, CBM data acquisition for decline curve constants follows, initial decline rate D_i , initial CBM flowrate Q_0 , and the hyperbolic exponent b .
- Assuming that field flowrate $\sum Q_t$ at any time during PP life must always be greater than Q_{min} , the number of active CBM wells needed to feed the PP can be estimated.
- When $\sum Q_t < Q_{min}$ is observed, additional CBM wells should begin production to maintain $\sum Q_t > Q_{min}$.

CHAPTER 3

SOLAR AND HYBRID POWER PLANTS

The solar energy sector has seen tremendous development and attention, owing to the belief that it will be the primary source of electricity in the future. The abundant solar energy is due to the heat and radiation supplied from the sun. The nuclear fusion reactions (especially of hydrogen and helium) within the sun's core creates 6 000 K surface temperature in sun's photosphere [49]. As a result, enormous amounts of energy are radiated from the sun through absorption (as short waves), scattering (as long waves), and reflection. The energy from the photosphere is emitted as photons throughout a distance of $1\,495 \times 10^{11} \text{ m} \pm 1.7\%$ to the earth's surface at a solar constant of $1\,367 \text{ W/m}^2$ [49]. Due to absorption, adsorption and scattering of irradiance⁸, solar radiation received on the earth's surface vary with location. The variation is also a result of sunspots and the non-circular path of the earth as it rotates around the sun [51]. As radiation arrives on the earth, it is observed as direct beam and/or diffuse radiation due to the path taken by the radiation wave. Diffuse radiation is that which passes through clouds, dust, etc., before reaching the earth's surface, while direct beams reach the earth's surface without being scattered by the atmosphere. As a result, the total useful solar radiation is the sum of diffuse and beam radiations.

There are three main components of irradiance used to determine solar potential in solar systems, and these are [52]:

- Direct Normal Irradiance (DNI)
- Diffuse Horizontal Irradiance (DHI)
- Global Horizontal Irradiance (GHI).

DHI is the amount of solar radiation per unit area by a surface that is not under a shadow and not coming from direct radiation [52]. GHI is defined as the gross amount of shortwave

⁸ Irradiance: the energy per unit time that strikes a unit horizontal area per unit wavelength interval, where the typical unit is $\text{Wm}^{-2} \text{ nm}^{-1}$ [50].

radiation received by a surface parallel to the earth's horizontal plane. GHI, DNI, and DHI are related by the following formula [52]:

$$GHI = DNI \times \cos\theta + DHI \quad (3.1)$$

Where, θ is the angle between the beam and the receiving object.

DNI can be represented by [53].

$$DNI = \int_{year} I_b(t) dt \quad (3.2)$$

Where,

I_b = beam radiation.

Two leading technologies are used to harness energy from the sun for EG: solar Photovoltaics (PV) and Concentrated Solar Power (CSP). DNI is typically used in solar systems to validate sites for concentrating solar power [53]. At the same time, GHI is normally used for validating PV harvesting technologies.

3.1 Solar Photovoltaics

Solar PV is a technology that converts energy from the sun into electrical energy by applying the photovoltaic effect. The photovoltaic effect was discovered by Becquerel (1839) [54] in a study when electrical effects occurred during the reaction of electrodes dipped in electrolytes. The electrical effects produced a photocurrent when solar light illuminated electrodes covered by copper or silver halide salts. After the discovery by Becquerel (1839) [54], many studies by Smith (1876) [55], Maxwell (1876) [56], Adams & Day (1877) [57], Fritts (1883) [58], and Siemens (1885) [59] followed in the belief that the photovoltaic effect could supply the earth with electrical power. After poor performances of other materials, Kingbury & Ohl (1952) [60] discovered maximum photo effects in silicon, which led to the discovery of the p-n junction. A p-n junction is a device made of semiconductors (p-type-positive and n-type-negative) that regulates the flow of electric current in a circuit, as shown in Figure 3.1.

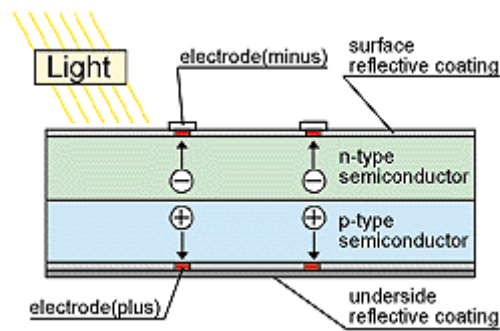


Figure 3.1. Positive and negative-type junctions regulating current flow in a circuit [61]

When radiations from the sun hit the semiconductor, electrons spring up and are attracted by the negative type semiconductor while causing an increase in electrons in the semiconductor. The positive type semiconductor with fewer electrons attracts electrons from the n-type, causing a flow of electrons, known as electricity.

The conversion of energy from the photons to electrical power is not as efficient as fossil fuel-based power-generating mechanisms. For example, the CCGT and Solar plant types in Table 2.2 show efficiency ranges of 50 – 60 % and 18 – 20 %, respectively. Solar radiations, in the form of photons, are radiated on the silicon-based surface where loss mechanisms, transport, and transfer processes occur [56]. Figure 3.2 shows the photovoltaic conversion taking place in a standard solar cell.

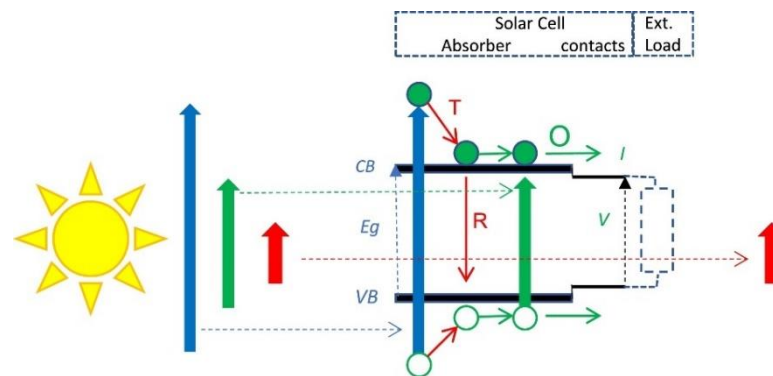


Figure 3.2. Photovoltaic conversion in a solar cell [56]

First, energy is transferred from photons to electrons in the valence band (VB) of the silicon-based surface. The blue arrow in Figure 3.2 represents total energy of the photon. The electrons are energized to energy levels equal to the photon energy, hf , where h is Planck's

constant, and f is the wave frequency [56]. The transfer of energy only occurs after energy level is in the conduction band (CB), and not in the forbidden energy gap (Eg) [56]. The red arrows, T and R in Figure 3.2 represent energy lost via thermalisation (T), and recombination (R, ReCOMB) occurring after energy transfer in the VB. The green arrows represent the transfer of energy that leads to output power, where maximum efficiency of the mechanism is equivalent to the product of current (I) and voltage (V),

$$P = I \times V \quad (3.3)$$

Currently, SUNPOWER produces the most efficient solar panels at 22.8 % efficiency value [62].

A cell is the basic unit of solar PV and would be too small to generate significant amounts of electricity alone. Photovoltaic cells are connected in series and/or parallel to produce more power. Solar farms or solar parks are areas of large PV installations for generating vast amounts of electricity. They are a construction of many arrays connected. In contrast, arrays are made up of many modules connected, and modules are many cells connected, as shown in Figure 3.3.

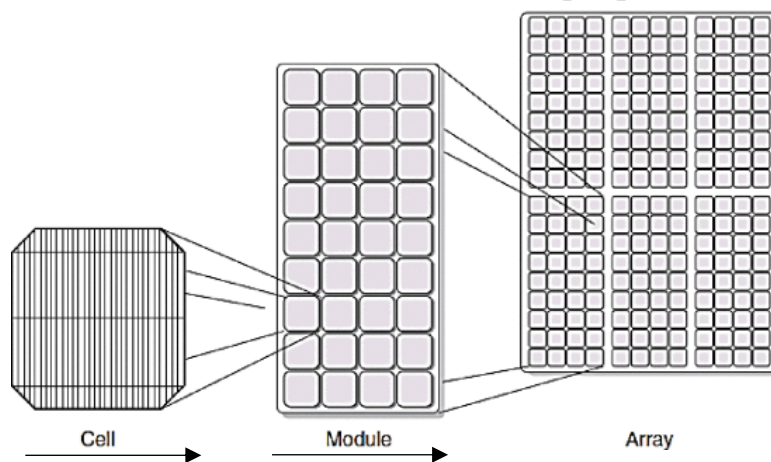


Figure 3.3. Presentation of a solar cell, module, and array [63]

The power generated in PV is direct current (DC), a DC-AC inverter connects the solar farm to the city AC grid. Figure 3.4 shows connections of arrays at currently the world's largest solar farm located in India and with a capacity of 2 245 MW [64].



Figure 3.4. World's largest solar farm located in India [65]

3.2 Concentrated Solar Power – CSP

Concentrated solar power (CSP) technology extracts thermal energy from solar radiation like conventional fossil fuel power generating mechanisms using combustion to generate heat (like the ST, adopting the Rankine cycle). CSP comprises concentrators, receivers, storage systems, and power conversion devices [66]. CSP uses mirrors to concentrate the solar flux, to heat the working fluid (WF), also known as the heat transfer fluid (HTF), in the receivers. The WF in the receiver boils upon heat transfer, and the vapor turns a turbine that generates electricity. Thermal Energy Storage (TES), typically using molten salt, makes it possible to store energy for times of high demand and improves the system flexibility. CSP without a storage unit operates with capacity factors ranging from 20 % to 40 % [67]. But the CSP with storage capability reaches to a capacity factor of 75 % for the most advanced power plants [67]. *The thermal aspect of CSP makes it possible to combine with other thermal PPs.*

There are four methods used in CSP systems [66] [67]:

1. Parabolic Trough Collectors (PTC) - The technology uses a receiver located on the focal point of parabolic mirrors. The receiver transfers solar energy to HTF, which transports energy to the steam generator, where heat exchange occurs. Here, the HTF transfers heat to water, converting it to steam. Then superheated high-pressure steam rotates the turbine blades to generate electricity. To generate more electricity, receivers are connected to loops, generating more heat. Approximately 16 187 m² to 20 234 m² of land is required to generate 1 MW of capacity [66], see Figure 3.5a and Figure 8.7. Parabolic trough technology uses mirrors called concentrators to direct thermal energy from the sun to the receivers called heat collectors (or heat absorbers) [68]. The absorbers are long pipes located in the middle of the PTC. They accommodate the WF, which has desired specific heat capacity, such as oil (can reach 400 °C) or molten salt (can reach 550 °C).
2. Linear Fresnel Reflectors (LFR)- Uses the exact mechanism of PT, differing in that it uses arrays of almost flat reflectors to concentrate irradiation (Figure 3.5b).
3. Solar tower/Central receiver (CT) - Heliostats⁹ are utilized to ensure that the boiler located on the solar tower receives the irradiance. The technology can be connected to a storage facility, allowing it to generate electricity during low to no solar irradiance (Figure 3.5c).
4. Parabolic dish- This technology uses reflective dishes to concentrate solar radiation to receivers. This is the least common CSP system (Figure 3.5d).

⁹ Heliostat: A device including mirrors, ensures that the tower collector is constantly receiving solar irradiation [69].

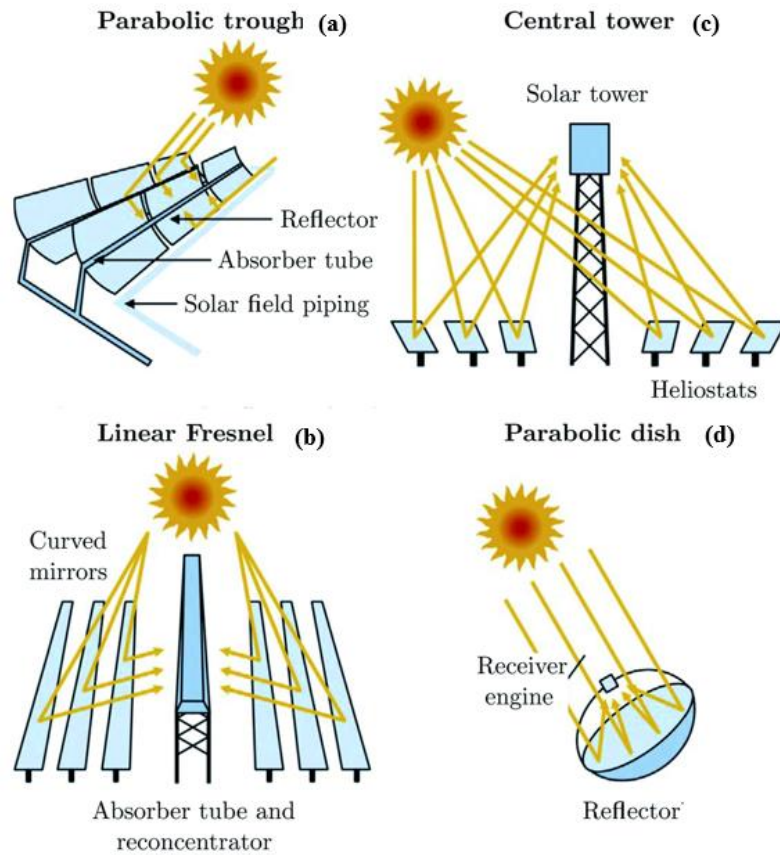


Figure 3.5. Types of solar thermal technologies [70]

Table 3.1 shows that the PTC technology has the least development risk, high efficiency, and can use different WFs. PTC PPs are mature technologies that generate over 90 % of the CSP capacity [71]. Figure 3.6 shows the schematic of a CSP PTC facility.

The Multi-Criteria Decision Analysis (MCDA)/Multi-Criteria Decision Making (MCDM), discussed next, is the preferred method to determine the feasibility of CSP application.

Table 3.1. Typical features of solar thermal technologies [72]

CSP technology type	Working fluid	Steam conditions, [°C/bar]	Thermal efficiency, [%]	Tech. Development risk
Solar Tower	Steam/water, molten salt, air	540/100 - 160	30 – 40	medium
Parabolic Trough	Synthetic oil HTF, water/steam, molten salt, air	360 – 540/100	30 – 40	Low
Linear Fresnel	Steam/water	260/50	-	Medium

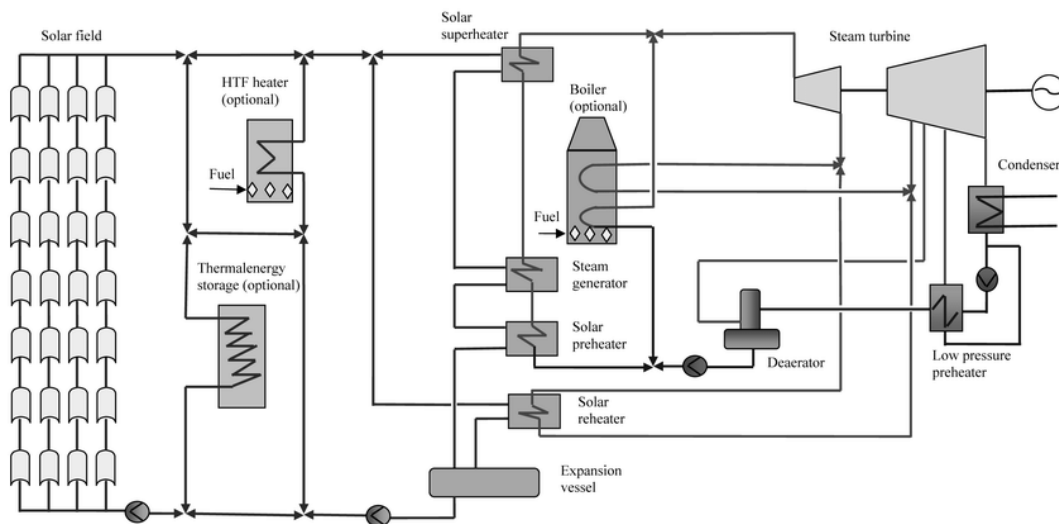


Figure 3.6. Schematic of a large-scale parabolic trough solar power plant [73]

3.3 Energy Storage

Both CSP and PV systems face the challenge of storing generated energy. Storage is an important part/aspect of solar systems since several factors cause slow and fast variations in solar intensity. Abrupt weather changes, changes in seasons, cloud cover, and windstorms, among many others, significantly affect the intensity of solar irradiance and, ultimately, the power output. Figure 3.7 shows the variation of irradiance (supply) and consumption

(demand) during a typical day (in the UK). There is a mismatch between the demand and supply, especially between 11.00 hrs. and 00.00 hrs. The high solar irradiance during the day and increased power demand from 16.00 hrs. to 22.00 hrs. highlight the need for storage or other solutions.

Since CSP systems have TES facilities, storing the energy as heat and using it to generate electricity during peak hours is easier. For massive PV systems, it is challenging to store electrical energy. However, electrical power can be stored in electrochemical systems (such as batteries) or converted into other energy forms. Akbari et al. (2019) [74] summarize the storage technologies for PV as Electrical Energy Storage (EES) and TES, choice of which depend on the end use of generated energy.

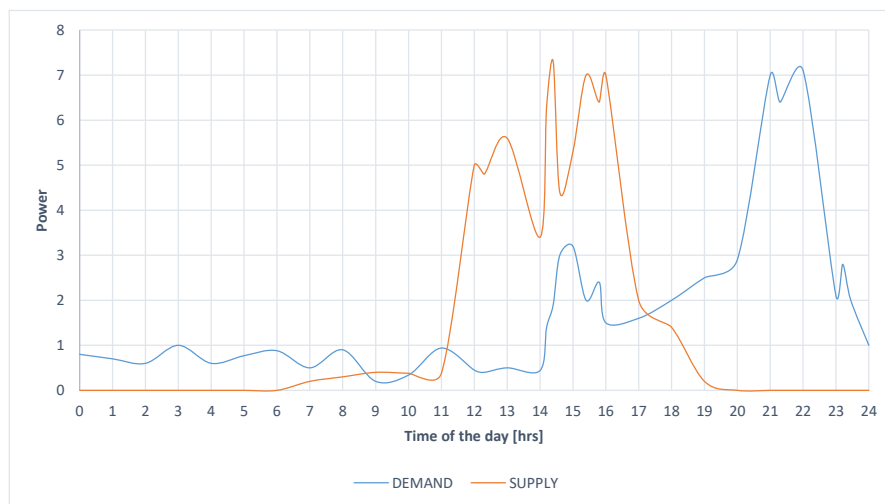


Figure 3.7. Typical variation of irradiance (supply), and consumption (demand) for a day of variable cloud (Adopted from [51])

Scholars have different opinions on which system (PV or CSP) is most preferred, considering storage facilities. PV is the most accepted and widely adopted technology, owing to being cheap and readily available for use, while CSP is the less popular one.

Akbari et al. (2019) [74] outline the electrical and thermal energy storage utilities for PV that could store energy ranging from 2 to 7.2 hours and with capacities ranging from 3.2 MWh to 250 MWh, concluding a potential for PV with battery storages. Considering the increased demand from Figure 3.7 lasting 7 to 8 hours, some technologies presented by Akbari et al. (2019) [74] would not be able to store needed energy throughout high-demand times of the day.

Ibrahim et al. (2012) [75], in an outline of electrical energy storage for PV, highlight the wide range of commercially available storage technologies under development and research. Maronga et al. (2021) [76] evaluate PV and CSP systems to supply power for the mining sector in Zimbabwe and concludes that PV systems with battery storage offers the preferred performance, while CSP with TES showed great potential for more extensive facilities. The authors did not consider the results that could have been achieved by huge power plants, say over 100 MW. Most literature on solar systems compares the growing and most preferred PV systems for small facilities (households, factories, farms, etc.) with the CSP systems reserved for huge facilities. Boretti & Castelletto (2021) [77] compares CSP and PV of capacities greater than 100 MW. Boretti & Castelletto (2021) [77] consider dispatchibility¹⁰ as a factor that should be looked into, as it justifies the adoption of CSP systems over PV systems. After comparing the performance of a CSP PTC plant without TES, CSP PTC with TES, with four PV power plants in America (all with capacities greater than 100 MW), Boretti & Castelletto (2021) [77] concludes that CSP without TES could provide comparable performances, at an acceptable cost, reaching the mass production of the current PV technologies. Accordingly, in this study we consider CSP without TES since the technology can be easily coupled with fossil fuel technologies like a CCGT power plant to perform as a hybrid ISCC power plant.

3.4 Power Generation Potential

Solar power generation is generally classified as the theoretical, technical, and economic potential [78]. The theoretical potential is the net annual solar radiation in a suitable region. The technical potential considers the theoretical potential and solar power technologies, while the economic potential estimates the cost of investment in comparison to conventional energy sources. The technical potential can be calculated as [79]:

$$TPSE = DNI \times EF \times A \times PR \quad (3.4)$$

¹⁰ Dispatchibility: The ability to produce after sunset or when there is cloud cover [77].

Where,

TPSE- Technical potential of CSP plant, [kWh/year]

DNI- Direct solar irradiance value, [kWh/m²/year]

EF- Efficiency for the solar system, [%]

A- Area available, [m²]

PR- Performance ratio for PV modules

The efficiency of PT solar technology ranges from 15 % to 21 %, and the PR can be taken at 70 % [78] [79].

To estimate the theoretical, technical and economic potential the location of the solar facility has to be known. The next section describes the most common method used to determine the most suitable location for the solar facility.

3.4.1 Plant Location and Multi-criteria Decision-Making (MCDM)

Plant location is among the most critical considerations for CSP, and determining the most suitable place for CSP is a complex decision-making problem. This is because there are many conflicting objectives and criteria to be considered.

The Multi-Criteria Decision Analysis (MCDA) method is used to solve complex decisions. [80]. Conflicting criteria are typical in assessing alternatives: cost and some quality measure is another criterion, easily in conflict with the cost. MCDM is involved with organizing and handling multiple-criteria decision and planning problems. The objective is to help decision-makers who are confronted with either of these problems.

The Analytic Hierarchy Process (AHP) method is the most applied MCDM method, as suggested by the references in Table 3.2 which summarizes the CSP site selection literature review using the AHP method.

Table 3.2. Feasibility of concentrating solar power literature review

Study	Country	Reference
CSP	Algeria	[81]
CSP and PV	China	[79]
CSP and PV	Iran	[78]
CSP	UAE	[80]
CSP	Morocco	[82]
CSP and PV	Morocco	[83]
CSP and PV	Tanzania	[84]
CSP and PV	Greece	[85]

3.4.1.1 Analytic Hierarchy Process (AHP)

The AHP organizes, analyzes, and selects the most feasible options based on mathematics and psychology [86]. The method is used to help decision-makers conclude their complex problems (in this case, the best location for CSP) by comparing available options (in this case, available sites) using selection criteria and sub-criteria suggested by Saaty (1980) [87].

Initially, the goal must be defined, followed by establishing of the criteria to be used in the process. For example, in this case, our goal is to find the most suitable site for CSP. The criteria are used to compare and select the most feasible location from the range of potential areas. The AHP applies a pairwise comparison to assign weights for the decision criteria competing against each other for prominence. Saaty (1980) [87] developed a table to show how one criterion could be more important than the other. Table 3.3 shows the AHP weighing scale, where each entry represents the importance of the i^{th} criterion to the j^{th} criterion. Furthermore, the relative importance of the j^{th} criterion to the i^{th} criterion is the reciprocal of a_{ij} , as shown in Table 3.3.

Table 3.3. AHP importance scale [87]

Intensity	Definition (<i>i</i> with respect to <i>j</i>) Relative importance	Values a_{ij}	Numbers a_{ji}
1	Equal importance	1	1
2	Intermediate (between 1 and 3)	2	1/2
3	Moderate importance	3	1/3
4	Intermediate (between 3 and 5)	4	1/4
5	Strong importance	5	1/5
6	Intermediate (between 5 and 7)	6	1/6
7	Very strong importance	7	1/7
8	Intermediate (between 7 and 9)	8	1/8
9	Extreme importance	9	1/9

The following are the steps taken when conducting AHP,

1. Determine the goal of the analysis
2. Determine the criteria and sub criteria
3. Assuming n criteria, set a pairwise comparison matrix $A [n \times n]$:

$$A = \begin{bmatrix} a_{11} & a_{12} & \dots & a_{1n} \\ a_{21} & a_{22} & \dots & a_{2n} \\ \dots & \dots & \dots & \dots \\ a_{n1} & a_{n2} & \dots & a_{nn} \end{bmatrix} \quad (3.5)$$

4. Get preference on the importance of each criterion against others, based on the recommendations from experts and/or literature.
 - a. Where a_{ij} is the importance of the i^{th} criterion to the j^{th} criterion, and the importance of the j^{th} term is $1/a_{ij}$.
 - b. The importance is based on the scale of importance by Saaty (1980) [87] shown in Table 3.3.
5. Obtain weight for each criterion. First, normalize matrix $A [n \times n]$ to matrix $[w_j]$. The normalized priority matrix is calculated by dividing the assigned numerical by the sum of values in the same column. Finally, the average of each row is calculated to give the weight for each criterion.

6. Calculate the consistence ratio (CR) to check or guarantee consistency of recommendations by experts or literature. The CR must be less than 10 % to satisfy consistency.

a. The consistency ratio is given by:

$$CR = \frac{CI}{RI} \quad (3.6)$$

Where, RI is the random index representing the deviation of matrices and is taken from Table 3.4.

CI is the consistency index and is given by:

$$CI = \frac{(\lambda_{max} - n)}{(n - 1)} \quad (3.7)$$

Table 3.4 shows the pairwise random indices to be used in the AHP method.

Table 3.4. Random consistency indexes [87]

n	1	2	3	4	5	6	7	8	9	10	11	12
RI	0	0	0.58	0.9	1.12	1.24	1.32	1.41	1.45	1.49	1.51	1.54

Where λ_{max} is the maximum eigenvalue obtained from matrix A ($n \times n$), and is given by:

$$\lambda_{max} = \frac{\sum_j^n (\sum_{i=1}^n A_{ij}) w_j}{A_{ij}} \quad (3.8)$$

7. Determine the land suitability index, by integrating MCDM with Geographic Information System (GIS) software according to following equation:

$$LSI_i = \sum_{j=1}^n w_j x_{ij} \times \prod_k^n EC_{ik} \quad (3.9)$$

Where, LSI_i is land suitability index of area i , x_{ij} is the value of the area (of the land in consideration) under the reclassification of j . w_j represents the assigned weight to the relative criterion j . EC_{ik} is the binary variable, such that if the respective area is under restricted areas then $EC_{ik} = 0$, and installation for CSP is not feasible, otherwise $EC_{ik} = 1$.

The MCDM-GIS integration is performed by using software such as ArcGIS, QGIS, GRASS GIS, SAGA GIS etc.

CHAPTER 4

HYBRID POWER PLANTS

Hybrid power plants combine at least two technologies, including renewables, non-renewables, or energy storage facilities, to generate electricity from a single facility [88] [89]. Renewable Energy Systems (RES), like solar and wind, depends on uncontrolled climatic characteristics. Therefore, hybrid PPs can provide optimal performance. Hybrid power generation has the following advantages:

- Environmentally friendly- Hybrids including RES consume less fuel, reducing GHG emissions.
- Dispatchable generation- Hybrid PPs produce an uninterrupted power supply.
- Optimal performance- Some combinations increase PP overall efficiency.

The system combination may include the following technologies, wind turbines, photovoltaics, CSP, Electrical Energy Systems (EES), geothermal power, hydropower, biomass, natural gas oil, coal, or nuclear power [89]. So, hybrid PPs could be PV-oil, wind-PV, wind-PV-coal, or CSP-natural gas, producing more predictable, controllable, and reliable electricity. However, the current study focuses on the solar-gas hybrid system, the Integrated Solar Combined Cycle (ISCC) PP.

4.1 Integrated Solar Combined Cycle (ISCC) Systems

The CCGT system is attractive because it has preferable performance, high efficiency, and low GHG emissions. The CCGT system utilizes two cycles, the Brayton cycle and the Rankine cycle, which can be coupled with other technologies to construct a hybrid configuration. Typically, the Rankine cycle is used to couple the CCGT system with other technologies. The ISCC system is a hybrid configuration that utilizes the effect of solar thermal in a CCGT power station. This means, the hybrid system can produce electricity as a conventional CCGT PP and an ISCC hybrid. This is an advantage because electricity can be generated irrespective of irradiance availability. The ISCC technology is a sustainable

method for EG by combining the technologies of CSP and CCGT. The technology has efficiencies typically 5 % higher than those of CCGT power plants [90]. There are several ISCC plants in the world, but not as many considering that solar energy is abundant in most areas of the world.

4.1.1 Technology, System Design and Equipment

The working principle is the same as the CCGT PP, but with the inclusion of the solar input, while having almost the same equipment types (mentioned in Chapter 2, CCGT working principle subsection). Significant changes are found in the ST (sizing of the ST) and balance of point (BOP) equipment. When we consider the purpose of including the solar cycle to boost the power output, then the BOP equipment, like pumps, cabling, piping, motor control centers, etc., must be capable of coping with the increased ST capacity. Figure 4.1 is a schematic of an ISCC PP using PTC.

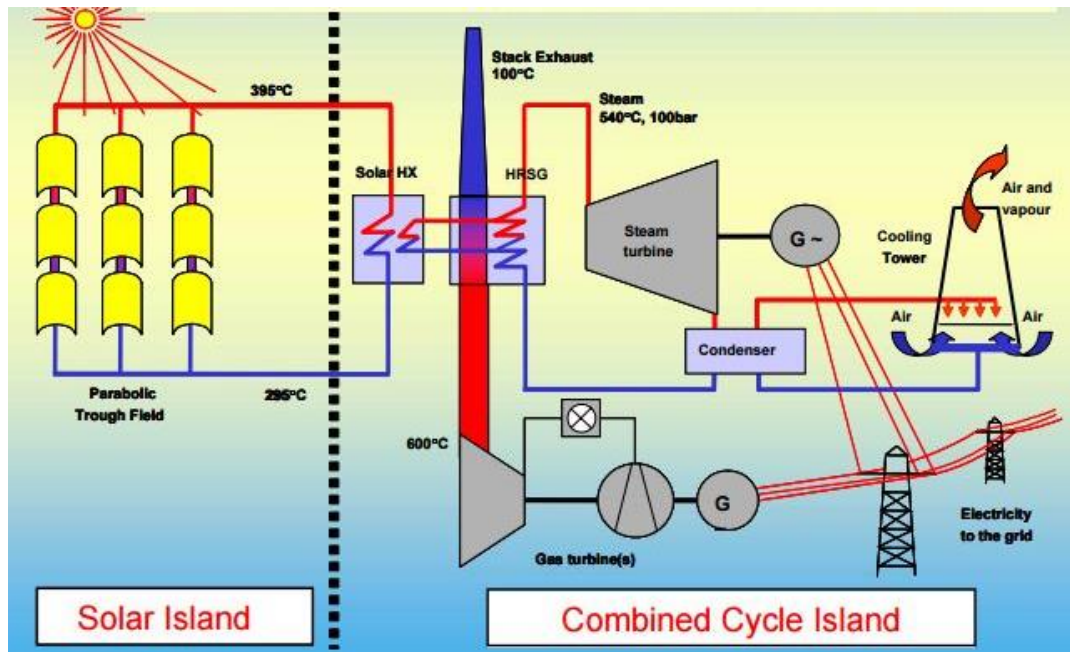


Figure 4.1. Integrated Solar Combined Cycle [91]

The concentrated solar part transfers energy by either the application of Direct Steam Generation (DSG) or the use of a working fluid (WF), using one of the solar thermal technologies mentioned in Chapter 3 (Concentrated solar power section). Either of the

technologies is used to generate steam which is then injected into the HRSG or directly into the ST (see Figure 4.1) [66]. Table 4.1 shows selected studies on ISCC. Most studies adopt the PTC technology while utilizing DSG solar integration.

Table 4.1. Integrated Solar Combined Cycle (ISCC) applications

Location	Solar type	Solar integration	Results	Reference
Almeria and Las Vegas	PTC, LFR, CT	DSG, air preheating	PTC performed better than others, using DSG	[92]
Dunhuang	PTC	HTF	Potential power in optimization strategies	[93]
Iraq	PTC	DSG	The technology saves fuel, reduces peak demand, and reduces carbon emissions	[94] [95]
Greece	PTC	HTF	ISCC PPs offer a flexible transition from CCGTTPs	[96]
China	PTC	DSG	ISCC PPs perform better than CCGTTPs	[90] [97]
Iran	PTC	DSG, HTF	Integration with DSG lowers cost of electricity, and increases output power	[98]
Algeria	PTC	HTF	Authors made a model that can predict solar to electricity of the hybrid	[99]

4.1.2 Solar Integration

Fundamentally, integration of the solar cycle depends on the purpose of the operator, where two options are available [66]:

1. Power boost- This option increases the PP power output by generating additional steam in the ST.
2. Heat rate improvement- PP power output remains constant, while the fuel required to maintain the designated power level is reduced.

When integrating solar energy into a combined cycle, some questions must be answered:

1. Which solar thermal technology must be used?

- a) To determine the best technology to use, Zachry (2012) [66] suggests performing an economic evaluation for each technology to determine the LCOE and compare different solar thermal inputs from other technologies. Many studies in Table 4.1 prefer adopting PTC because the technology has matured and is easily understood.
2. How much solar thermal must be added to the bottoming cycle?
 - a) The quantity of solar thermal to be added, if a power boost is chosen, depends on the desired HRSG arrangements and ST capacities [100]. Breeze (2016) [101] suggests that the solar input should be kept to 10 % or less of the total PP energy input.
 3. In the HRSG, where is the best place for adding solar thermal?
 - a) When a thermal technology is chosen, the combined cycle can be integrated based on temperature capabilities. For example, CT, PTC, and LFR generate high-temperature, medium-temperature, and low-temperature steam, respectively. High-temperature solar technology (CT) generates steam over 540 °C, which can be directly administered to the High pressure (HP) steam line of the GT [66]. Medium-temperature technologies using the PT are considered the best and most preferred technology when integrated into the HP drum of the HRSG [66] [102]. Most LFRs fall under low-temperature solar technology, generating steam up to 270 °C. Due to low temperatures, the technology can be integrated into the Low pressure (LP) admission line or combined with the cold reheat line [66].
 4. Where in the HRSG must the feedwater be extracted from the solar boiler?
 - a) The most preferred method is to take the feedwater from the HP feedwater pump outlet, and to maximize feedwater heating, use flue gases from the GT, and reduce the quantity of input solar thermal (thus, also reduce the size of the solar field). Thermodynamically, the most efficient way to input steam for a three-pressure steam generator (see Section 2.3.2) is the HP evaporator [66].

4.1.3 Assessment of Integrated Solar Combined Cycle Power Plant

To investigate the feasibility of coupling solar thermal and CCGT PPs, authors used different methods. Table 4.2 lists important literature exploring several aspects of the ISCC PPs.

Table 4.2. Assessment of ISCC PP

Analysis	Location	Software	Remarks	Reference
CT vs PT integration with a CCGTTPP	Middle East	NREL	CT saved more fuel than PT, due to integration used. The ISCC also produced less electricity than CCGTTPP, though it reduced fuel consumption	[66]
Techno-economic assessment/ Power boost	Greece	TRNSYS	The simulation proved the feasibility of integrating large solar fields in conventional power plants	[96]
Performance and comparison	South Australia	Bird Clear Sky process simulation	The proposed plant was both economic and exergy efficient	[103]
DSG-ISCCPP integration	India	C++, Engineering Equation solver 2010.	The proposed plant had an increased output capacity, reduced efficiency, reduced LCOE, and reduced payback	[104]
3 E methods on CCGT and ISCC PPs	China	EBSILON	The proposed system offered reduced fuel consumption and reduced CO ₂ emissions	[105]
PTC, LFR, and CT comparison for an ISCC system	Spain and USA	N/A	ISCCs using DSG improve electricity generated, and PT proved to be the best technology for DSG	[92]
CCGT to ISCC conversion	Iraq	Energy Equation Solver	The output power is highly proportional to irradiance, increasing benefits in efficiency, performance, and economics	[95]
ISCC Optimization	China	EBSILON, TRNSYS	The proposed integration resulted in increased efficiency and reduced LCOE	[90]
ISCC modeling	Algeria	MATLAB	Operating data and simulating data showed a good alignment	[99]
General performance evaluation	N/A	EBSILON	The study provides different system optimization analyses that can be applied for desired results in an ISCC system	[97]

CHAPTER 5

COAL BED METHANE

5.1 Natural Gas

Natural gas is a fossil fuel from organic debris and inorganic matter deposited under earth's surface for millions of years. Natural gas is primarily made of methane (CH_4), with slight traces of impurities like carbon dioxide (CO_2), nitrogen, sulfur, etc. After generation in source rocks, natural gas can be categorized according to trapping mechanisms in the geological formations as conventional or unconventional natural gas, where:

- Conventional gas is trapped in reservoir rocks capped with impermeable layers and can be produced from a well without artificial lift technologies.
- Unconventional gas is trapped in the source rock, requiring different production methods. Types of unconventional gases include shale gas, tight gas, CBM, and natural gas hydrates.

Compared with other fossil fuels, natural gas is the cleanest fossil fuel when combusted. The increasing GHG emissions from fossil fuels (especially coal and oil) have shifted the use of fossil fuels to natural gas. Natural gas is considered a bridge fuel to transition from using non-renewables to using clean RES. Natural gas is more environmentally sustainable than coal because coal releases approximately 70 % more GHGs [15] [16]. Since most natural gas is methane (CH_4), mainly CO_2 and water (H_2O) are released as by-products. In power generation, natural gas has the highest energy conversion efficiencies [106]. Presently, natural gas is the premium fossil fuel of the world economy for a sustainable environment. With worldwide policies ensuring the cost of carbon emissions, natural gas has the potential to increase its share in the power generation sector significantly.

5.2 Coal Bed Methane

Coal bed methane (CBM), also known as coal bed gas, coal seam gas, or coal mine methane, is an unconventional natural gas resource, produced and extracted from coal beds. CBM is a life-threatening entity in coal mines, which had to be vented for safety, but it has become an essential global resource. CBM plays a vital role in the energy industry, and there are significant field exploitations in the USA, Canada, India, Australia, and China [107]. The produced CBM is sold as pipeline gas in the aforementioned countries or used to generate electricity.

Fig 5.1 shows the global CBM market share by application. Power generation takes the largest share, 40.6 % of the total application, because power generation from CBM is not as expensive as other fossils (G. R, n.d.). A report by Grand View Research (2019) [108] points out that CBM power generation is expected to be the fastest-growing application from 2020 to 2027 at a Compound Annual Growth Rate (CAGR) of 6.6 %.

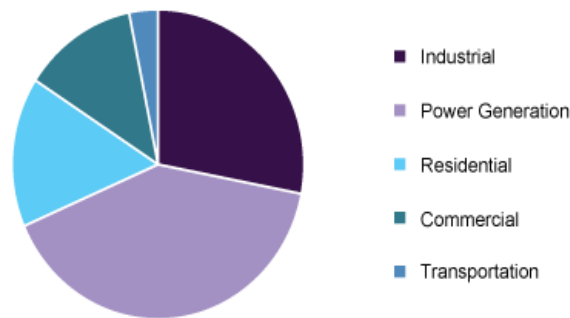


Figure 5.1. Global CBM market share, by application [108]

Table 5.1, shows prominent members of the CBM resources in the Asian-Pacific Economy Cooperation (APEC) group of countries.

Table 5.1. CBM resources in major APEC economies [109]

Member	CBM resource [Trillion m ³]
Australia	8 – 14
Canada	17.9 – 76
Indonesia	12
Russia	83.7 (17 – 113)
China	36.8
United states of America	21.4

5.3 Origin of Coal

Coal is a sedimentary rock composed of carbon and hydrocarbons formed from dirt and plants buried under water, subjected to heat and high pressure for millions of years [110]. Changing of peat¹¹ to coal under high pressure and temperature is known as coalification. The black or brownish-black sedimentary rock is grouped into different ranks depending on coalification, carbon content, and the number of impurities. The ranks are used to evaluate the maturity, calorific value, and volatile matter content per unit mass of coal. To quantify thermal maturity, vitrinite reflectance can be measured by obtaining the percentage of incident light reflected from the vitrinite substance found in coals. Vitrinite is a type of maceral found in organic matter in coals, and the reflectance increases from lignite to anthracite coals. Coal is classified into the following foremost ranks [110],

- Anthracite- A black type of coal with the highest carbon content and heating value and is the highest ranking. It contains 86 % to 97 % carbon and has negligible impurities.
- Bituminous (grouped into low volatile bituminous, medium volatile bituminous, high volatile bituminous-A, low volatile bituminous B, high volatile bituminous C)- The black or dark brown coal contains bitumen and has a carbon content ranging from 45 % to 86%.
- Subbituminous (grouped into subbituminous A, subbituminous B, and subbituminous C) - The dull to dark brown coal is low-rank coal containing 35 % to 45 % and has a lower heating value than anthracite and bituminous coal.
- Lignite- Brown coal is the lowest-ranking coal, with carbon content ranging from 25 % to 35 %. The low-ranking coal has the most moisture content, which is the reason for its low heating value along with low carbon content.

5.4 Origin of Coal Bed Methane

After changing the physical and chemical properties of organic remains, coalification also results in the generation of natural gas called CBM containing various gases in which CH₄

¹¹ Peat: Partially decomposed vegetable matter, usually mosses.

amounts to 80 – 99 % [111]. The gas content per metric ton of rock ranges from 0.0003 – 18.66 m³/tonne [112]. 1 % to 20 % of the remaining gas mixture comprises carbon dioxide, nitrogen, hydrogen sulfide, and sulfur dioxide.

CBM is generated by two subsurface processes, biogenic and thermogenic. Biogenic gas, mainly composed of CH₄ and CO₂, converts coal molecules to gas by the action of micro-organisms residing in the coal and is primarily produced in low calorific value coals [113]. Due to increased temperatures underground, thermogenic gas is formed during the conversion of subbituminous to bituminous coals.

Lower-rank coals, such as subbituminous C and lignite, produce mostly biogenic coal seam gas. In comparison, higher rank coals, like low volatile bituminous and anthracite coals, are more likely to present as thermogenic gas play. Most prolific CBM is generated in medium-volatile bituminous rank [114] [115]. According to Qin et al. (2017), 53 % of total CBM resources are from middle to high-rank coal reservoirs, and the potential producible resources from these ranks are estimated to be about 31.6 % of the resources. Figure 5.2 shows the hydrocarbon (HC) generation from different coal types and the relative gas abundance.

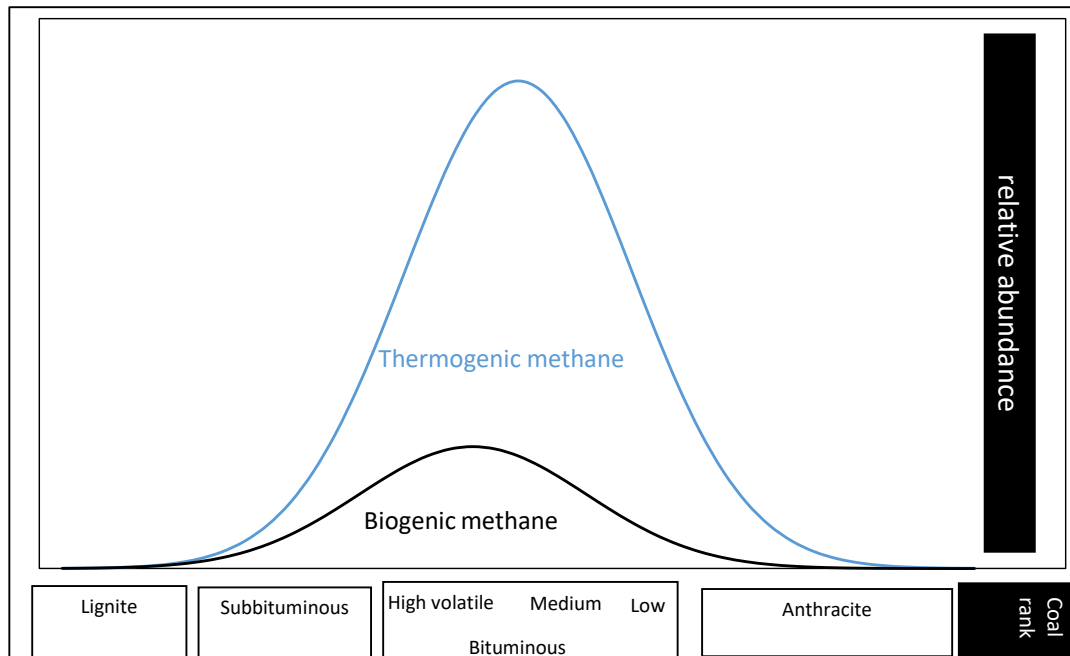


Figure 5.2. Hydrocarbon generation during coalification (Adopted from [114] and [115])

5.5 Adsorption Capacity and the Langmuir Isotherm

Adsorption is mass transfer of gases onto solid surfaces (or solutes onto liquid surfaces) [116]. Adsorbed phase does not necessarily retain gas properties: it exhibits liquid-like features [117]. Therefore, it is preferably called adsorbed phase instead of adsorbed gas. Adsorption capacity is the amount of CH₄ that can adsorb on the coal surface per unit mass (or volume) [118]. It is an essential parameter for estimating CBM OGIP and the exploitation potential [119]. The equilibrium state in the sorption¹² process with respect to pressure is typically described by a Langmuir Isotherm, shown in Figure 5.3 [120].

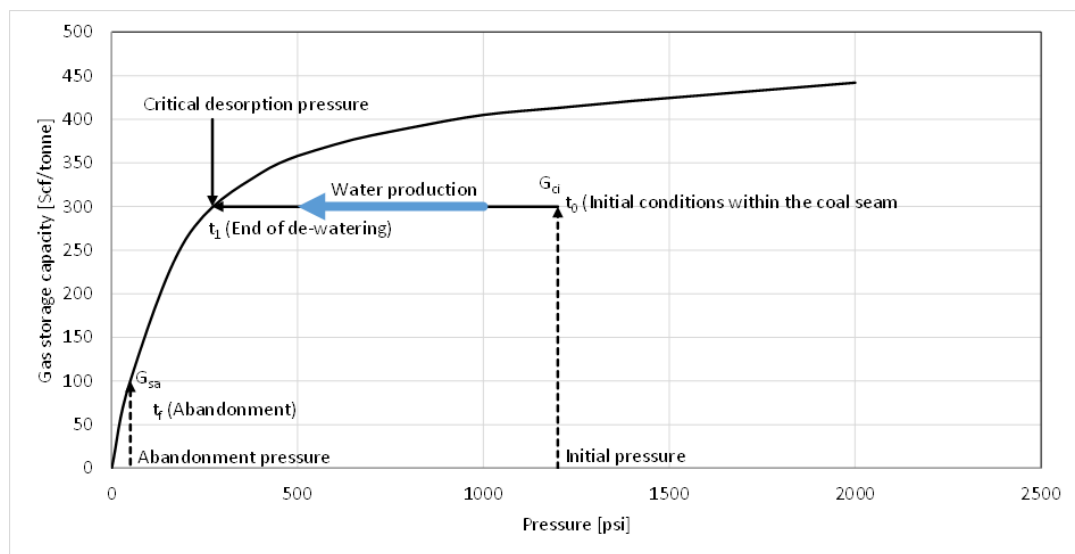


Figure 5.3. CBM operating conditions are shown on a typical Langmuir Isotherm.
(Adopted from [121])

¹² Sorption: In this context, general name referring to the two-way adsorption/desorption [113].

5.6 Coal Bed Methane Deposition

Coal is a dual-porosity medium¹³. The porosity of coals is from original deposition (matrix porosity) and secondary porosity (cleats) due to various mechanisms and stresses acting on the coal formation. CBM is mainly stored as adsorbed phase on the micro-pores of the coal matrix surface, and a small fraction of it is kept in the fractures or the cleat system as free gas, as shown in Fig 5.3.

Absorbed methane is diffused into the coal matrix, while adsorbed methane is kept in the micro-pores of the matrix surface by weak Van Der Waal forces. However, it is generally thought that most methane is attached through adsorption [122].

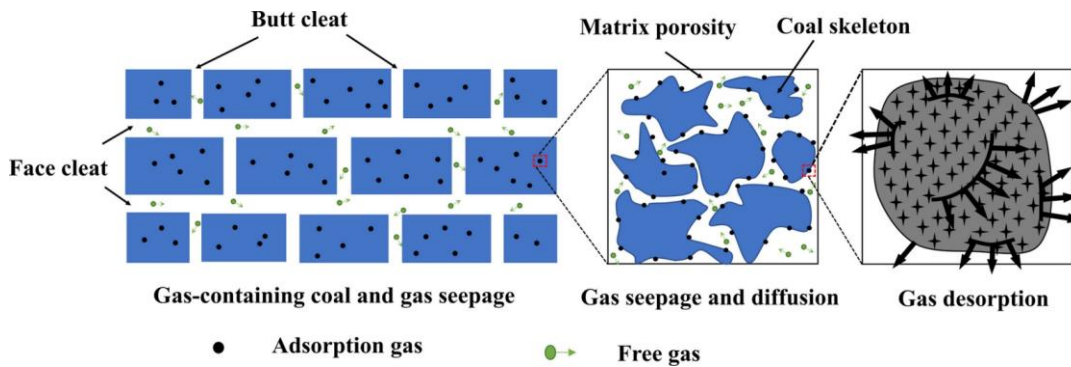


Figure 5.4. Adsorbed and free gas on a coal surface [123]

The adsorption of CBM on the coal surface exhibits a non-linear relationship with pressure. The Langmuir isotherm introduced in the previous section governs the adsorption of gas on coal seams with the isothermal adsorption equation [120]:

$$V_{adsorption} = \frac{V_L \times p}{p + p_l} \quad (5.1)$$

Where,

¹³ Dual-porosity medium- are comprised of pores and cleats, where face cleats and butt cleats are observed for coals.

$V_{adsorption}$ - Adsorbed volume, [m³/tonne].

V_L - Langmuir volume, representing the maximum adsorptive capacity of the coal, [m³/tonne].

p - Pressure of the coal formation, [MPa].

p_L - Langmuir pressure, pressure at which adsorbed volume of gas is half of V_L , [MPa].

Due to the dual storing ability of coals the total original gas in place (OGIP) is given by:

$$OGIP = G_a + G_f \quad (5.2)$$

Where,

G_a – Adsorbed gas.

G_f – Free gas.

5.7 Coal Bed Methane Resources and Reserves

In the hydrocarbon industry, quantities of oil and gas can be defined as either resources or reserves based on economic and social viability, the feasibility of production, and available geological knowledge. Fig 5.4 represents the definitions used to classify resources and reserves. The horizontal axis represents the range of uncertainty in the estimated hydrocarbon quantities, while the vertical axis represents the certainty of the hydrocarbon quantities. The maturity ranges from undiscovered hydrocarbon in place (also known as original hydrocarbon in place) to discovered hydrocarbon initially in place. Prospective resources are hydrocarbon quantities estimated to be potentially producible from undiscovered accumulations. Contingent resources are estimated quantities from discovered accumulations and are more likely to be recoverable than prospective resources. *Reserves* are hydrocarbon quantities that are commercially producible from known accumulations.

Before estimating producible hydrocarbon quantities, resources must be estimated, and Table 5.2 shows some of the methods used for estimating OGIP in the gas industry. As observed from Table 5.2, the methods used to estimate OGIP can be grouped into Volumetric

methods (conventional resource calculations) and Performance methods (methods relying on the historical data of gas produced).

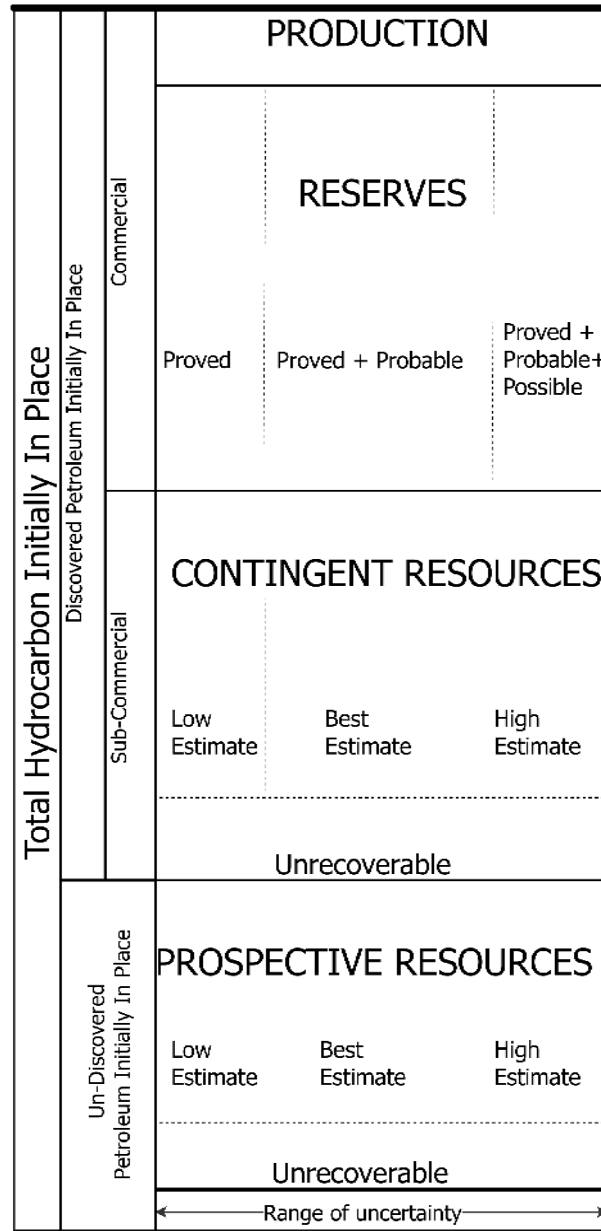


Figure 5.5. Resource classification (Adopted from [124])

Table 5.2. Resource/reserve estimation literature review

Method	Model	Resource type	Reference
Probabilistic	Volumetric equation	Unconventional (Shale gas)	[125]
Deterministic Probabilistic Probabilistic	(and Material Balance Equation (MBE) Volumetric, MBE, Flowing Material Balance (FMB)	Conventional (Geo- pressured) Conventional	[126] [127]
Deterministic Probabilistic	and 3D geometrical framework, Volumetric- MCS	Unconventional (CBM)	[128] [129]
Deterministic Probabilistic	and Volumetric, decline curve (modified), MBE	Unconventional (CBM)	[130]
Deterministic	Langmuir model, Volumetric	Unconventional (CBM)	[131]

5.8 CBM Reserve Estimation

The volumetric OGIP formula for a conventional reservoir (free gas in place) is given by Equation 5.3 [130]:

$$G_f = A \times h \left(\frac{43\,560 \times \varphi \times (1 - S_{wi})}{B_{gi}} \right) \quad (5.3)$$

Where,

G_f = Original Gas in Place (for CBM, this is the free gas in cleats), [SCF].

A = Rock area gas is drained from, [Acre].

h = Rock formation thickness, [ft.].

φ = Total porosity, includes matrix and fracture porosity, [fraction].

S_{wi} = Initial water saturation [fraction].

B_{gi} = Gas formation volume factor at initial conditions, [ft³/SCF].

The adsorbed phase gas volume in-place is calculated using Equation 5.4.

$$G_a = 1\,359 \times A \times h \times \rho_c \times G_c \quad (5.4)$$

Where,

A = Rock area, [Acre].

h = Rock formation (coal seam) thickness, [ft.].

ρ_c = Coal bulk density, [g/cm³].

G_c = Adsorbed methane content, [SCF/tonne].

Therefore, total OGIP for CBM after Equation 5.2 is given by:

$$G_t = A \times h \left(\frac{43\,560 \times \varphi \times (1 - S_{wi})}{B_{gi}} + (1\,359 \times \rho_c \times G_c) \right) \quad (5.5)$$

The equation for total initial gas in place can be represented with Equation 5.6, by substituting Equation 5.1 for G_c in equation 5.5, accounting for both ash weight and water weight to give:

$$G_t = A \times h \left(\frac{43\,560 \times \varphi \times (1 - S_{wi})}{B_{gi}} + 1\,359 \times \rho_c \times (1 - f_a - f_w) \frac{V_l \times p}{p_l + p} \right) \quad (5.6)$$

Where, S_{wi} [fraction] is initial water saturation in the cleats. If coal seam is initially invaded by water, $S_{wi} = 1$. Particularly if the coal seam is below the water table, cleats and macropores are assumed to be initially fully saturated with water. And, CH₄ is only present as the adsorbed phase on micro-pores.

5.8.1 Uncertainty in OGIP and Probabilistic Methods

The total hydrocarbon found in the subsurface is not established with 100 % certainty. The two significant reasons for this uncertainty, among several others, are the following:

- Rock formation uncertainty- rock formations that accumulate hydrocarbons are beyond human sight, and geophysical errors are expected even when direct measurements are done (through cores).
- Reservoir heterogeneity- spatial variations in thickness, matrix porosity, permeability, pressure, gas content, etc.

Limitations of geophysical surveys, and possible survey errors inherent in all collected data, regardless of the care and competence of data collectors, are factors contributing to the uncertainty in calculations [132]. Such survey errors include sampling, coverage, non-response (when surveys fail to get a response to questions), adjustment (the difference between an adjusted statistic and the population parameter), measurement, and processing errors [132].

When using a mathematical relationship to calculate OGIP, as in Equation 5.4, one substitutes unique values for the parameters (porosity, water saturation, gas density, etc.). Due to uncertainty in estimated parameters, a single OGIP value calculated using a deterministic method rarely, if ever, truly represents the actual amount. This leads to uncertainty in OGIP estimations, and calculated OGIP can either be positively or negatively biased due to such uncertainty [133]. Therefore, particularly if the calculation is sensitive to the values of involved parameters, computations should be repeated to account for variability in parameter values, generating a range of OGIP values with associated probabilities [134]. Stochastic methods are applied to solve such challenges in the probabilistic evaluation of OGIP. One commonly used method in the oil and gas industry to estimate the total

hydrocarbon in place is the Monte Carlo Simulation (MCS). MCS is explained in greater detail in the Methodology chapter.

5.8.2 Recovery Factor and Uncertainty in Reserves

As indicated in Fig 5.4, the estimation of reserves (producibile quantity initially in place) follows the estimation of total hydrocarbon in place. This is usually done by multiplying the total hydrocarbon initially in place by a recovery factor (RF). RF changes according to resource type and the drive mechanism associated with the production of hydrocarbons, and it is heavily dependent on fluid displacement [135]. Table 5.3 shows RF values used in the referenced studies.

Table 5.3. The overall proportion of CBM expected to be recovered from total resources (ordered according to increasing RFs)

CBM Recovery factor, [%]	Reference
20 – 45	[136]
20 – 60	[137]
27.8 – 31.6	[138]
50	[139]
50	[140]
50 – 60	[141]
64.70	[142]

5.9 Coal Bed Methane Production

The coal seams where CBM is produced from, are often unmineable due to their depth, enveloped with an impermeable rock layer at the top (e.g. shale, which prevents fluid migration) and saturated with water (depositional water or groundwater). Therefore, CBM is produced by drilling several wells into the coal seam (Figure 5.6). For production, CBM adsorbed in coal micropores has to desorb and travel through the cleats to the wellbore (see Figure 5.3). Per the Langmuir isotherm in Figure 5.3, release of CBM adsorbed on the coal is governed by pressure. Assuming the coal bed cleats are fully saturated with water, between

initial pressure and critical desorption pressure there is no space available for desorbed free gas. Initial water production (de-watering, see Figure 5.7) is essential as it lowers the pressure in the cleats to initiate the desorption of CH_4 from the coal and opens room for free gas, before CH_4 can be produced [143]. After the production of water, once the critical desorption pressure is reached, adsorbed CBM begins to desorb from the coal matrix. When free gas exceeds a critical saturation, it is coproduced with the water in the cleats, and both fluids flow to the well. In Figure 5.3 high gas content in the cleats is noticeable between critical desorption pressure and abandonment pressure.

Fig 5.7 shows the three production stages of CBM in conjunction with CBM-coproduced water: The Dewatering stage, the Stable stage (primary production), and the Decline stage. Initially, the production of CBM depends heavily on water production, which is known as primary production. Water production is dominant in the early stages of CBM wells, as shown in Figure 5.7, where the volume of water coproduced is greater than that of CBM produced.

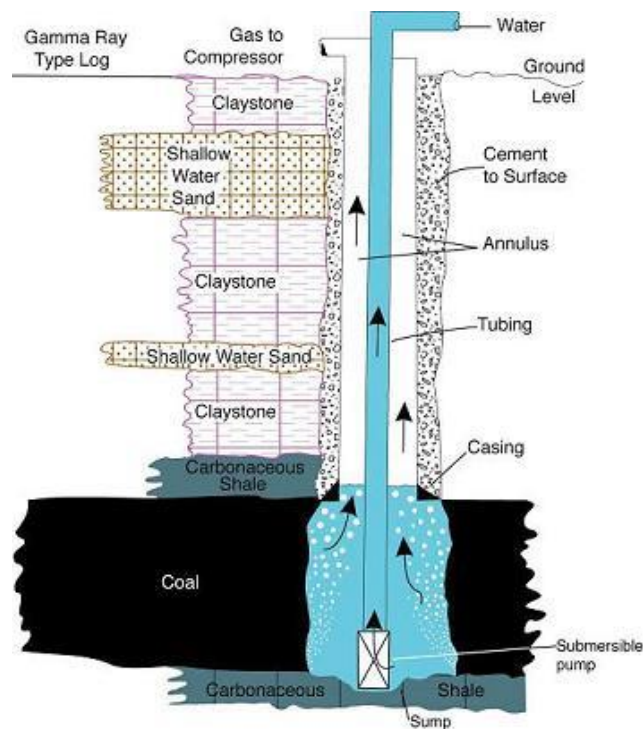


Figure 5.6. Schematic of CBM extraction process [144]

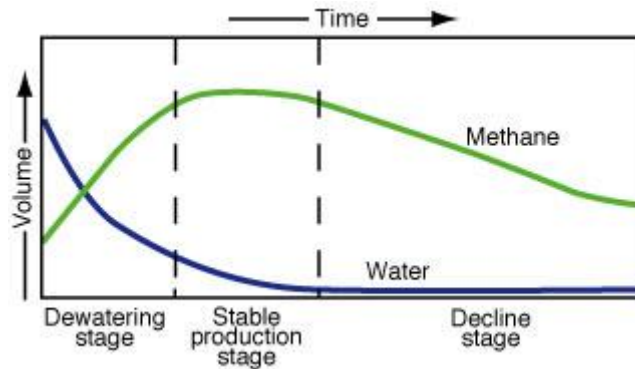


Figure 5.7. Production stages of CBM [145]

5.9.1 Temperature Effect on Adsorption

The adsorption of gas increases with pressure and decreases with temperature. Cai et al. (2019) [146] obtained adsorption curves for bituminous coal (Figure 5.3) showing that the adsorption content decreases as temperature increases. This suggests that with temperature rise, more CH_4 desorbs as free gas. Thermal stimulation of CBM can be achieved by using heat sources (for example, electromagnetically excited nanoparticles) that can be dispersed into the formations during hydraulic fracturing [147]. Nevertheless, Figure 5.3 also shows that a 0.1 MPa pressure decrease causes a much more significant reduction in adsorbed content (from $\sim 9.6 \text{ cm}^3/\text{g}$ to $\sim 7.8 \text{ cm}^3/\text{g}$, 18.8 % content change), compared to a $70 \text{ }^\circ\text{C}$ temperature increase (from $\sim 9.6 \text{ cm}^3/\text{g}$ to $\sim 8.5 \text{ cm}^3/\text{g}$, 11.5 % content change). Increasing the temperature of large volumes of subsurface rock by $70 \text{ }^\circ\text{C}$ would be much more energy-intensive than simply reducing the pressure by producing water (and then desorbed gas) filling the cleats and pores. So, the temperature increase is not a feasible mechanism for CBM production.

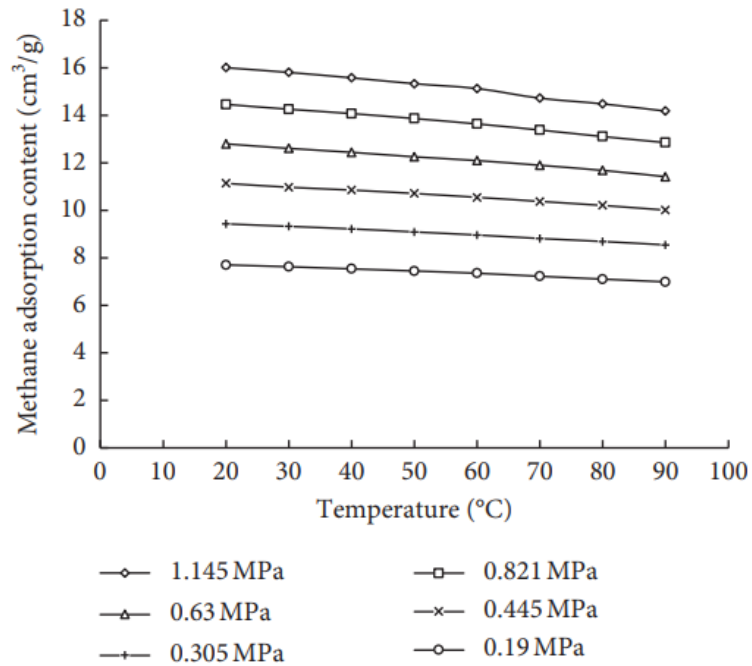


Figure 5.8. Methane adsorption content curves for bituminous coal [146]

5.9.2 Coal Bed Methane Production Analysis

The Langmuir isotherm in Figure 5.3 shows a non-linear relationship between the gas content and the pressure, suggesting that the decline rate is expected to be hyperbolic (see Figure 5.9). Okuszko et al. (2007) [148], in a study to determine the decline performance of CBM wells, divide the production profile into two stages as:

1. Inclining trend- During the initial stages of CBM production, water production reduces reservoir pressure and allows gas to desorb. Consequently, water saturation reduces while gas relative permeability increases, which favors gas deliverability.
2. Declining trend- After the gas rate peaks, the decline starts because of the decreasing reservoir pressure.

CBM flows from the reservoir into the well in three stages: unsteady state flow, steady-state flow, and declining flow (Fig 5.9). After the stable production stage the production of CBM

declines similar to a conventional gas well. Typically, the empirical equation based forecast method (decline curve analysis) developed for conventional wells is performed for the CBM well after the peak production rate.

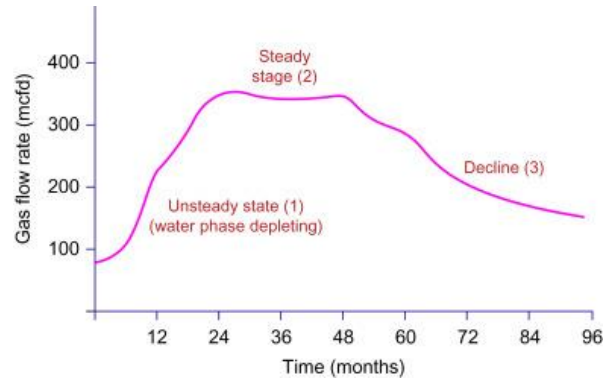


Figure 5.9. Stages in gas production [149]

Okuszko et al. (2007) [148] performed a fifty-year CBM production forecast simulation, and their results show that the decline rate followed a hyperbolic profile after 30 years of production. This suggests that for better establishment of a decline trend, long term history data is required. However, not many CBM wells have produced long enough to have adequate data for matching. Therefore, the decline trend can be matched with b values ranging from 0 to 0.6 [148].

For virgin seams, Thakur (2009) [150] defines the term “specific gas production” as a characteristic of coal seam and is a measure of initial gas production from a 100-ft borehole drilled in the coal bed. When the fracture length is known, specific gas production is used to forecast both vertical and horizontal wells. Table 5.4 provides specific CBM rates for coal seams in the United States.

Table 5.4. Specific gas production for CBM seams in United States [150]

Coal seam	Depth [ft.]	Rank	Specific gas production [MCFD/100 ft.]
Pittsburgh	500 - 1 000	High vol. bituminous	15
Blue Creek	1 400 - 2 000	Low vol. bituminous	9
Sunnyside	1 400 - 2 000	High vol. bituminous	9
Pocahontas	1 400 - 2 000	Low vol. bituminous	8
Pocahontas	800 - 1 200	Medium vol. bituminous	5

5.9.3 Decline Curve Analysis for Gas Wells

Arps (1945) introduced the use of decline curves to estimate recoverable gas and predict conventional well performance. Arps (1945) [151] empirical production rate decline equation is given as:

$$q(t) = \frac{q_i}{(1 + bD_i t)^{1/b}} \quad (5.7)$$

Where:

$q(t)$ – The production at time (t)

q_i – Initial production rate

b – Rate of decline constant

D_i – initial decline rate, [days⁻¹]

t – time

Arps (1956) used the Equation 5.9 to estimate the production decline rate and assigned constants for decline types as:

1. Exponential decline- $b = 0$
2. Hyperbolic decline- $0 < b < 1$
3. Harmonic decline- $b = 1$

Since $b = 0$ for exponential decline Equation 5.9 reduces to:

$$q = q_i e^{-dt} \quad (5.8)$$

The cumulative production is then given by:

$$Np = \int q dt = q_i e^{-dt} = \frac{q_1 - q_2}{D} \quad (5.9)$$

For hyperbolic decline ($0 < b < 1$), the flow rate is given by:

$$q = \frac{q_i}{(1 + bD_i t)^{1/b}} \quad (5.10)$$

The cumulative production is given by:

$$Np = \left(\frac{q_i^b}{(b-1)D_i} \right) \times (q^{(1-b)} - q_i^{(1-b)}) \quad (5.11)$$

Lastly for harmonic ($b = 1$), the flowrate is given by:

$$q = \frac{q_i}{(1 + D_i t)} \quad (5.12)$$

The cumulative production is given by:

$$Np = \frac{q_i}{d_i} \times \ln \left(\frac{q_i}{q} \right) \quad (5.13)$$

Depending on the value of the decline exponent, b , the three forms of decline have different shapes when plotted on a Cartesian plane or semi-log plot.

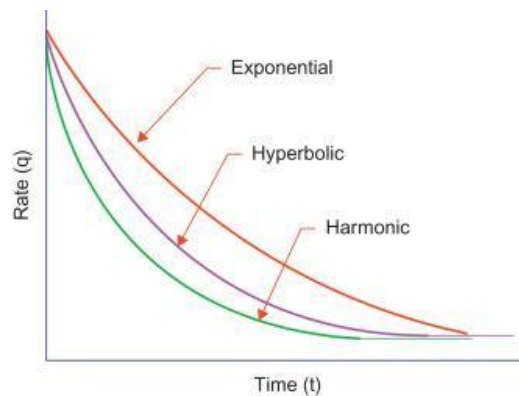


Figure 5.10. Production decline curves used in oil and gas [149]

According to Okuszko (2007) [148] and Shen et al. (2008) [152], the CBM b values range between 0 and 0.6 as shown in Figure 5.11.

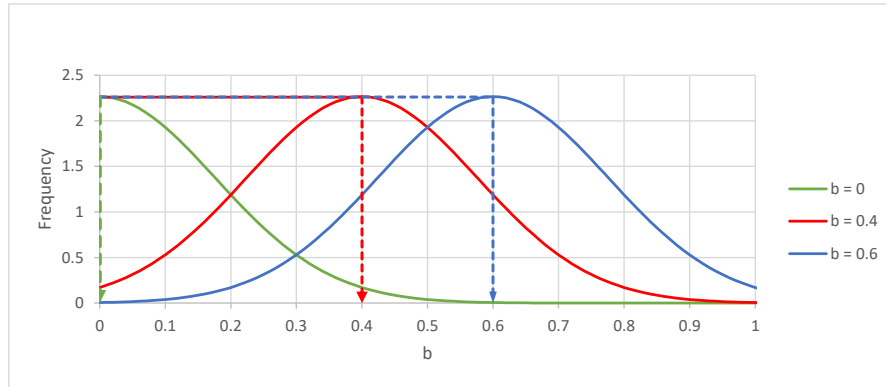


Figure 5.11. Coal bed methane decline curve b value range

5.10 Enhanced CBM Production

The adsorption behavior of CH_4 on coals governs the main processes of CBM accumulation, storage, and recovery. Thus, it is essential to understand the sorption characteristics of coals to enhance CBM recovery. Goraya et al. (2019) [141] elaborate on the significance of the adsorption isotherms (Equation 5.1) that about 50 - 60 % of CBM recovery can be realized under primary depletion, while enhanced methods can boost the recovery up to about 80 %. Such enhancements are possible through selective adsorption, where a displacing gas (e.g., CO_2) is injected to displace adsorbed CH_4 [141]. This process is called enhanced CBM production (ECBM).

5.11 Productivity Enhancement by Hydraulic Fracturing

Unconventional natural gas like CBM is produced from formations with ultra-low matrix permeability down to 0.0001 mD – 0.00001 mD [153]. CBM production require substantially different production schemes, as suggested in Sections 5.10 and 5.11. Hydraulic fracturing (HF) is a crucial stimulation measure for CBM, which produces cracks in coal formations when fracturing fluid is continuously pumped into the wellbore. As high pressure is applied, the formation eventually cracks, creating new passageways for CBM to

flow, consequently improving CBM production. The fundamental purpose of HF is connect the well to the fractures of ultra-low permeability formations and increase or extend the life of a low producing wells.

CHAPTER 6

ZIMBABWE AND THE STUDY AREA

Among the 53 African countries, Zimbabwe emits a global share of 0.03 % of fossil CO₂, yet the country has not been exempted from the catastrophic events cultivated by global warming [154]. Zimbabwe has been affected by droughts, epidemics, floods, and storms, causing damages worth approximately 0.18 % to 0.28 % of the country's Gross Domestic Product (GDP), endangering approximately 60 000 persons per million population [155] [156]. With the aforementioned in mind, every country must aim to develop methods to reduce GHG emissions in the atmosphere. Of the 0.03 % CO₂ global emissions share of Zimbabwe, approximately 30 % is from the thermal PPs [157]. Table 6.1 shows Zimbabwe's GHG emissions by sector.

Table 6.1. GHG emission by sector, Zimbabwe [158]

GHG emission source	Share (%)
Power generation	30
Buildings ¹⁴	29.1
Industrial combustion	18.4
Transport	12.5
Non-combustion ¹⁵	10

Adding to the climate change-related challenges, Zimbabwe suffers great poverty, such that 50 % of the country's population live below the food poverty line [159]. At most 52.7 % of Zimbabwe's population has electricity access, and frequent power outages increase the dependence on fuelwood [160]. Fuelwood delivers 61 % of the total energy required, and

¹⁴ Buildings: The building sector contributes when emissions are from the direct use of fossil fuels (for heating or cooking), and from electricity generation in the building.

¹⁵ Non-combustion: This is when fossil fuels are consumed without being combusted, for example, fuels can be used directly as solvents, lubricants, and other products.

approximately 6 MMts of fuelwood is depleted per annum [161]. Most of the tree cover land is lost due to power poverty driving the unsustainable chopping of trees for fuelwood. Between 2001 and 2020, Zimbabwe lost 15 % of its forest area to fuelwood purposes, emitting 83.2 million tonnes (MMts) of CO₂ [162].

Zimbabwe has an installed capacity of 2 210 MW, producing an average of 1 100 MW, against a projected peak demand of 2 200 MW [163]. The electricity is mainly generated from the Kariba hydropower station (64 %) and Hwange thermal power station (33 %) [163]. In as much as hydroelectric power is taking a larger share in EG, there has been a reduction in reliability due to the increased temperatures from global warming. In 2019, the Kariba dam water level was deficient, so there was a notable decrease in the generated electricity [164].

To solve the power poverty problem, the Zimbabwean government plans to expand and construct new coal-fueled PPs [157]. Since more than 30 % of Zimbabwe's CO₂ emissions are from EG, expanding and increasing coal-fueled PPs appears unsustainable considering UN Sustainable Development Goals (SDGs). At this point, it is essential to point out that the approximate 30 % share of power generation in Table 6.6 is from old, poorly serviced and seldom delivering coal-fueled PPs, such that increasing the capacity would increase the percentage of GHG emission. Nevertheless, Zimbabwe has CBM and solar potential. It receives 1 753 to 2 483 kWh/m² of direct normal irradiance [165] [166]. Zimbabwe can benefit from this abundant irradiance and CBM potential. The use of CBM is more sustainable than coal because coal releases approximately 70 % more GHGs [167].

6.1 Zimbabwe: Country Overview

Zimbabwe, a landlocked country and a member of the Southern African Development Community (SADC), is located in the southern region of Africa (see Figure 6.1), with just above 15 million population. The country is surrounded by Zambia, South Africa, Botswana, and Mozambique.

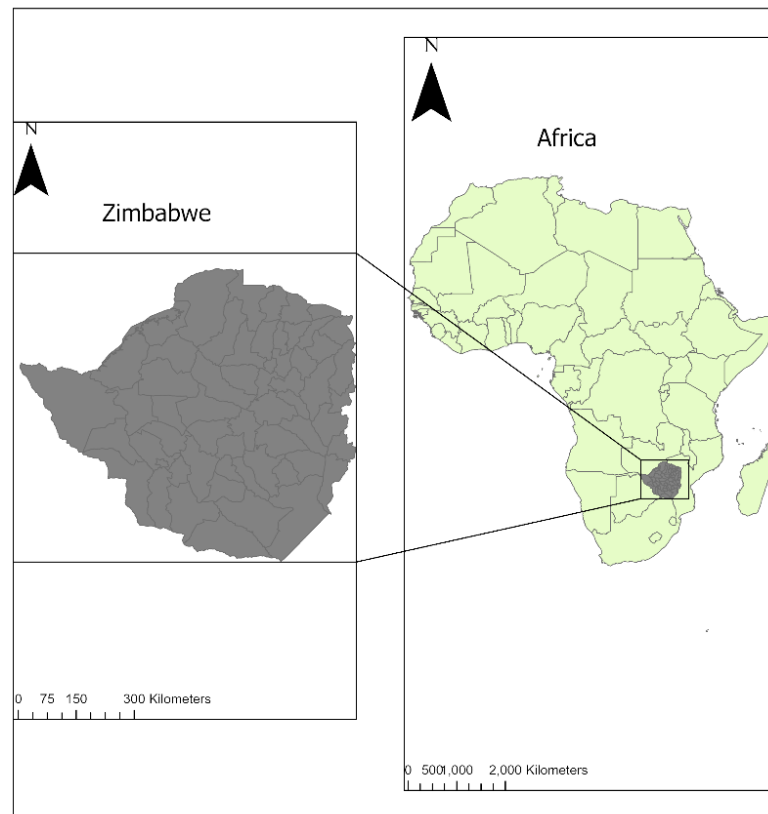


Figure 6.1. The landlocked country of Zimbabwe

Zimbabwe is blessed with minerals and renewable & non-renewable resources. Once the world's third-largest gold producer, with the world's 38th largest coal reserves of 1.1 MMst, with potential CBM exceeding the total of SADC resources, the nation has faced many economic challenges over the past forty years [168]. Irrespective of the abundant resources, just above half the population has access to electricity, accompanied by frequent blackouts. Power poverty has led to the poverty, high mortality rates, and destruction of trees, among other challenges.

Over the past forty years, the country has had inflation fluctuate between -2.4 % and 24 411 %, owing to many political complexities [169]. Zimbabwe, once the breadbasket of Africa, has over half its population living below the food poverty line. These economic challenges should be a result of energy poverty because energy plays a pivotal role in economic growth. After all, many production and consumption activities require power as an input.

6.2 Zimbabwe Energy Sector

The Ministry of Energy and Power Development (MoEPD) supervises the energy sector in Zimbabwe. At the same time, the National Energy Policy (NEP) provides the framework for the supply and utilization of energy [157]. The Energy Regulatory Act [Chapters 13: 23] of 2011 describes that the Zimbabwean Energy Regulatory Authority (ZERA) is responsible for [157],

- The expansion and security of supply for a better economy
- The regulation and licensing of energy from any energy source
- The efficiency of energy and the protection of the environment
- The maintenance and promotion of competition within the industry
- The promotion, identification, and encouragement of employment and development of renewable energy resources
- Advising the minister of energy on all issues in the energy industry

Figure 6.2 shows the regulatory structure of the MoEPD, where ZETDC is the Zimbabwean Electricity Transmission and Distribution Company, ZPC is the Zimbabwean Power Company responsible for the generation of electricity, and IPPs represent all Independent Power Producers.

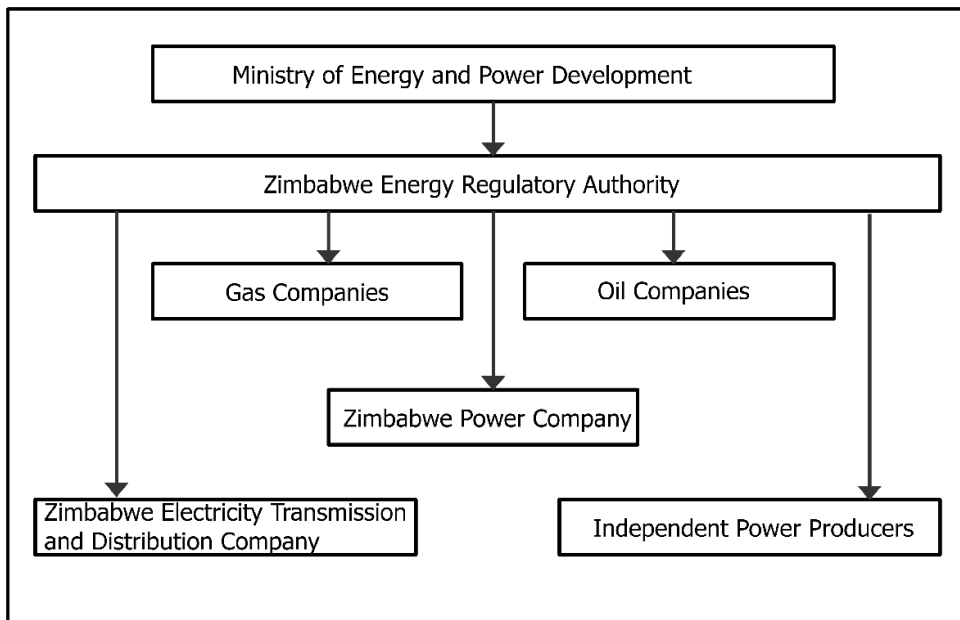


Figure 6.2. The structure of the power sector in Zimbabwe [157]

6.2.1 Current Acts and Policies

Zimbabwe energy sector is regulated by some of the following Acts and Policies in Table 6.2.

Table 6.2. Acts governing Zimbabwe’s energy sector [157]

Act	Primary goal
Electricity Act	Generation, transmission, distribution, and supply of electricity.
Environmental Management Act	Establish the National Environment Council and Environmental Management Agency.
Hydrocarbon Act	Establish the Hydrocarbon Regulatory Authority and its functions
Energy Authority	Establish the Energy Regulatory Authority

Table 6.3. Policies governing Zimbabwe’s energy sector [157]

Policy	Primary goal
National energy policy	Promote optimum supply and utilization of energy in a safe, sustainable manner.
Zimbabwe’s intended Nationally Determined Contribution	To contribute to the global climate target and ensure food security.
Zimbabwe’s National Climate Change Response Strategy	Create provisions targeted toward climate change issues, understand threats, and find ways to reduce them.
Zimbabwe’s Climate Policy	Create a low carbon development economy
2030 Agenda for Sustainable Development	Goal 13 of UN Sustainable Energy for All (SE4ALL) states to take urgent action to combat climate change and its effects.
Vision 2030	Reduce poverty, and raise employment, to transform Zimbabwe into an upper-middle-income economy.

6.2.2 Ongoing Plans of the Zimbabwean Government

With the 13th global goal for sustainable development, the Zimbabwean government integrated climate change energy policies for Renewable Energy (RE) targets based on Nationally Determined Contributions (NDC). The targets were handed over to the United Nations Framework Convention on Climate Change (UNFCCC) [157]. The National Renewable Energy Policy of Zimbabwe (NREP) set targets for the following RE types shown in Table 6.4.

Table 6.4. RE targets by the Zimbabwean energy sector [157]

RE type	MW capacity target by 2030
Large hydro	1 050
Small hydro	150
Grid solar	1 800
Bagasse and other RE	275
Wind	100
Total	3 375
Technology specific targets under NREP	2100

Due to the cost, low efficiencies, and unreliable supply of renewable energy, the Zimbabwean government also has non-renewable energy projects. These projects are summarized in Table 6.5.

Table 6.5. Non-renewable energy targets by the Zimbabwean energy sector [170]

Non-renewable energy project type	Description of project
Hwange expansion project	Expanding the plant by adding 600 MW installed capacity
Hwange life extension project	Extend the life of old units up to 25 years
Bulawayo repowering project	Rekindle the plant to full capacity
Munyati repowering project	Upgrade the inefficient units and increase capacity

6.3 Power Generation in Zimbabwe

Zimbabwe has an installed power capacity of 2 210 MW but generates at most half of the capacity against an estimated peak demand of 2 200 MW [163]. The nation generates electricity from five main power stations governed by ZPC, four coal-fueled and one hydroelectric (Kariba Hydroelectric Plant). The Hwange power station is located in the North-Western region of Zimbabwe, with an installed capacity of 920 MW. The 920 MW capacity comprises 4×120 MW and 2×220 MW units, currently generating 20 to 40 % of Zimbabwe's electricity needs (ZPC, 2022). Situated in Zimbabwe's second-largest city, Bulawayo power station had an installed capacity of 120 MW, which was downsized to 90 MW, and is currently generating only up to 30 MW (ZPC, 2022). In the capital of Zimbabwe is the Harare power plant, which has three stations, namely,

- Station 1- Had a capacity of 21 MW but was decommissioned in 1970
- Station 2- Had an initial capacity of 75 MW, but was downsized to 20 MW
- Station 3- Has a capacity of 60 MW

The total dependable capacity from stations 2 and 3 is 50 MW. The last coal-fueled power plant is located in Munyati, a city between Harare and Bulawayo. The plant initially had a capacity of 120 MW but currently functions with a capacity of 100 MW (ZPC, 2022). The Kariba South hydropower station is Zimbabwe's most significant power-generating PP, with a capacity of 1 050 MW. The plant generates over 60 % of the total generated power in Zimbabwe, as shown by the generation statistics in Table 6.6.

Table 6.6. Zimbabwe's power plants and generation statistics[163]

Station	Capacity [MW]	Generated	Generated
		[MW] 10/5/2022	[MW] 23/12/2022
Kariba	1 050	745	233
Hwange	920	397	430
Munyati	100	18.5	18
Harare	50	12	0
Bulawayo	90	0	0
Total	2 210	1 172.5	681

For decades, the Kariba power station has been the main and sustainable source of electricity. However, owing to climate change, the water levels at Kariba have been decreasing with time. Towards the end of November 2022, Zimbabwe stopped generating electricity at the Kariba South Power Station of the Kariba Dam, birthing power outages lasting 19 hours per day [171]. From 10/5/2022 to 23/12/2022, Zimbabwe's power output almost halved, with an increase in the use of coal.

6.4 Past Studies on Power Generation in Zimbabwe

There have been studies aiming to increase the renewable energy share, reducing CO₂ emission, and increasing electricity accessibility, among others goals, in Zimbabwe. Ziuku et al. (2014) [172] investigated the potential of concentrating solar power in Zimbabwe, and their results indicate CSP potential. However, Ziuku et al. (2014) [172] only considered the technical potential and omitted economic evaluation, which is one of the main challenges RES faces. Kaseke (2014) [173], in a comparative cost assessment of power outages and generation expansion, found the frequency of power outages astonishing and concluded the need for power generation expansion. Kaseke (2014) [173] recommended expanding Zimbabwe's thermal plants (which can solve power poverty but increase CO₂ emission) and the Kariba hydropower plant. Makonese (2016) [174] reviews the potential of Zimbabwe's energy resources and concludes the adoption of RES, including solar and hydropower. Al-Ghussai et al. (2020) [175] compared a standalone wind, PV, and a PV/wind hybrid to maximize RES percentage in Gwanda, Zimbabwe. Their results preferred using the PV/wind hybrid offering economic benefits and the best technical performance. Samu et al. (2019) [176] evaluated the potential of a 10 MW grid-connected wind plant in 28 locations in Zimbabwe. The best results with the least energy generation cost of 77.23 \$/MWh were observed for Ruwa. Maqhuzu et al. (2019) [177] investigated the effect of co-firing municipal solid waste with coal in thermal PPs and concluded the potential reduction of SO_x, CO₂, and CH₄ emissions.

6.5 Zimbabwe's Coal Reserves

Zimbabwe has 553.4E+06 tons of coal reserves, making it rank 38th globally of countries with most coal reserves [178]. The coal in Zimbabwe mainly falls under the upper Karoo group and the lower Karoo group formations in the North-Western areas of the country as shown by Figure 6.3. The areas with coal and associated CBM include Lupane, Hwange, Lubimbi, Lusulu, Sebungu, Lubu, Busi, Sengwa, Gokwe, Nyamandlovu, Bari, Kaonga, Gwaai, Kamativi, and Dete. Alluvial plain coal¹⁶ and freshwater-lake shoreline coal¹⁷ are the two types of sedimentological types of coal identified through intensive lithological studies and correlation of borehole records from coal occurrences in Zimbabwe [180]. Studies after Lepper (2005) [180] show that the Alluvial plain coal deposits dominated the Gokwe and Nyamandlovu areas, while the freshwater-lake shoreline coal deposits were found in Wankie (present day Hwange), Lusulu, Lubu, Busi to Sengwa. The Alluvial plain coal and freshwater-lake shoreline coal areas mentioned above are all within the North-Western areas of Zimbabwe.

¹⁶ Alluvial plain coal: Restricted, high-ash, and thick coals found in narrow and fault-boarded intermountain depressions [179].

¹⁷ Freshwater-lake shoreline coal: Coal deposits accumulated on in-fill surfaces of interdistributary lakes and bays [179].

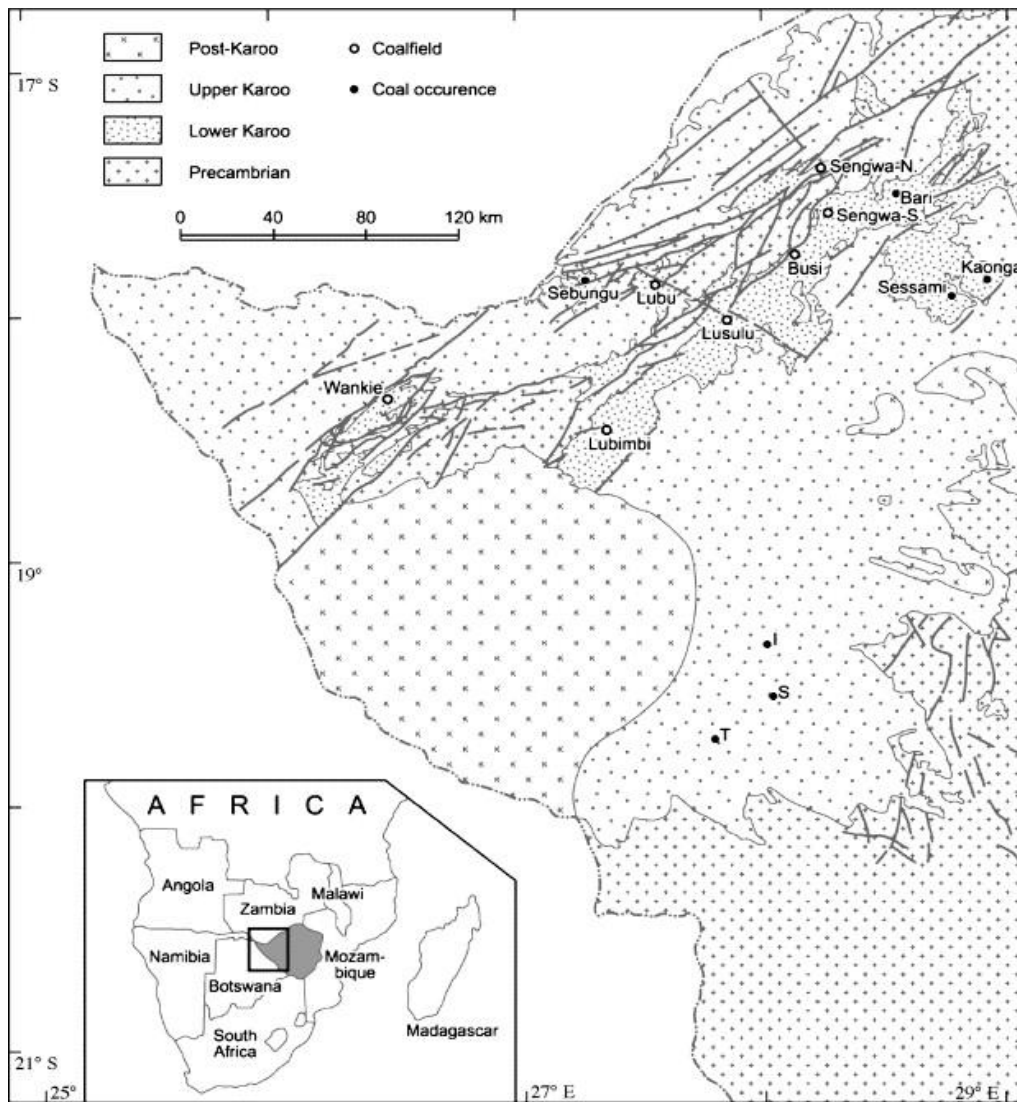


Figure 6.3. Coal-occurrences and location of coalfields in Zimbabwe [180]

The alluvial plain coal in Gokwe and Nyamandlovu is enclosed in fine-grained sediments and is primarily thin and discontinuous. This type of coal has an extremely low economic significance. In contrast, the lake shoreline coal amounts to a high economic relevance, where the coal seams are approximately 17m (50+ ft.) thick and are embedded in carbonaceous mudstones [180]. Table 6.7 shows the representative coal qualities for Zimbabwe.

Table 6.7. Metallurgical coal qualities for Zimbabwe [181]

Coal Properties	Composition
Carbon content, %	64
Moisture content, %	0.8
Ash content, %	9.8
Volatile matter content, %	26.3
Heat value, BTUs/lb.	12 811.7

Using the information from Moyo (2012) [181], the distribution of coal ranks in Zimbabwe ranges from bituminous high volatile C to bituminous medium volatile, with some areas containing low rank sub-bituminous coal.

6.6 Coal Bed Methane Potential in Zimbabwe

The North-Western formations of Zimbabwe contain coal and associated CBM. The basin covers an area of approximately 45 566 km², covering the upper and lower Karoo structures shown by Figure 6.3. The study areas of Zimbabwe are coal and carbonaceous shale formations that contain an average of 2 to 5 m³/tonne of CBM [182]. The study area shown in Figure 6.4 has since been some hope for secure and sustainable EG after the discoveries of potential CBM. The wild cat well tests began before the end of 1991 and turned the potential of CBM in Zimbabwe to “probable” [183]. Shangani Energy Exploration (Pvt. Ltd) drilled what they believe to be Africa’s first CBM production well (OGJ, 1995) near Shangani river, which cuts through Tshotsholo, Lubimbi, and Kamativi. Studies by OJG (1991:1995) [183], Maponga (2014) [184], Mukwakwami (2014) [168], and Sibanda (2018) [185] confirm the existence of CBM, but there have not been any publicly available studies on the total gas in place, and the techno-economic studies on the gas. For CBM exploration to commence at a large scale, some degree of confidence must be met, typically by extensive evaluations of reservoir conditions, production forecasts, and other economic viabilities.

6.7 Zimbabwe: Study Area

The study area falls under the Karoo Supergroup¹⁸ formation in the southern part of Africa, which is of both scientific and economic importance. The Karoo-aged basin provides a crucial fossil understanding of Permo-Triassic evolution, providing information on potential fossil fuels [186]. The Karoo Supergroup hosts coal reserves, accounting for approximately 10 % of the world's total reserves [187]. The Medium- to low-volatile bituminous to semi-anthracite coal deposits are superimposed by sandstones, mudstones, and the Pebbly Arkose formations [188]. Figure 6.4 and Figure 6.5 show the study area, and the distribution of the Karoo Supergroup in South-Central Africa, respectively.

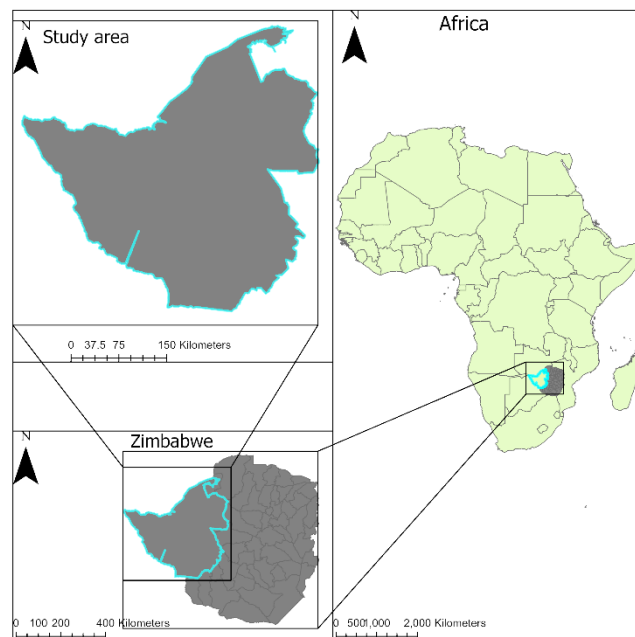


Figure 6.4. Geological location of study area

¹⁸ Supergroup: A set of more than one associated formation sharing certain lithological characteristics

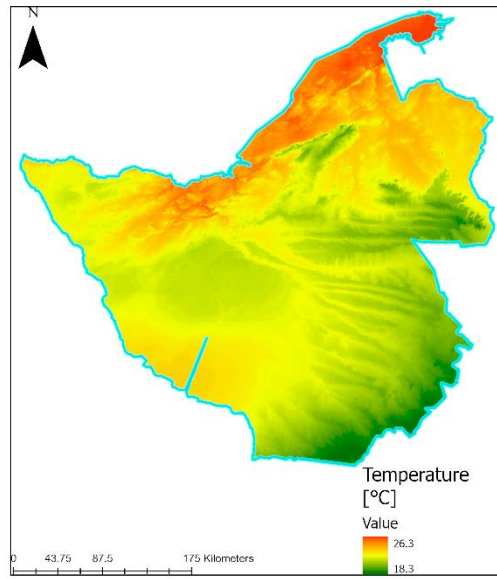


Figure 6.6. Yearly average temperature map of the study area (adopted from [166])

CHAPTER 7

PROBLEM STATEMENT

The past studies on power generation in Zimbabwe, (mentioned in Section 6.4) can be grouped into renewable and non-renewable energy studies. All these studies considered the use of either the renewables or the non-renewables. Some challenges of using fossil fuels to generate electricity include conventional oil and gas depletion, exacerbated pollution, and accelerated climate change. The disadvantages of using only RES include unreliability, low efficiency, high capital cost, and low dispatchability. Generally, the past studies mentioned in Section 6.4 have been conducted to reduce or eliminate power poverty in Zimbabwe, though following areas were left unaddressed or incomplete:

- CBM potential- to the best of this author's knowledge, there haven't been any extensive studies on the potential of CBM in Zimbabwe.
- Techno-economic and environmental analysis of generating electricity from CBM.
- Non-renewable energy systems- Most studies focused on coal fueled old, to-be-serviced plants and newly proposed thermal PPs. Though expanding old thermal PPs and constructing new ones can solve power outage and accessibility issues, carbon sequestration should be implemented to capture and store CO₂ to address the climate change issue.
- Renewable energy systems- many studies have been conducted to improve or increase the RE share in Zimbabwe, but not many have addressed the challenge of reliability and dispatchability. For example, Zimbabwe has an annual average of 8.3 sun hours per day for solar systems. This means that there will not be electricity generation for 15.7 hours, considering there is no TES. The same can be said for wind energy without energy storage facilities. Feasibility studies by Al-Ghussain et al. (2018) and Samu et al. (2019) indicate the insignificant improvement of including TES and that hybridization of RES does not increase generation capacity but offers a better energy mix. If renewables are to be adopted, work must be done to improve reliability and dispatchability.
- Most studies have focused on PV, leaving out the CSP potential.

- Hybrid renewable and non-renewable energy studies for Zimbabwe.

Therefore, to address the aforementioned issues, in this study we focus on the assessment of CBM-Solar hybrid power plants to address the issue of power poverty, and climate change (SDG 7 and SDG 13).

Listed below are some of the problems that current study seeks to assess:

- How feasible is an ISCC-PP using CBM-CSP hybrid?
- Addition of solar will eliminate the need for how many additional CBM wells? Or how much additional MWh will be generated?
- What is the best possible site for ISCC PP?
- What are the requirements from CBM and CSP side?

Major issues to be addressed for the success of hybrid CBM-ISCC PP are:

- Estimation of CBM reserves.
- Selection of site which meets both CBM and CSP criteria.
- Techno-economic and environmental assessment of the hybrid.
- Fuel consumption, production rate & number of CBM wells.

CHAPTER 8

METHODOLOGY

The assessment of a CBM-based solar-gas system for this study is grouped into 4 major parts, namely:

1. Suitable site selection which meets CBM and CSP criteria simultaneously.
2. The estimation of CBM in-place and production modeling.
3. The feasibility of concentrating solar power for an ISCC hybrid.
4. Techno-economic and environmental analysis of the proposed system.

We begin with the estimation of OGIP since the proposed system (ISCC) will have most of the system fueled by natural gas (CBM in this case) and a considerable percentage by solar power. After estimating OGIP for the whole region, the most suitable location for gas exploration is determined. The intersection of CSP-suitable sites and CBM-preferred sites will be a subset of CBM-preferred sites and the most feasible location for concentrating solar power. The chosen study area (Figure 6.4) is analyzed separately for CBM and CSP potential, as shown in Figure 8.1 which outlines the methodology framework of the current study.

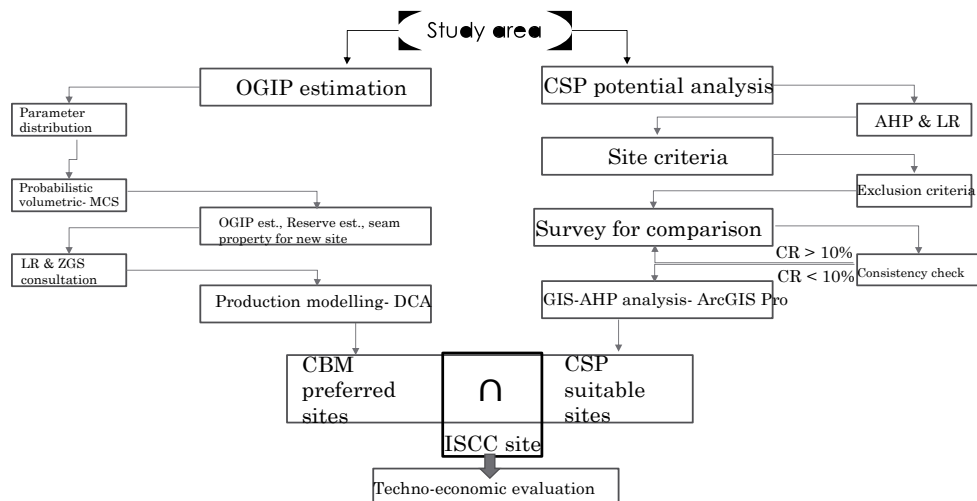


Figure 8.1. Methodology for choosing ISCC site

8.1 Assessment of Coal Bed Methane Generated Power

The investigation of CBM economic potential from the study area for EG is adopted from the study done by Sarhosis et al. (2016) [45] who investigated the potential of producing CBM from virgin coal seams for EG in South Wales, UK. Authors proposed to fuel a CCGT PP using CBM and found that the CBM-CCGT process offered an economical option for EG.

After verifying its applicability, the same PP computer model(s) described in Sections 8.5 and 8.6 are utilized to assess the feasibility of standalone CCGT PP as well.

8.1.1 Site Selection for Coal Bed Methane

Site selection criteria for CBM (given in Table 8.1) were developed based on previous successful field applications. The criteria highlight the advantages and disadvantages of the parameters, their economic significance, environmental impact, and their importance in site selection for CBM exploration.

Table 8.1. Site selection criteria

Selection criteria	Value	Reference
Resource Area	>1 km ²	[190]
Gas content	>7 m ³ /tonne	[191] [192]
Depth of coal seams	400 m < D < 1 000 m	[193]
Coal seam thickness	>5 m	[191] [192]
CBM Resource Density (RD)	>1 million m ³ /ha	[45]
Coal rank	Above Bituminous	[194]
Permeability	>5 mD	[195]
Reservoir pressure	>0.50 psi/ft.	[195]

8.1.2 Resource Density

Resource density is the ratio of the resource estimate to the surface area, and is given by [165]:

$$RD = \frac{G_P}{A} \quad (8.1)$$

Where,

RD = Resource density estimation, [Bm³/km²].

G_P = P10, P50, or P90 resource estimate, [Bm³].

A = P10, P50, or P90 surface area, [km²].

Resource densities are used to compare potential hydrocarbon sites with producing sites to have an idea of the feasibility of producing from potential sites.

8.2 Original Gas in Place Estimation

There are two fundamental methods for the estimation of total hydrocarbon in place, namely:

1. The deterministic method uses mathematical relationships, where one substitutes unique values for parameters (porosity, water saturation, gas density, etc.) to obtain a single OGIP value. The calculated OGIP value rarely, if ever, truly represents the actual value.
2. The probabilistic methods are adopted to account uncertainties in parameters, where simulations (calculations of various combinations) are performed to obtain multiple results.

To account for uncertainty in OGIP of the study area, probabilistic method is performed using the Monte Carlo Simulation (MCS) based on equation 5.5.

8.2.1 Monte Carlo Simulation

The Monte Carlo Simulation (MCS) is a stochastic method commonly used by engineers in the oil and gas industry to estimate the original HC in-place and/or reserves [196] and to account for errors and uncertainties in different calculations [133]. In MCS, probable distributions of parameters (such as normal distribution, triangular distribution, etc.) are used to generate several possible results. The method's success heavily depends on the selection and careful analysis of model parameters [134]. Using the MCS produces a range of results with the ability to report likelihood of values as P10, P50, and P90. Engineers or organizations can utilize these results for major decisions.

According to Zahner (1997) [197], the calculation of OGIP for CBM has the following forms of uncertainty:

- Initial adsorbed gas content (G_c) - Measurements from core samples often give inaccurate results.
- Net thickness (h_{net}) - There are different opinions in the industry on what density cut-off value should be used to determine the pay zone thickness.

The MCS for CBM OGIP estimation follows the procedure presented in Figure 8.2:

- 1) The process begins with gathering data representative of the North-Western region of Zimbabwe. Required data is obtained from various sources, as listed in Table 8.2.
- 2) Field data establishes parameter value range and distribution type. Available data is analyzed using histograms to determine distribution type (for example, Weibull, triangular, gamma, etc.). The mean, mode, maximum, and minimum values determine the distribution type, as well as distribution profile.
- 3) Parameter distributions are randomly sampled to be used in the calculations.
- 4) Objective function (OGIP) calculations are repeated for each set of randomly sampled parameters.
- 5) The cumulative density function (CDF) of the calculated results is plotted and analyzed.
- 6) The MCS is repeated with different sample counts (e.g., $10^2, 10^3, 10^4$ samples) until there is no significant change in the CDF plot, to establish that results are stochastically repeatable.

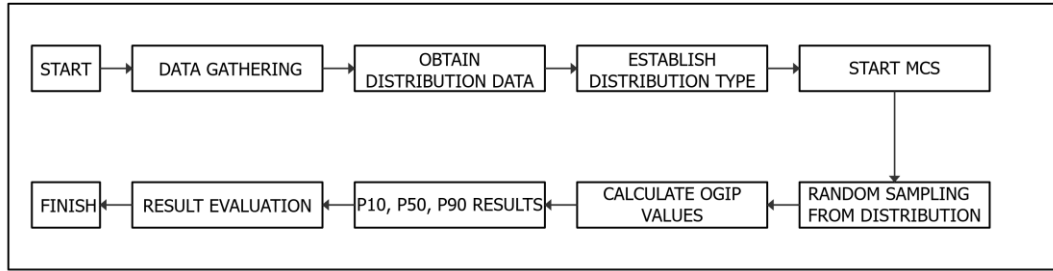


Figure 8.2. Flow chart of MCS methodology used in this study

In essence, because G_c values are available in literature, OGIP is calculated using Equation 5.5. But Equation 5.5 is reduced to Equation 8.1 after data analysis, recognizing that the cleats are filled with water. Such that, the total OGIP (G_t) is given by:

$$G_t = 1\,359 \times A \times h \times \rho_c \times G_c \quad (8.2)$$

And the reserve is estimated by the following formula:

$$Reserves = OGIP \times RF \quad (8.3)$$

8.2.2 Field Data and Analysis

Per Equation 8.2, required parameters for OGIP analysis are now the target area A [Acres], coal seam thickness h [ft], coal density ρ_c [g/cm³], and gas content G_c [SCF/tonne]. Table 8.2 shows the min-max values of parameters representing the region of Karoo basin within Zimbabwe, from resources that were available during the course of this study.

Table 8.2. Karoo basin CBM data for the study area of Zimbabwe

Parameter	Min	Max	Reference
Area [Acre]	1.12E+07	1.26E+07	ARCGIS Pro
Thickness [ft.]	5.58	66.73	[198] [180]
Density [g/cm ³]	1.35	1.75	[165]
Gas content [SCF/tonne]	5.58	66.73	[199] [200]
Seam Avg. Depth [ft.]	328	3 280	[198] [180]

The North-Western region of Zimbabwe is a coal-rich region, identified by alluvial plain coal and freshwater-lake shoreline coal [180]. Alluvial plains and freshwater-lake shoreline coals are either in water or between water bodies. This is supported by the information in Table 8.3. Table 8.3 provides details on the hydrogeology of the North-Western region of Zimbabwe which has high potential for groundwater, suggesting that the coal seams are under the water table. Therefore, we expect no free gas initially in the cleats, and $S_{wi}=1$.

Table 8.3. Hydrogeology of the study area of Zimbabwe

Location	Aquifer type [201]	Water table depth [ft] [201]	Seam depth [ft]
Area between Hwange-Western districts and Lupane-Southeastern districts	Unconsolidated, Save Alluvial Aquifer, Umzingwane Alluvial aquifer, Grootvlei/Limpopo	16.4 - 131.2	114.8 - 3280.8
Hwange-Lubumbi and Sengwa North-Lusulu districts	Cretaceous Sedimentary intergranular/fracture	32.8 - 49.2	65.6 - 1312.3

8.2.2.1 Area

The area is estimated using ArcGIS Pro, a mapping software for creating and working with spatial data. First, we establish the target area (North-Western region of Zimbabwe) as shown in Figure 8.3. Area values are found as Max: 51 000 km² and Min: 45 566 km². The difference in the values for the area is because we considered the gross (Figure 8.3) and net (land potentially available for exploration) areas. Figure 8.3 shows the synopsis of Min. and Max. areas taken for this study. The data distribution for the target area is shown in Table 8.4.

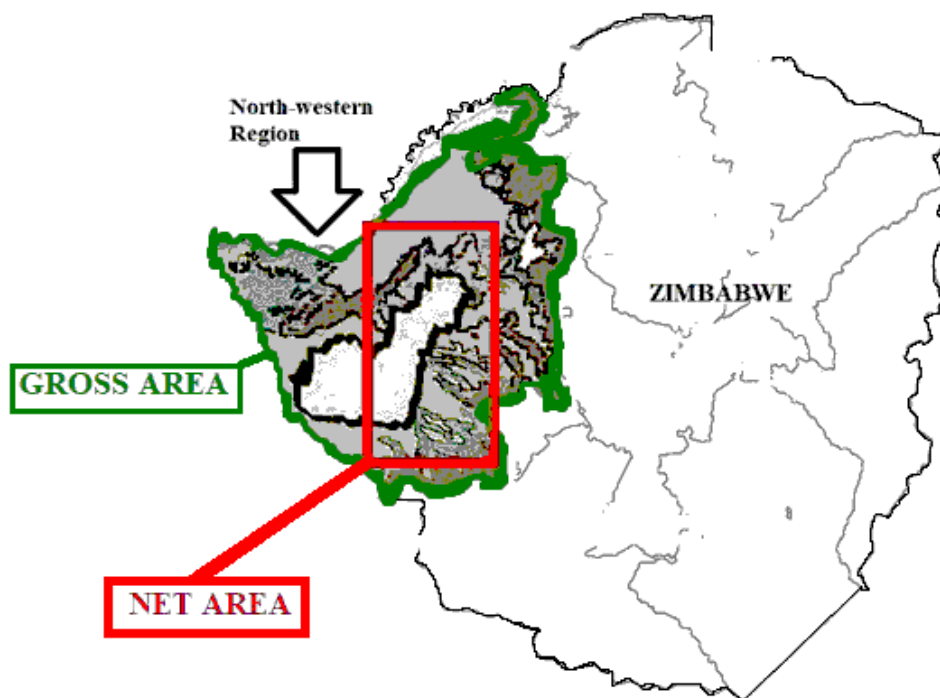


Figure 8.3. Target area

Table 8.4. Histogram of target area

Area [Acres] (ArcGIS Pro)	
Descriptive statistics	Numerical value
Min	1.12E+07
Max	1.26E+07
Mode	1.19E+07
Median	1.19E+07
Mean	1.19E+07
SD	8.51E+05
Data count	243

Area [Acre]	Frequency
1.13E+07	30
1.135E+07	30
1.14E+07	18
1.145E+07	15
1.15E+07	30
1.155E+07	25
1.16E+07	25
1.165E+07	20
1.17E+07	25
1.175E+07	20
1.18E+07	5

8.2.2.2 Coal Density

Since the Karoo basin stretches across Botswana and Zimbabwe, as shown in Figure 6.5, current study adopted the values calculated for Botswana by Kubu Energy [202] due to the scarcity of coal density data from Zimbabwe. The data distribution for coal density is shown in Table 8.5.

Table 8.5. Histogram of coal density data [202]

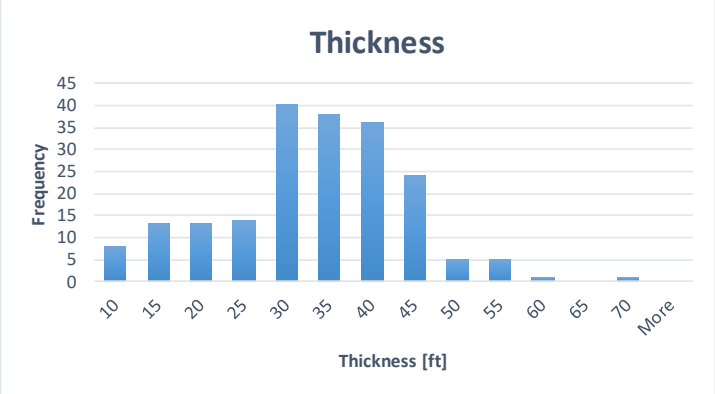
Coal density [g/cm ³]		Histogram																						
Descriptive statistics	Numerical value																							
Min	1.35	<p>The histogram displays the frequency distribution of coal density data. The x-axis represents density in g/cm³, with bins at 1.35, 1.4, 1.45, 1.5, 1.55, 1.6, 1.65, 1.7, and 1.75. The y-axis represents frequency, ranging from 0 to 45. The distribution is roughly bell-shaped, peaking at 1.65 g/cm³ with a frequency of approximately 40.</p> <table border="1"> <caption>Histogram Data</caption> <thead> <tr> <th>Density Bin [g/cm³]</th> <th>Frequency</th> </tr> </thead> <tbody> <tr><td>1.35</td><td>0</td></tr> <tr><td>1.4</td><td>25</td></tr> <tr><td>1.45</td><td>30</td></tr> <tr><td>1.5</td><td>28</td></tr> <tr><td>1.55</td><td>25</td></tr> <tr><td>1.6</td><td>30</td></tr> <tr><td>1.65</td><td>40</td></tr> <tr><td>1.7</td><td>28</td></tr> <tr><td>1.75</td><td>25</td></tr> <tr><td>More</td><td>0</td></tr> </tbody> </table>	Density Bin [g/cm³]	Frequency	1.35	0	1.4	25	1.45	30	1.5	28	1.55	25	1.6	30	1.65	40	1.7	28	1.75	25	More	0
Density Bin [g/cm³]	Frequency																							
1.35	0																							
1.4	25																							
1.45	30																							
1.5	28																							
1.55	25																							
1.6	30																							
1.65	40																							
1.7	28																							
1.75	25																							
More	0																							
Max	1.75																							
Mode	1.65																							
Median	1.58																							
Mean	1.57																							
SD	0.16																							
Data count	232																							

8.2.2.3 Thickness

Thickness data is gathered from Pollok (1984) [198], Oesterlen & Lepper (2005) [180], and Padcoal (Pvt) Ltd (2011) [203]. Most of the data representing the target North-Western area of Zimbabwe is from Ntuba, Lubu, Sengwa South, Lusulu, Hwange, Lupane, and Gokwe districts. The data from these locations represent the whole area considered in this study, and the distribution is shown in Table 8.6.

Table 8.6. Thickness data [180] [198] [203]

Histogram of thickness data [ft.]	
Descriptive statistics	Numerical value
Min	5.58
Max	66.73
Mode	38.25
Median	31.33
Mean	30.86
SD	11.0
Data count	200



8.2.2.4 Gas Content

The gas content values were read from the depth vs. gas content plot in Barker (2006) [199] courtesy of Shangani Energy Exploration, as shown in Figure 8.4. The data distribution for gas content is shown in Table 8.7.

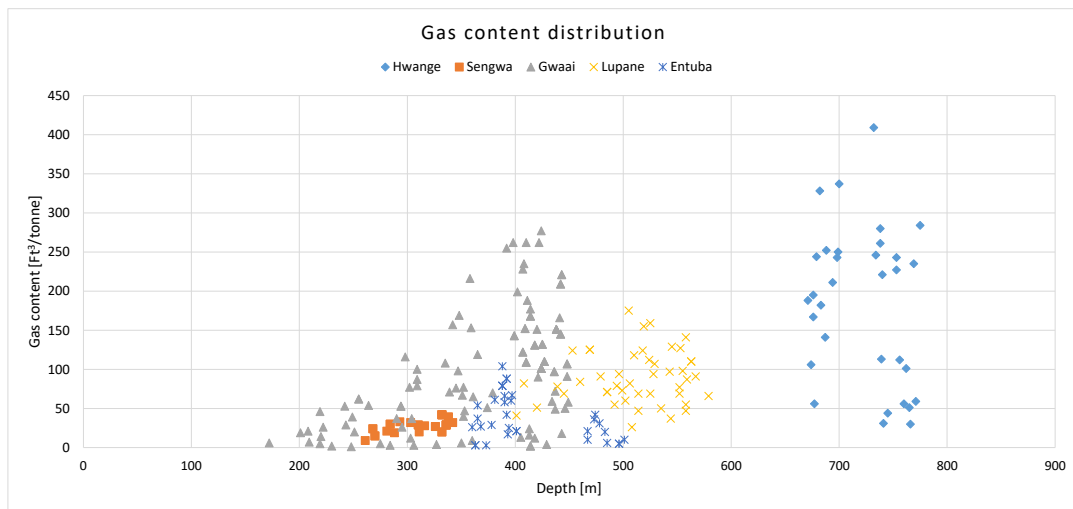
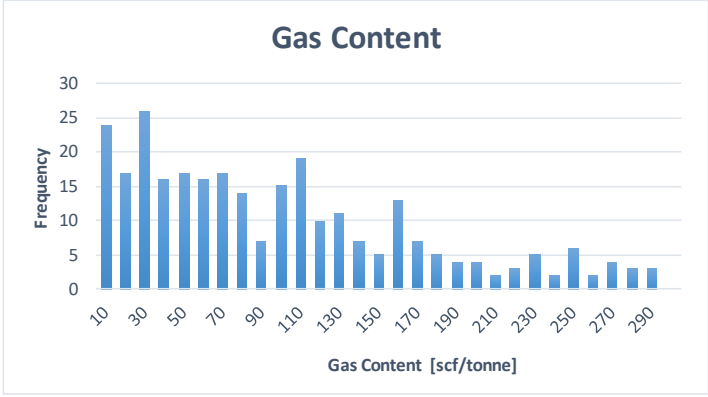


Figure 8.4. Gas content values from desorption testing (Adopted from [199])

Table 8.7. Histogram of gas content data [199]

Gas content [SCF/tonne]		
Descriptive statistics	Numerical value	Histogram
Min	1.0	 <p>The histogram, titled 'Gas Content', displays the frequency distribution of gas content data. The x-axis represents Gas Content in SCF/tonne, ranging from 10 to 290 with major ticks every 20 units. The y-axis represents Frequency, ranging from 0 to 30 with major ticks every 5 units. The distribution is unimodal and slightly right-skewed, with a peak frequency of approximately 26 occurring between 30 and 40 SCF/tonne. The data count is 284.</p>
Max	290.0	
Mode	29.0	
Median	77.0	
Mean	93.98	
SD	72.85	
Data count	284	

8.2.3 Parameter Distribution

Histograms representing the parameter distributions are obtained, as shown in Tables 8.3 to 8.6. The raw gas content, density, and thickness data follow a triangular distribution with visible Min, Max and mode values. Therefore, triangular distribution is used for gas content, density, and thickness. The uniform distribution is chosen for the area since we only determined Maximum and Minimum values. Table 8.8 below summarizes the parameter distribution of the primary data.

After the evaluation of the OGIP, the CBM most preferred site is evaluated using the criteria given in Table 8.1.

Table 8.8. Summary of parameter distributions

Parameter	Descriptive statistics	Numerical value
Area [Acre]	Min	1.12E+07
	Max	1.26E+07
TYPE OF DISTRIBUTION: Uniform	Mode	
	Median	1.19E+07
	Mean	1.19E+07
	SD	8.51E+05
	Data count	243
Thickness [m]	Min	5.58
	Max	66.73
TYPE OF DISTRIBUTION: Triangular	Mode	38.25
	Median	31.33
	Mean	30.86
	SD	11.0
	Data count	200
Coal density [g/cm ³]	Min	1.35
	Max	1.75
TYPE OF DISTRIBUTION: Triangular	Mode	
	Median	1.58
	Mean	1.57
	SD	0.16
	Data count	232
Gas content [SCF/tonne]	Min	1.0
	Max	290.0
TYPE OF DISTRIBUTION: Triangular	Mode	29.0
	Median	77.0
	Mean	93.98
	SD	72.85
	Data count	284

8.3 Site Selection for Concentrated Solar Power

GIS tools are combined with the multi-criteria decision-making method (MCDM) to determine the potential site for CSP as shown in Figure 8.5.

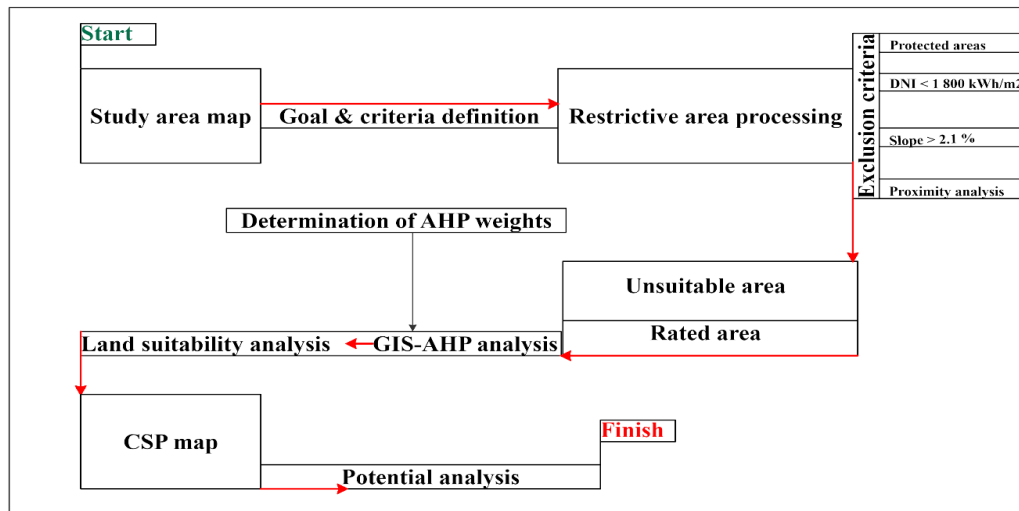


Figure 8.5. Methodology for Concentrated Solar Power potential analysis

The methodology presented in Figure 8.5 contains three main processes:

1. Initially, the goal and criteria are defined to remove unsuitable layers (regions) from the study area map, by applying spatial tools in ArcGIS Pro. The unsuitable region represents all the areas that can never be suitable for CSP.
2. Secondly, the GIS-AHP analysis (Section 3.4.1), and the land suitability analysis are performed in ArcGIS using the spatial tools.
3. Lastly, perform calculations to determine the proposed plant's theoretical, technical, and economical performance.

The site for the ISCC power plant should be suitable for both CBM and DNI technologies, i.e. should:

- 1) be close to CBM field, to reduce hydraulic losses and compressor requirements in the transportation pipelines, and
- 2) receive adequate sun light.

8.3.1 Criteria Definition

Because standalone CSP is one of the most expensive power-generating technologies, misjudgments can lead to tremendous economic penalties. Based on the references that

studied CSP feasibility (Table 3.2), *climate factors (e.g. irradiance and temperature), orography, location, and water availability* assures maximum plant performance, territorial efficiency, and maximum achievable productivity. Consequently, climate factors, orography, and location are used in the MCDM-AHP, to exclude unsuitable areas.

8.3.2 Data Collection

Relevant data search and standardization are carried out, and the data is collected as spatial data (from references in Table 8.9 and is normalized in ArcGIS Pro software.

Table 8.9. Data sources for Concentrated Solar Power site selection

Criterion	Data source
Solar irradiance	SolarGIS [166]
Orography	USGS, United States Geological Survey [204]
Power grid	Worldbank [205]
Roads	MapCruzin [206]
Water availability	Africa Groundwater Atlas [207]

8.3.3 Solar Irradiance

The performance of CSP plants is significantly affected by DNI to generate electricity. For financial accounts, regions having DNI values less than 1 800 kWh/m²/yr. must be excluded in the first stage. Areas with the greatest DNI would be considered the most appropriate after using the AHP method, the higher the irradiance, the higher the theoretical potential. Table 8.10 shows the solar resource and site selection ranges of cumulative annual DNI, typically preferred for CSP application.

Table 8.10. Solar resource and site selection [208]

Not recommended	$\text{DNI} \leq 1\,600 \text{ kWh/m}^2/\text{yr.}$
Recommended	$1\,600 \text{ kWh/m}^2/\text{yr.} \leq \text{DNI} \leq 2\,000 \text{ kWh/m}^2/\text{yr.}$
Better performance	$\text{DNI} \geq 2\,000 \text{ kWh/m}^2/\text{yr.}$

8.3.4 Orography

Orography is a study of topographic relief, concentrated on the detailed and precise description of mountains and elevated terrains like hills. The adoption of CSP PPs (especially the employment of PTC) requires flat lands [82]. The inclination of the area determines suitability of the site for CSP [79]. According to Tazi et al. (2018) [209], the suitable slope should be less than 2.1 %, with excellent slopes ranging between 0.5 % to 1 %.

8.3.5 Location

The most suitable location for any PP is near the road network and electricity grid. This is because the location has to be close to residential areas for easy transportation of workers and close to the grid, making it cheaper to have a plant-grid connection. A PP close to a power grid, roads, and railways offers low capital and maintenance costs.

8.3.6 Water resources

Since the proposed system is an ISCC PP, water plays a crucial role in the bottoming cycle. Water can be used as a cooling agent for cleaning the concentrators, especially in windy areas. Qoaidar & Liqreina (2015) [210] highlight high water consumption in CSP systems and that 90 % of the water is used for wet cooling while 10 % is used for cleaning. Therefore, there is need for a water body close to the PP.

8.3.7 Restrictive Area Processing

After defining the criteria, the AHP method is applied to couple each criterion to its appropriate weight. The weights are then used in ArcGIS to determine the most appropriate location for concentrating solar power.

When performing the MCDM-AHP in ArcGIS, the initial step is to exclude all unsuitable sites for CSP based on expert logic and legal directives. According to Sun et al. (2021) [79]; Haddad et al. (2021) [81]; Ghasemi et al. (2019) [78]; Merrouni et al. (2018) [82]; and Alqaderi et al. (2018) [80], the areas that must be excluded are summarized in Table 8.11.

Table 8.11. Exclusion criteria and averaged values adopted for current study

Excluded layers		Buffer limitation	Remarks
Protected areas	World heritage sites	300 m – 500 m	No installation within 300 m from the site
	National parks	300 m – 500 m	No installation within 300 m from the site
	Biosphere ¹⁹	300 m – 500 m	No installation within 300 m from the site
	Conservation areas	300 m – 500 m	No installation within 300 m from the site
Climate	DNI	< 1 800 kWh/m ²	Zones with DNI of less than 1 800 kWh/m ² must be excluded
Orography	Slope	> 2.1 %	Zones with slopes greater than 2.1 % must be excluded
Proximity	Power lines	200 km	Zones located more than 200 km from the power grid are not included
	Water supply	30 km	Areas 30 km away from the site are excluded

The criteria in Table 8.11 is compiled to exclude all areas that might result in poor plant performance, destruction of essential sites, disturbance of the biosphere and ecosystem, high initial capital cost, increased maintenance cost, and the disturbance of ongoing activities. After excluding these locations, the next step is to carry out the GIS-AHP analysis and the

¹⁹ Biosphere: Anywhere on earth where life exists.

land suitability analysis in ArcGIS Pro. The final step in ArcGIS Pro (using Equation 3.9) is to develop a map representing all potential sites for concentrating solar power.

8.4 Assessment of Concentrated Solar Power

Solar power generation potential is generally classified as the theoretical, technical, and economic potential [78], as described in detail in Section 3.4. The power generation potential is calculated using Equation 3.4 [79]:

$$TPSE = DNI \times EF \times A \times PR \quad (3.4)$$

After verifying its applicability, the same PP computer model(s) described in Sections 8.5 and 8.6 is utilized to assess the feasibility of standalone CSP as well.

8.5 Evaluation of the ISCC PP

The site for the proposed ISCC PP is the intersection of the potential CBM sites (established using Table 8.1) and potential CSP sites (Figure 8.5). In order to evaluate the feasibility of adopting the solar-gas system, a comparison is made among different technologies. First, the ISCC is compared with the standalone CSP PP and standalone CCGT PP. Then, ISCC is compared with Zimbabwe's current electricity-generating technologies.

A techno-economic and environmental analysis is carried out for three different technologies for the potential ISCC PP site, namely:

1. CSP PP, modeled using NREL's System Advisor Model (SAM) (Figure 8.6).
2. CCGT PP (CCGT_ISCC²⁰), modeled using EBSILON (Figs. 8.7 and 8.8).
3. ISCC PP, modeled using EBSILON (Figure 8.7).

EBSILON Professional and SAM are power/electrical system simulation software from different vendors. They both use algorithms based on physical equations, polynomials, and

²⁰ CCGT_ISCC: It indicates CCGT model is derived from hybrid model by blocking CSP component.

characteristic curves to model various machinery, electrical components, and whole systems, including power plants. Both EBSILON and SAM allow changing any practical parameter of the plant one can think of. However, original template files already model real life functioning plants. Thus, in order to base the analysis on real life plants only following parameters were changed, plant capacity (which automatically changes other parameters like gas intake rates, heat rates, ST capacity, plant efficiency, COE, power output, etc.) and the number of solar collectors (which automatically changes other plant parameters like ST capacity, plant efficiency, capacity factor, COE, etc.)

The System Advisor Model (SAM) is a software that estimates the technical and financial aspects of power plant facilities. SAM models several RES including PV systems, battery storage facilities, CSP systems, wind power farms, biomass plants, etc. Figure 8.6 shows the steps to modelling renewable energy using SAM.

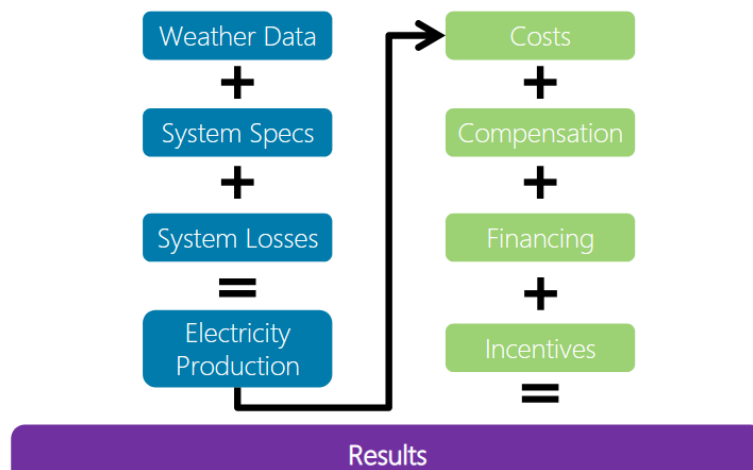


Figure 8.6. Steps to modelling RES in SAM [211]

EBSILON Professional is a system planning and simulation software. It allows user to simulate any PP thermodynamic cycle process, calculate performance and efficiency of a PP under various operating conditions. The PP model types readily available in the software include hard coal thermal PP, CSP, ISCC, cooling cycles, CO₂ capture systems, etc.

The performances of the 3 PP technologies are compared using following parameters:

1. Output power- Calculations performed using Equations 2.8 and 3.9
2. Fuel consumption- EBSILON (simulated)

3. Plant efficiency- Equation 2.6
4. Cost of electricity- Equation 2.5
 - a. For CSP PP calculations, SAM is used to estimate the cost of electricity.
 - b. For CCGT PP calculations, the fuel cost is determined by the heat rate of the GT modelled in EBSILON, while other LCOE parameters are taken from specific values given in Table 8.12. Figure 8.8 shows the schematic of EBSILON's CCGT Siemens SGT5-4000F PP.

Since the ISCC model template might be optimized for the solar-gas system, EBSILON's CCGT Siemens SGT5-4000F PP is used estimate the heat rate of a CCGT PP. This is done to analyze the difference in LCOE between a CCGT_ISCC and a standalone CCGT PP.

- c. For ISCC PP calculations, fuel cost is determined by the heat rate of the GT modelled in EBSILON (Figure 8.7), and other parameters are estimated based on the specific values in Table 8.12.
5. Pay Back Period (Li et al., 2015)

$$R_{ann} \times \frac{[(1+i)^{PBP} - 1]}{[i \times (1+i)^{PBP}]} = C_{TPC} \quad (8.4)$$

Where R_{ann} is the annual net income, i is the real debt interest, PBP is the payback period, and C_{TPC} is the annual average investment.

6. GHG emissions-

$$GHG = Fluegas_2 \cdot M \times Fluegas_2 \cdot XGHG \times 1000 \quad (8.5)$$

Where, $Fluegas_2 \cdot M$ is the mass flow of flue gas, $Fluegas_2 \cdot XGHG$ is the GHG type, e.g. N₂, CO₂, etc.

Table 8.12 shows the technical, environmental and economic parameters used in this study.

Table 8.12. Input parameters

Parameter	Value	Unit	Reference
GT unit	235	\$/kW	[100] [212]
ST unit	860	\$/kW	[100] [212]
DSG field	770	\$/kW	[100] [212]
ET field	330	\$/kW	[100] [212]
Land cost	2.8	\$/kW	[100] [212]
Con, Eng., Cont. fees	0.1	\$/kW	[100] [212]
O & M factor of GT	0.05	%	[100] [212]
O & M factor of ST	0.02	%	[100] [212]
O & M factor of SF	0.015	%	[100] [212]
Real debt interest	0.08	%	[100] [212]
Plant life	30	Years	[212]
Sol life	30	Years	[212]
Gas price	0.266	\$/m ³	[213]
Average Irradiance	2 200	kWh/m ² /yr.	[166]
Solar hours ²¹ full load	3 029.5	hrs.	[214]
Fixed charge ratio for CSP	0.072	%	[211]
CSP capital cost	5 627.00	\$/kW	[211]
CSP Fixed O & M	66.00	\$/kW	[211]
ISCC capacity ratio	87	%	[215]
CCGT capacity ratio	87	%	[215]
CSP capacity ratio	31	%	[211]
ZW COE	0.12	\$/kWh	[216]
CCGT capital cost	1 100	\$/kwh	[42]
CCGT fixed O & M	6	\$/kWh	[42]
CCGT variable O & M	3	\$/MWh	[42]
Coal-gCO ₂ eq/kWh	820		[16]
Gas-gCO ₂ eq/kWh	490		[16]

²¹ Solar Hours: hours in a day significant DNI is received by the collectors.

8.6 Modeling the ISCC PP

The study uses EBSILON and SAM to model for ISCC PP and CSP PP, respectively, because:

- SAM only simulates for RE technologies.
- EBSILON simulates all electricity generating technologies. However, during the time of study, the CSP model in EBSILON did not have functions to manipulate or change the plant's parameters.

Power output of ISCC (and CCGT) systems are simulated using EBSILON's Siemens model templates (SGT 4 000 F GT- SGT5-4000F 50 Hz gas), where the desired GT capacity controls the CBM intake. The schematic diagram of the proposed ISCCPP (or standalone CCGT PP) is shown in Figure 8.7.

To model the ISCC,

1. The flow in Figure 8.7 is allowed to perform as is, changing the number of collectors (thus changing the solar capacity to a desired capacity) and the GT's desired power.

To model the CCGT_ISCC,

1. The thermo-liquid flow is shut, disconnecting the solar cycle from the other components of the system.
2. The SGT5- 4000F 50 Hz's capacity is changed to suit the desired plant capacity.

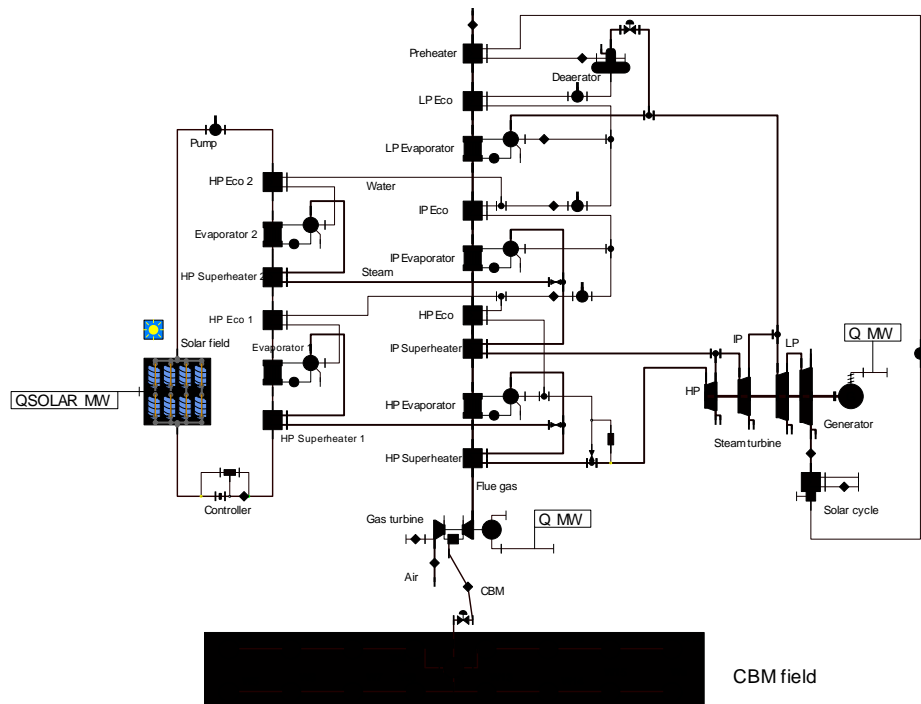


Figure 8.7. EBSILON's ISCC SGT 4 000 F [217]

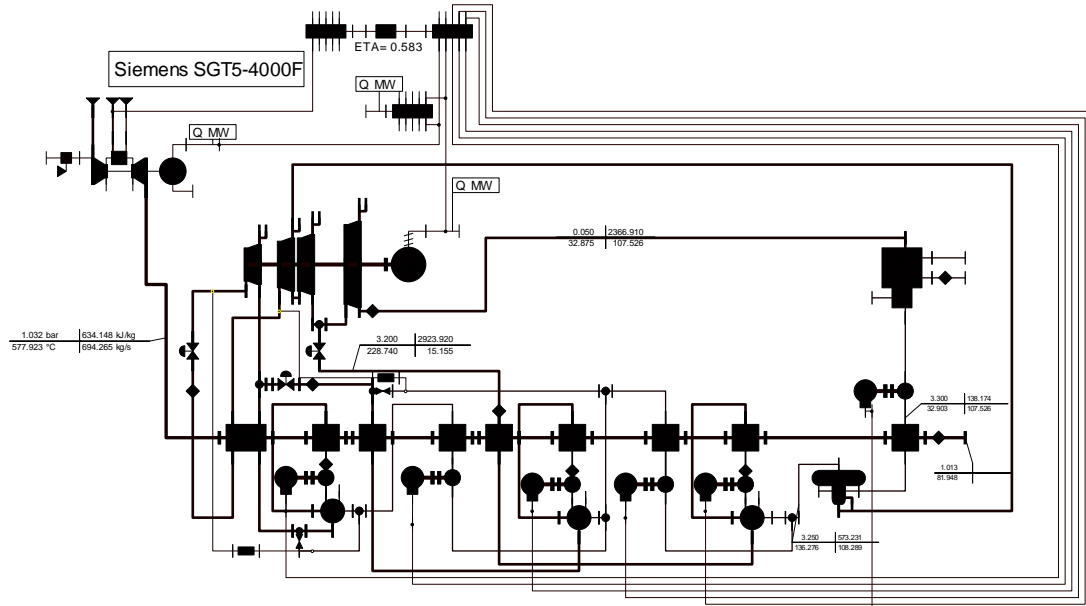


Figure 8.8. EBSILON's CCGT Siemens SGT5-4000F [217]

CHAPTER 9

RESULTS

9.1 Zimbabwe Coal Bed Methane Evaluation

Since a significant percentage of the power is generated from firing CBM, firstly a wide-range CBM assessment is completed as it narrows down suitable locations for the ISCC PP. We begin by estimating the OGIP in the region and specific sites, overlapping with top candidates for concentrating solar power (gross area Figure 8.3). The OGIP results calculated by MCS are represented by a histogram (Figure 9.1), a CDF (Figure 9.2), and tabulated in Table 9.1. The CDF plot yields P10, P50, and P90 values of the total CBM in place for the study area of Zimbabwe. Whilst conducting the MCS, E+02 and E+03 combinations generated fluctuating curves representing inconsistent P10, P50, and P90 values as shown by the CDF in Figure 9.2. More stable results were produced from E+04 and E+05 combinations. Precisely, the MSC produces consistent results after 25 000 runs. These variation of OGIP values can be quantified by a Sensitivity analysis (SA) in response to specific input ranges.

P90 means there is a 90 % probability (90 % of the time) that actual hydrocarbon in-place will be less than or equal to the low estimate (P90, 706 Bm³). Therefore, it is estimated that the study area sits on 706 Bm³ of CBM.

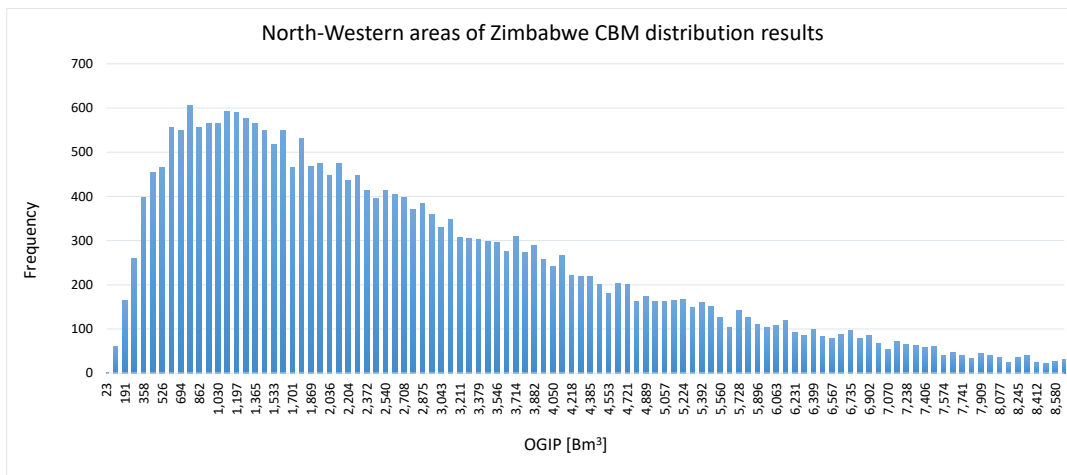


Figure 9.1. Histogram of OGIP values calculated by MCS

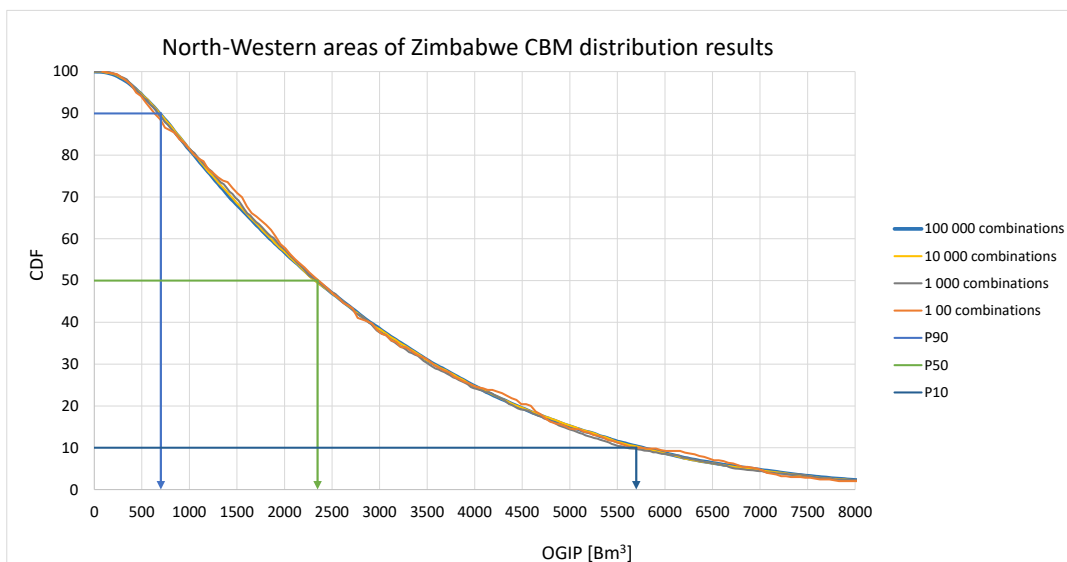


Figure 9.2. CDF of OGIP values obtained for different combinations

Table 9.1. CBM OGIP and reserve estimates

Probability	Trillion Cubic Feet [Tcf, E+12]	Billion Cubic meters [Bm ³ , E+09]	Reserves [Bm ³ , E+09] RF = 50 % [141]
P10	201.3	5 699	2 850
P50	82.8	2 347	1 174
P90	24.9	706	353

9.1.1 Sensitivity Analysis

Sensitivity analysis (SA) is a method to quantify the amount of variation a system (or model) has in response to specific ranges in input [218]. To understand how sensitive the output (in our case, the OGIP) is to the input parameters, we performed a one-factor-at-a-time²² (OFAT) analysis to find out which parameter could potentially impact OGIP results, hence contribute most uncertainty to the model [218].

First, input values for each parameter are set to their mean value. The output of the mean values is the baseline. Figure 9.3 shows a tornado plot of the inputs (area, thickness, density, and gas content) used in this study against the output (OGIP). In Figure 9.3, the bars illustrate the range of results produced when each parameter is set to Min. and Max. while keeping other parameters constant. The parameter having the greatest effect is on the top. The parameter at the bottom represents the one with the least effect. The middle line in Figure 9.3 represents the baseline when the mean values are used for gas content, thickness, area, and density, respectively. Per parameter ranges considered in this study, according to Figure 9.3, gas content has the most significant effect on the OGIP, followed by the thickness of the coal seam. The effect of gas content and coal seam thickness is significant. However, it is important to point out that the values for these two parameters were taken directly from the Karoo basin (North-Western areas of Zimbabwe). Area has a small impact perhaps because percentage change between the Max and Min is little. Table 9.2 shows the

²² One-factor-at-a-time: Also known as one-variable-at-a-time (OVAT).

percentage change in OGIP with respect to percentage changes in parameters during OFAT study.

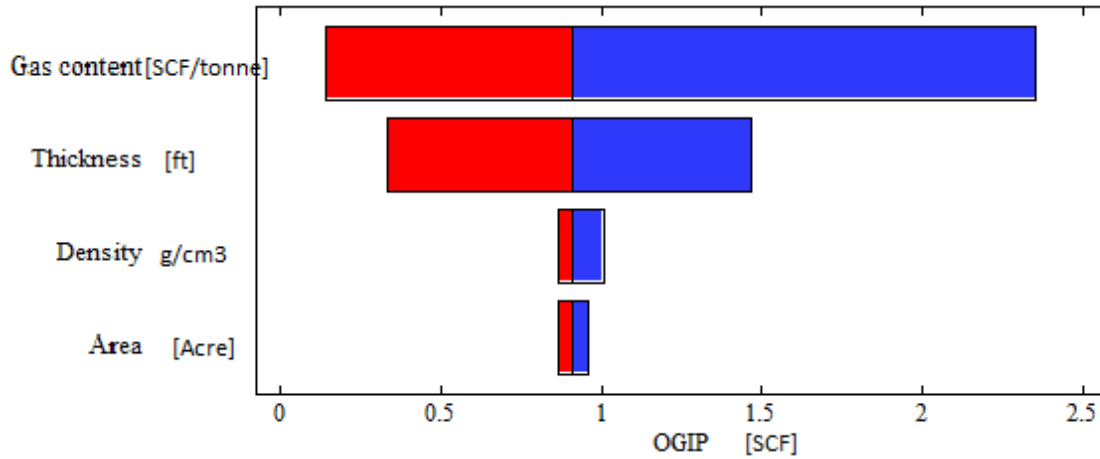


Figure 9.3. Sensitivity plot of OGIP to the input parameters

Table 9.2. Sensitivity of OGIP to input parameters

Parameter	Median	Variation in parameter		Variation in OGIP	
		- Δ %	+ Δ %	- Δ %	+ Δ %
ρ_{coal} [g/cm ³]	1.58	- 0.140	+ 0.115	- 0.027	+ 0.073
A [Acres]	1.19 x 10 ⁷	- 0.058	+ 0.058	- 0.032	+ 0.045
h [m]	31.33	- 0.822	+ 1.130	- 0.555	+ 0.545
G_c [SCF/tonne]	93.98	- 0.989	+ 2.086	- 0.636	+ 1.136

The results from Table 9.2 shows that the highest OGIP change is caused by G_c (-0.636 and + 1.136). For example, taking P90 (706 Bm³) as the OGIP value, G_c causes a change in the OGIP value from 701.5 Bm³ to 714.0 Bm³, which is not significant. Therefore, since the OGIP value is not too sensitive to specific ranges in the inputs (especially G_c in this case), the results in Table 9.1 are taken to represent the CBM resources in the study area.

9.1.2 Resource Density Comparison

Table 9.3 shows the CBM resource densities (RDs) calculated for the study area of Zimbabwe. The RD for the study area is found to range from 0.015 Bm³/km² to 0.113 Bm³/km². These values are comparable to major basins in Canada. This is significant because Canada is among the top 6 natural gas-producing countries in the world, considering that approximately 71 % of the production occurs in Alberta where there are abundant CBM reserves [219]. In fact, RD values range from 0.016 to 0.025 Bm³/km² in Alberta plains shallow basin, and from 0.034 to 0.071 Bm³/km² in Alberta plains deep basin [220]. This comparison signifies the CBM potential and opportunities for Zimbabwe. However, since the study area ranges from 1.12E+07 Acres to 1.26E+07 Acres which is huge, further screening is necessary to select the most preferred site for CBM exploration and concentrating solar power.

Table 9.3. CBM resource densities for the study area of Zimbabwe

	Resource estimate [Bcf]	Area [km ²]	Resource density [Bm ³ /km ²]
P10	201 300	50 585	0.113
P50	82 800	48 562	0.048
P90	24 900	46 134	0.015

9.1.3 Coal Bed Methane site Evaluation

To evaluate the study area for CBM exploration, criteria from Table 8.1 are compared with a range of values belonging to the study area, as shown in Table 9.4. This comparison qualifies the study area for CBM exploration except for the following drawbacks:

- 1) The CBM RD is less than the expected E+06 m³/ha.
- 2) The depth of seams for most regions range from 10 m to 300 m, much shallower than the preferred 400 m – 1 000 m range.
- 3) The gas content for some areas is less than the preferred 7 m³/tonne, ranging from 0.82 m³/tonne to 11.5 m³/tonne.

Using Figure 5.2 (hydrocarbon generation during coalification) and Table 6.7 (metallurgical coal qualities for Zimbabwe), the coal rank within the study area of Zimbabwe ranges from low-quality Subbituminous C to middle-quality high volatile bituminous.

Table 9.4. CBM site evaluation

Selection criteria	Site selection values	North-Western areas of Zimbabwe Values
Resource Area	>1 km ²	>1 km ²
Gas Content (G_c)	>7 m ³ /tonne	0.82 < G_c < 11.5 [m ³ /tonne]
Depth of coal seams (D)	400 m < D < 1 000 m	0 m < D < 1 000 m
Coal Seam thickness (h)	>5 m	0.1 m < h < 25 m
Resource Density (RD)	>1 E+06 m ³ /ha	1 10 ⁻⁵ < RD < 1 E+06 [m ³ /ha]
Coal Rank	Greater than Bituminous	High volatile A bituminous < CR < Subbituminous C

It is observed after the initial evaluation that the range in criteria used in Table 9.4 divides the study area into two main regions, for the reasons discussed next:

- Low seam depths dominate from the Lusulu-Lubu areas to the Sengwa North-Gokwe areas. The coal seam depths range from 0 m in Gokwe to approximately 350 m in Sengwa, with other areas in between Lusulu-Lubu and Sengwa North-Gokwe falling in the same range.
- Maximum coal seam thickness values are found in Gokwe, Lubu, and Lusulu. However, low coal thicknesses are dominant in those areas.
- Lowest gas content values are found in Sengwa area being less than 1 m³/tonne.
- The Hwange-Lupane area predominantly has the highest coal seam thickness and gas content values.
- The Hwange-Lupane area mostly has seam depths ranging from 600 m to 1 000 m.

Therefore, the study area is divided into two regions as:

- Region 1 contains all the area/zones between the Hwange-Gwayi river and Lupane and Gwaai.
- Region 2 contains all the area/zones between the Lusulu-Lubu areas and Gokwe-Sengwa areas.

Region 2 contains locations with the least preferred CBM parameters and is disregarded for further consideration in this study.

According to criteria in Table 8.1, region 1 (Hwange-Lupane area) is chosen as the most preferred site for CBM exploration. Figure 9.4 shows the Hwange-Lupane region which has an approximate area of 7 837 441 Acres (31 717 km²), approximately 70 % and 62.2 % of the Min and Max study area of Zimbabwe, respectively.

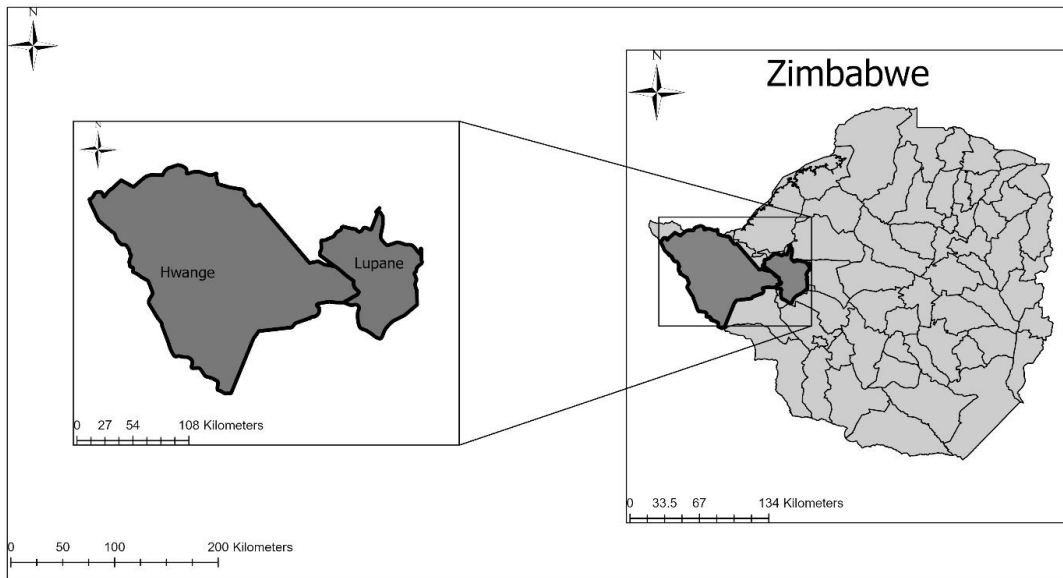


Figure 9.4. Geographical location of Hwange and Lupane regions of Zimbabwe

9.2 Concentrating Solar Power Evaluation

Per the overall methodology adopted in this study (see Chapter 8, Figure 8.1 and Sections 8.5 and 8.6), because we have rejected region 2 for CBM development, the most suitable location for CSP within region 1 (Hwange-Lupane area) should be the best location for the ISCC PP. Priority is given to CBM site because it has been established that an overwhelming fraction of power generated by the ISCC-PP will be from CBM. Site evaluation and selection steps for CSP in the Hwange-Lupane area is discussed in the remainder of this section.

9.2.1 Exclusion Zones

According to UNEP-WCMC (2022), Zimbabwe has 232 protected areas spread around the country. These protected areas include nature reserves, national parks, wilderness areas, national monuments, recreation parks, safari areas, sanctuaries, wildlife management areas, botanical reserves, state forests, and protected forests. The land cover map of the Hwange-Lupane area (Figure 9.5) shows that most of the land is covered with vegetation (which is beneficial because most of the land would not be occupied). However, the Hwange-Lupane region hosts over 25 % of Zimbabwe’s protected areas. Figure 9.6 shows the distribution of all protected areas over the study area, covering more than half of the Hwange-Lupane area.

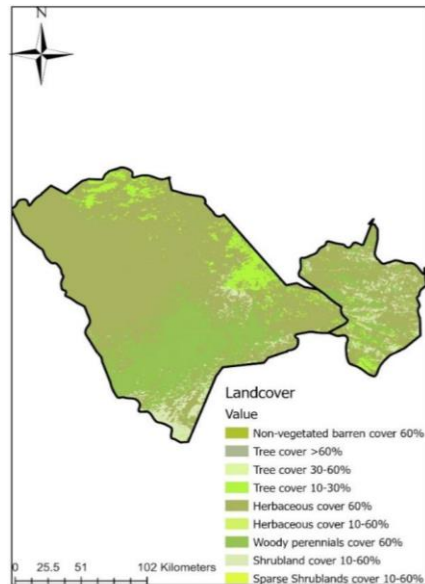


Figure 9.5. Land cover of Region 1: Hwange-Lupane area

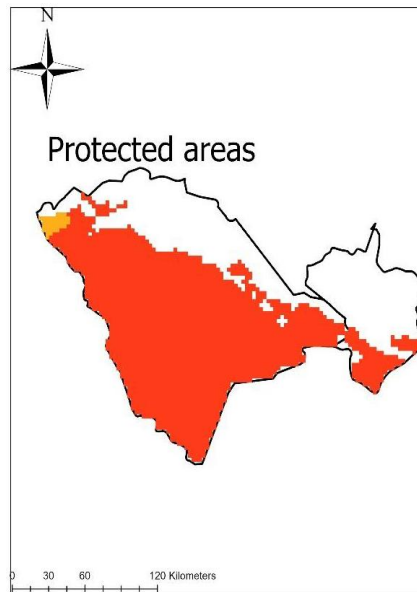


Figure 9.6. Protected area of Region 1: Hwange-Lupane area

9.2.2 Criteria for the Hwange-Lupane Region

The data collected from references in Table 8.9 is standardized in ArcGIS Pro. The Figures 9.5 to 9.9 represent the factors considered in the feasibility of CSP for the Hwange-Lupane area. Figure 9.7 shows the DNI distribution over the study area, ranging from approximately 1 800 to 2 400 kWh/m²/year. Accordingly, there was no need to exclude regions with DNI less than 1 800 kWh/m²/year since the observed least DNI is 1 799.6 kWh/m²/year.

Figure 9.8a shows the slope of the Hwange-Lupane area in percentage and Figure 9.8b in meters. Most of the area has a slope less than 2.1 %, while the Northern areas of Hwange have slopes ranging between 5 to 10 %.

Figure 9.9 shows the road, electricity grid distribution, and the water resource distribution over the study area, making the southern part of Hwange less suitable for concentrating solar power as it is far from the grid, roads, and the water body.

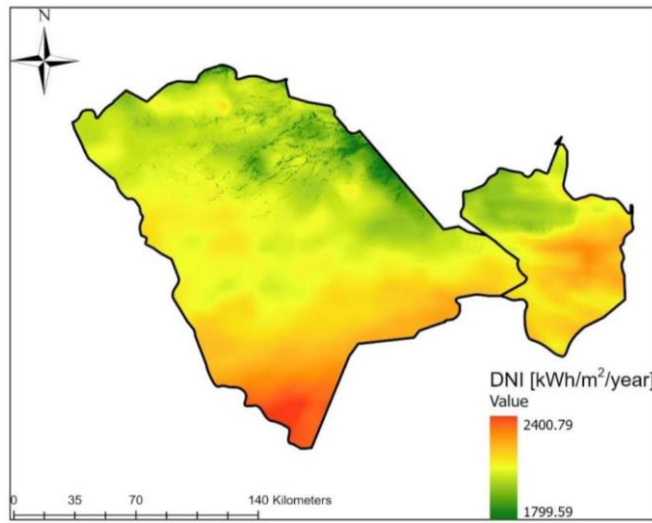


Figure 9.7. Direct normal irradiance of Region 1: Hwange-Lupane area

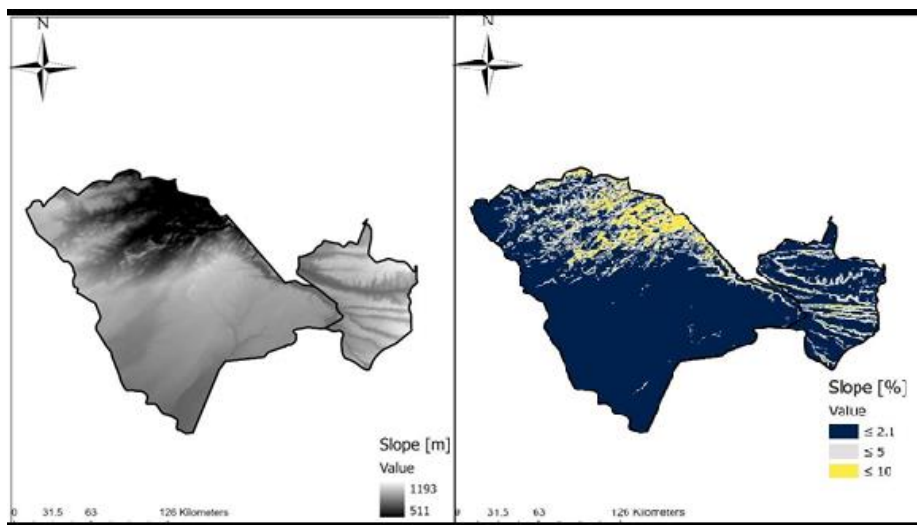


Figure 9.8. Slope data of the Region 1: Hwange-Lupane area

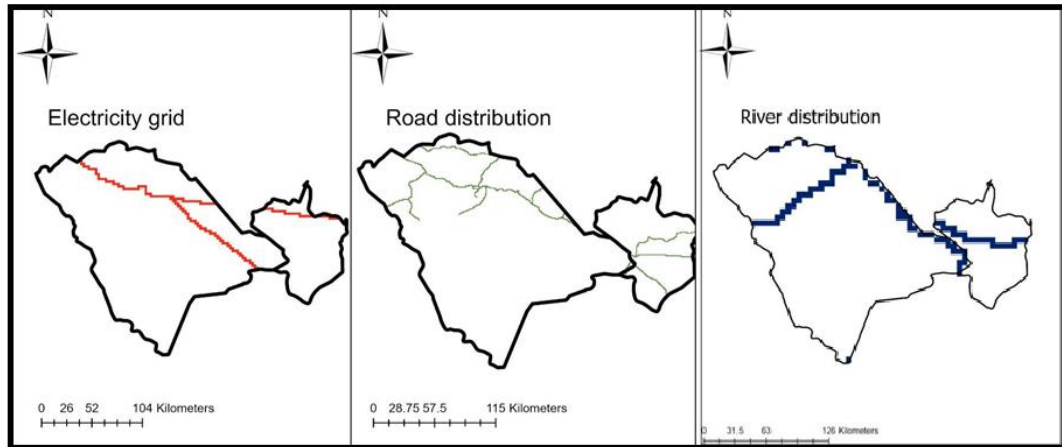


Figure 9.9. Electricity grid, road distribution, and river distribution data of Region 1: Hwang-Lupane area

9.2.3 Analytic Hierarchy Process

As described in Section 3.4.1, the AHP applies a pairwise comparison to get the weights of decision criteria. Using the weights, a pairwise comparison matrix is built, then normalized, and factored in Equation 3.9 to determine the land suitability index (LSI). The importance of each criterion is an arithmetic average of the recommendations from three experts in solar energy and/or pertinent literature provided in Table 3.2. Table 9.5. shows matrix $[A]$, representing the average of the combined results. Table 9.6 shows the normalized matrix $[w]$ corresponding to matrix $[A]$ in Table 9.5, with specified criteria weights. Solar irradiance (DNI) has the greatest weight at 55.46 %, followed by the slope at 26.87 %, proximity to the grid and road at 11.11 %, and water resources at 6.55 %.

Table 9.5. AHP pairwise comparison matrix [X]

	Solar irradiance	Slope	Proximity	Water resources
Solar irradiance	1.00	3.33	5.20	5.91
Slope	0.30	1.00	3.96	4.26
Proximity	0.19	0.25	1.00	2.48
Water resources	0.17	0.23	0.40	1.00
Summation	1.66	4.82	10.56	13.65

Table 9.6. Normalized matrix [w]

	Solar irradiance	Slope	Proximity	Water resources	Weights [%]
Solar irradiance	0.60	0.69	0.49	0.43	55.46
Slope	0.18	0.21	0.38	0.31	26.88
Proximity	0.12	0.05	0.09	0.18	11.11
Water resources	0.10	0.05	0.04	0.07	6.55

The consistency ratio, CR is calculated as (see Sec. 3.7 for details):

- $CI = \frac{(\lambda_{max} - n)}{(n-1)} = \frac{(4.190082 - 4)}{(4-1)} = 0.063$
- $CR = \frac{CI}{RI} = \frac{0.0063361}{0.89} = 0.071$

The CR is 7.12 %, and is less than 10 %, representing the consistency of collected data. Accordingly, the weights in Table 9.6 are used in the GIS-AHP analysis (in ArcGIS Pro).

Unsuitable regions were extracted, and Equation 3.9 is used with the help of Analysis tools in ArcGIS Pro. Most of the unsuitable area is in Hwange due to the constraints of the Hwange National Park and other protected areas, while most of the suitable land is in Lupane. Figure 9.10 shows the land suitable for CSP. The land suitable for CSP in Hwange and Lupane is 1

792 km² and 3 771 km², accounting for 5.6 % and 11.9 % of the Hwange-Lupane study area, respectively. The coordinates for corners of the rectangular/angular patches of selected land suitable for CSP are given in Table 9.7.

Table 9.7. Coordinates of the suitable land for CSP

Area coordinate	Region	
	Hwange	Lupane
1	26.31 °E and 18.14 °S	27.48 °E and 18.63 °S
2	26.82 °E and 18.13 °S	27.93 °E and 18.42 °S
3	26.32 °E and 18.39 °S	28.06 °E and 19.27 °S
4	26.86 °E and 18.40 °S	28.30 °E and 18.77 °S

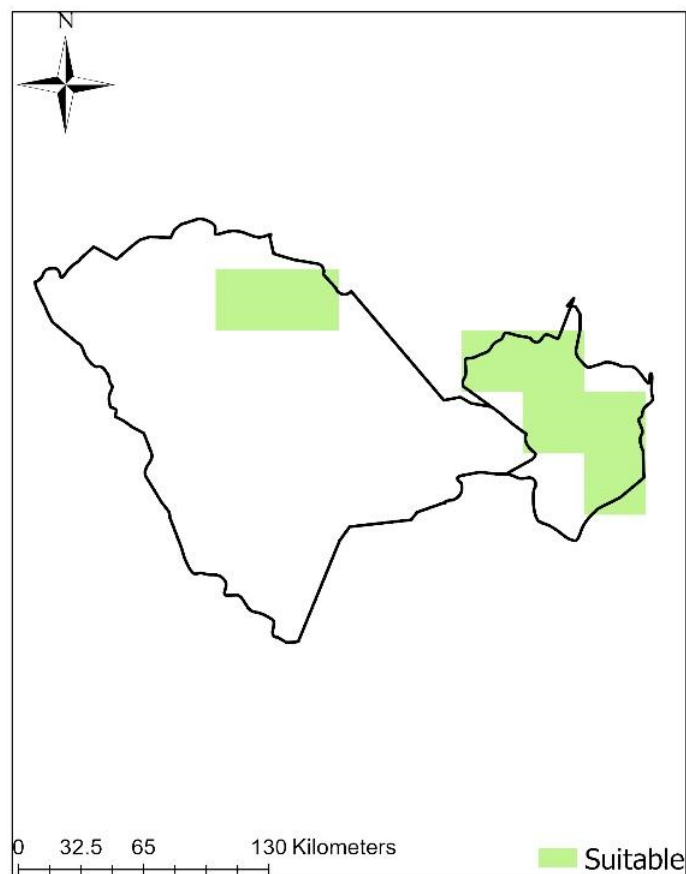


Figure 9.10. Land suitability for concentrating solar power

9.2.4 Power Potential of Land Suitable for CSP

The technical power potential (TPSE) for selected areas in both Hwange and Lupane is calculated using Equation 8.8. A probabilistic approach is adopted using STRATGRAPHICS 18 software [221] to perform MCS. This is to quantify the uncertainty in the calculation by estimating a range of values for the TPSE. Tables 9.8 and 9.9 show the summary statistics utilized to estimate the TPSE of selected areas in Hwange and Lupane, respectively. Similarly, Figures 9.11 and 9.12 show the CDF of TPSE results for Hwange and Lupane, respectively. Accordingly, the TPSE for the suitable area in Hwange and Lupane is estimated to range from 529 to 696 TWh/year, and 1 207 to 1 613 TWh/year, respectively, as shown in Table 9.10. Consequently, Lupane (with an area of 3 771 km² available for CSP) is the determined intersection for CBM development and CSP system since it has more land suitable for concentrating solar power.

At this point, the OGIP for Lupane region alone must be estimated, and it should be determined if the quantity is enough to sustain power generation at the proposed CCGT and ISCC PPs throughout life span of the plants.

Table 9.8. Summary of parameters used in MCS for the power potential of Hwange

	TPSE [kWh/year]	Area	DNI	Efficiency
Count	10000	10000	10000	10000
Average	6.12E+11	1.79E+9	1899.92	0.18
Standard deviation	6.19E+10	0.00	57.67	0.017
Coeff. of variation	10.11%	0.00%	3.04%	9.63%
Minimum	4.84E+11	1.79E+9	1800.00	0.15
Maximum	7.51E+11	1.79E+9	1999.97	0.21
Range	2.67E+11	0.00	199.97	0.06

Table 9.9. Summary of parameters used in MCS for the power potential of Lupane

	TPSE [kWh/year]	Area	DNI	Efficiency
Count	10000	10000	10000	10000
Average	1.41E+12	3.77E+9	2075.00	0.18
Standard deviation	1.53E+11	0.00	101.28	0.017
Coeff. of variation	10.82%	0.00%	4.88%	9.61%
Minimum	1.08E+12	3.77E+9	1900.00	0.15
Maximum	1.78E+12	3.77E+9	2249.98	0.21
Range	6.98E+11	0.00	349.98	0.06

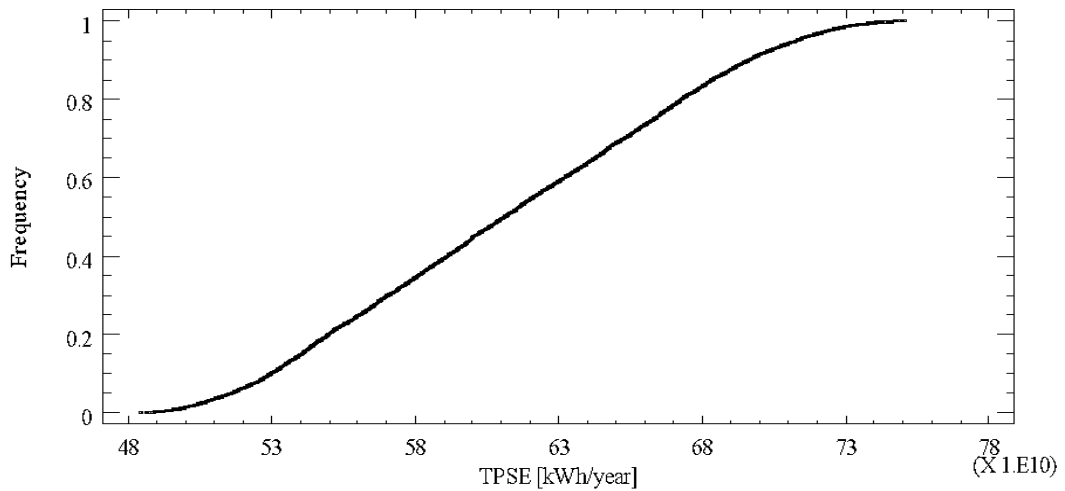


Figure 9.11. CDF of TPSE values for Hwange obtained from different combinations, P50 =611 TWh/year

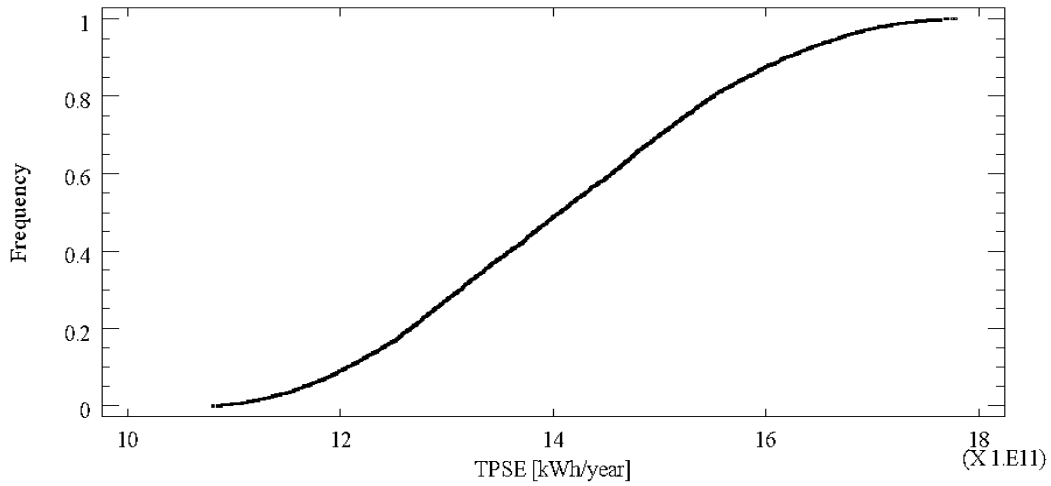


Figure 9.12. Cumulative distribution function of TPSE values for Lupane obtained from different combinations, P50 = 1 403 TWh/year

Table 9.10. Range of TPSE in percentiles

	TPSE [TWh/year]		
	P10	P50	P90
Hwange	529	611	696
Lupane	1 207	1 403	1 613

9.3 Lupane coal bed methane Evaluation

After applying the same methodology discussed in Sec. 9.1 (with input parameters from Table 9.11), the OGIP for the intersection of suitable CBM development and CSP sites is estimated as 250 Bm³ (P90 from Figure 9.13 and Table 9.12). This value will be used to determine the potential of burning CBM in CCGT and ISCC PPs throughout facility lifetime.

Table 9.11. MCS inputs for Lupane

Parameter	Descriptive statistics	Numerical value	Type of distribution	of Reference
Area [Acre]		1 892 621.08	Constant	[222]
Thickness [ft.]	Min	6.76	Triangular distribution	[180] [198]
	Mode	38.24		
	Max	66.72		
Coal density [g/cm ³]	Min	1.53	Triangular distribution	[165]
	Mode	1.54		
	Max	1.75		
Gas content [SCF/ton]	Min	26	Triangular distribution	[199] [200]
	Mode	69		
	Max	409		

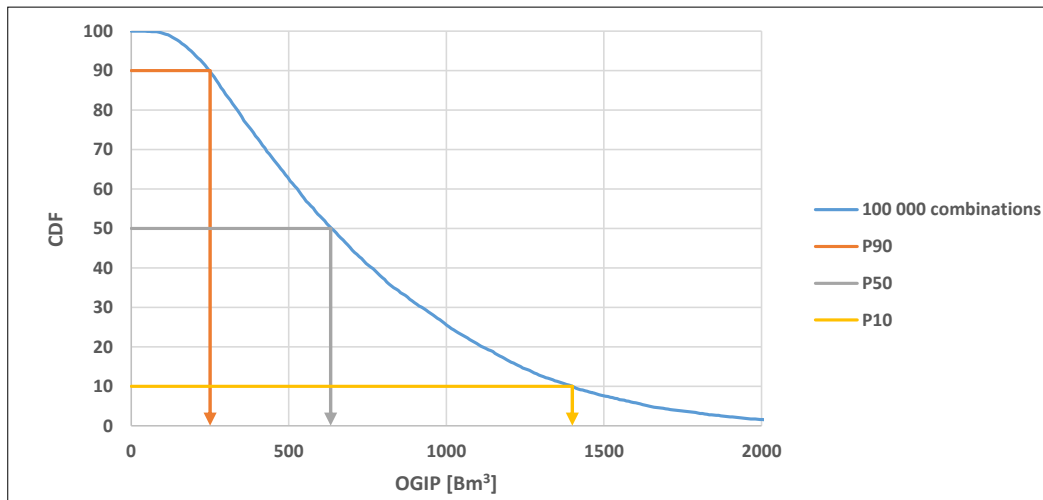


Figure 9.13. CDF of OGIP for Lupane

Table 9.12. CBM OGIP and reserve estimates for Lupane

Probability	OGIP [Tcf, E+12]	OGIP [Bm ³ , E+09]	Reserves [Bm ³ , E+09] RF = 50 % [141]
P10	49.4	1 400	700
P50	22.4	633	316.5
P90	8.8	250	125

9.4 Technical Analysis

Optimum power plant capacity and CSP contribution to total output should be determined before including fuel consumption, CBM field gas production rates, and well counts in the CBM-ISCC PP evaluation. This requires establishing a valid capacity factor (ratio of actual power output over theoretical maximum output, Sec. 2.5) for each power plant type (or technology). The capacity factor can be increased by improving the technical efficiency of the plant. For this purpose, the efficiency of the two primary components used for energy conversion in the plants should be analyzed:

1. The GT (Brayton cycle), used in the ISCC and CCGT systems.
2. The ST (Rankine cycle), used in all three plant types.

As ST is present in all three plant types, we focus on the ST efficiency. Table 9.13 shows the technical efficiency factors for the ST and the solar field which supports steam generation in a CSP component.

Table 9.13. The technical results of the Rankine cycle

Steam turbine (ST) efficiency factors		Solar field efficiency factors	
Isentropic efficiency	0.88 %	Optical efficiency	0.75 %
Polytropic efficiency	0.86 %	Thermal efficiency	0.89 %
Mechanical efficiency	0.998 %	Field efficiency	0.67 %

9.4.1 Capacity Factor for the CSP

The capacity factor for CSP (standalone or as part of ISCC) is typically low because the solar hours are relatively low. Figure 9.14 shows the typical hours when there is irradiance available for EG in Lupane region of Zimbabwe. From Figure 9.14, the effective average of annual solar hours is approximately 8.3 hours, denoting an average daily capacity factor of 34.6 % (= 8.3/24 hrs.) for CSP without TES.

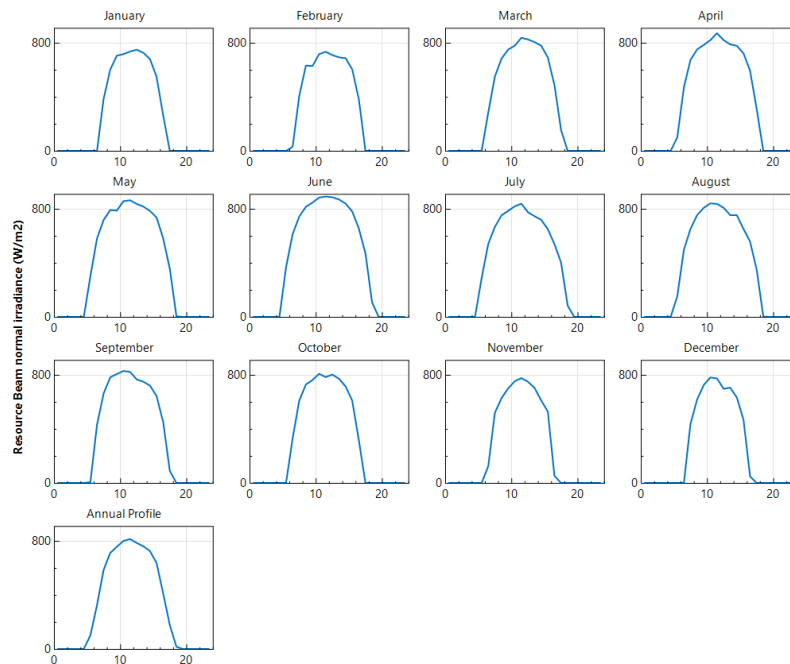


Figure 9.14. Monthly plots of solar hours vs Irradiance for Lupane region

The capacity factor for a CSP plant is simulated in SAM. The current study compares CSP, CCGT, and ISCC power plants. Considering the 600 MW target (Table 6.5) by the Zimbabwean government, study compares different capacities of the three technologies from 50 MW to 600 MW.

To determine the CSP capacity factor, an average is taken from different capacities of the CSP plant, simulated in SAM. The average capacity factor is important because it will be used to estimate the capacity factor of the CCGT and CSP without TES combination (ISCC). Figure 9.15 shows the relationship between the capacity factor and plant capacity operating in Lupane of Zimbabwe, simulated in SAM. The capacity ranges from 29.2 % (for the 600 MW CSP plant) to 31.9 % (for the 50 MW CSP plant). Accordingly, the average of 31 % is taken to represent the CSP capacity factor for current study.

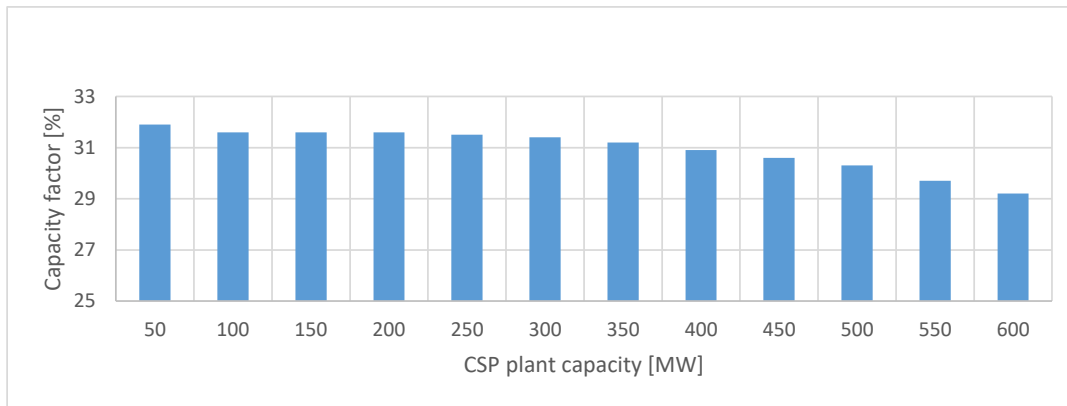


Figure 9.15. Total electric power to grid for Lupane from a CSP plant

9.4.2 Capacity Factor for CCGT and ISCC

To establish the capacity factor for ISCC cycle, consider, for sake of simplicity, a 100 MW ISCC-PP, hereafter designated as ISCC_{100MW}. Due to unpredictable weather changes, assume CSP will provide 10 % of the total theoretical power output (after Breeze, 2016 [101]). Hence, 90 % of output should be generated by the fossil fueled CCGT cycle. Assume capacity factors of 31 % (Section 9.4.1) and 87 % (after Alqahtani & Patiño-Echeverri, 2016 [215]) respectively for CSP and CCGT cycles of the ISCC. Consequently, 10 % of theoretical output is generated at a capacity of 31 % (solar cycle), and 90 % is generated at a capacity of 87 % (CCGT cycle). That is, the ISCC_{100MW} actually produces 81.4 MW (= 78.3 MW from the CCGT cycle + 3.1 MW from the CSP cycle). Therefore, if the capacity factors of 31 % and 87 % are applied for the CSP and ISCC, respectively, they actually translate to a 81.4 % capacity factor for the ISCC plant.

The two capacity factors for the ISCC PP (87 % after [215] and the calculated 81.4 %) are considered in the calculations, and the results for power output from ISCC system are shown in Figure 9.16. The difference in the actual power output for the two capacity factors is found to range between 5 % and 6 %. Since the difference is less than an arbitrary margin of 10 %, only one capacity factor can be utilized for ISCC calculations. Accordingly, the lower value of 81.4 % should be chosen such that the cost of electricity from the ISCC system is not underestimated. However, this conclusion will also be supported by LCOE calculations in the economic analysis section.

Figure 9.17 shows actual power output [kWh/year] from three types of PPs at different theoretical capacities [MW]. The CCGT PP generates the highest output for all capacities. For instance, a CCGT_{500MW} generates 3.8 billion kWh/yr. In comparison, an ISCC_{550MW} generates 3.91 billion kWh/yr., which is greater than the total power output by Zimbabwe’s five²³ fossil fuel PPs. This suggests that a single CCGT_{500MW} or ISCC_{550MW} technically performs better than the existing five coal-fired power plants. On the other hand, the CSP PP generates the lowest output due to the annual average of 8.3 sun hours per day, and that the CSP type considered herein is without TES. However, for CSP’s comparison sake with other PPs, an 8 hour TES facility is added to each facility from 50 MW to 600 MW in SAM. Figure 9.17 shows that the addition of TES facility increases the power output, irrespective of the fact that it is not comparable with CCGT and ISCC technologies.

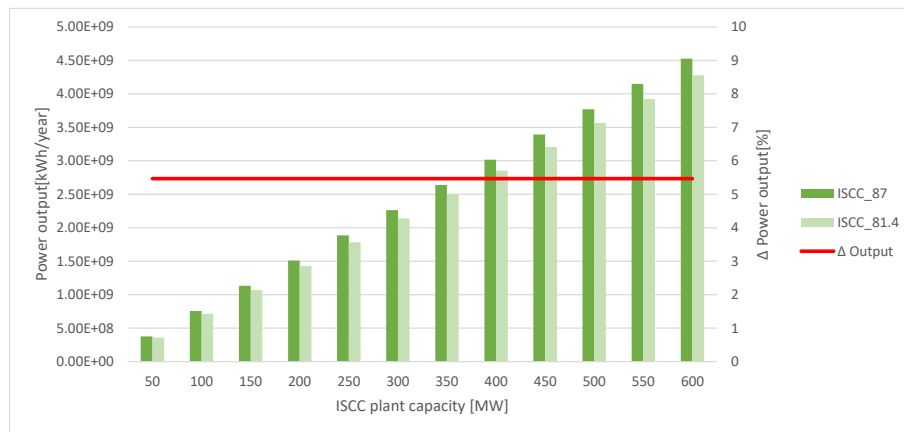


Figure 9.16. Actual power Output from ISCC systems at different theoretical capacities

²³ From 2017 to 2020, the five thermal PPs in Zimbabwe (Table 6.6) generated an average of 3.675 billion kWh/yr of electricity.

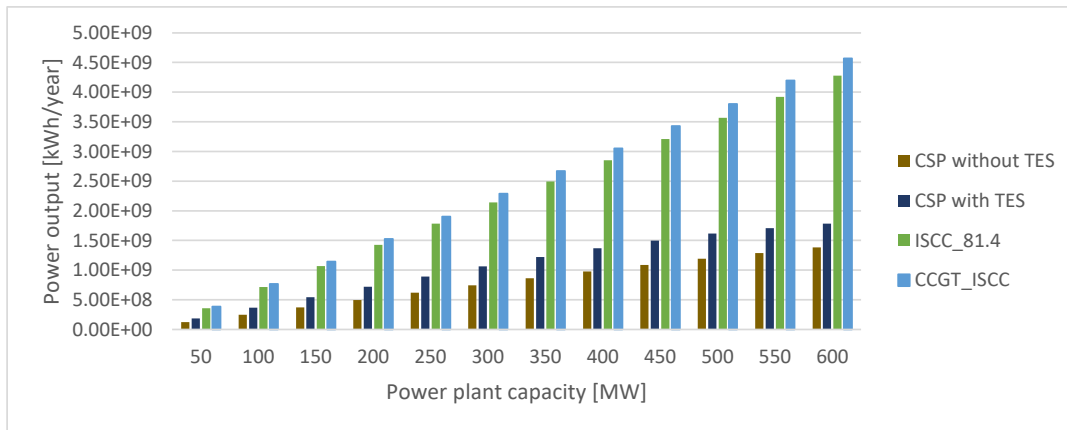


Figure 9.17. Actual power Output from CSP, CCGT and ISCC plants at different theoretical capacities

9.4.3 Overall Efficiency as a Function of Total Plant Capacity

The efficiency of the GT (CCGT) and the solar cycle (CSP) is calculated for the total capacity range considered in the analysis, as shown in Figure 9.18. The GT efficiency, fitted with a power trend line, suggesting a significant increase in efficiency with an increase in capacity. The solar cycle efficiency follows a near constant trend with an insignificant (0.19 %) change in efficiency with increasing plant capacity.

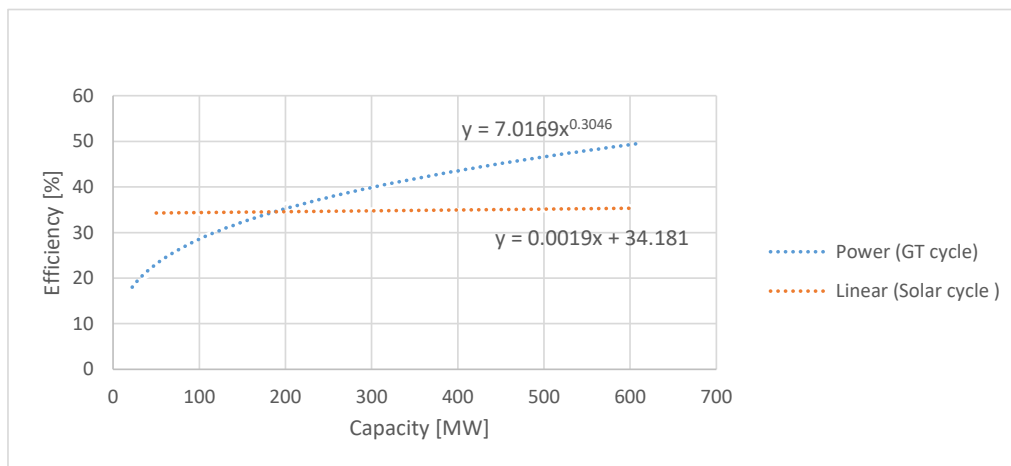


Figure 9.18. Efficiency of the gas turbine and solar cycle

9.5 Economic Analysis

The LCOE is utilized as a parameter for evaluating economics of power-generation. Table 9.14 shows Zimbabwe’s LCOE for various technologies, to be compared with the LCOE results (Table 9.14 in italics) obtained in this study.

Table 9.14. LCOE by technology for Zimbabwe [223]

Technology	LCOE [\$/kWh]
Biomass	0.130 – 0.170
Small hydro	0.075 – 0.110
Solar PV	0.170 – 0.220
Onshore wind	0.175 – 0.220
Coal	0.079 – 0.096
<i>CSP without TES</i>	<i>0.180 – 0.196</i>
<i>CSP with TES</i>	<i>0.119 – 0.146</i>
<i>CCGT</i>	<i>0.053 – 0.081</i>
<i>ISCC</i>	<i>0.050 – 0.069</i>

For LCOE calculations of current analysis, different capacities (from 50 to 600 MW) of the same technology are compared against each other. The LCOE for CSP is provided by SAM, Figure 9.19 shows LCOE for different capacities of the CSP PP with and without TES. From Figure 9.19, the inclusion of a TES facility significantly reduces the LCOE with a minimum of 30 % change.

LCOE for CCGT and ISCC are calculated in a spreadsheet, and a 10 % solar share is considered for each ISCC capacity. Figure 9.20 shows two set of results for ISCC LCOE because one calculation is considered at a capacity factor of 87 %, while the other is 81.4 % (as discussed in the technical analysis section). Figure 9.20 also shows a near constant difference in LCOE depending on the ISCC system capacity factor. The mean difference in the LCOE values is 6.79 %. This is under the arbitrary 10 % margin, so the ISCC_81.4 LCOE values are considered in the remaining analysis, to avoid underestimating the cost of electricity for ISCC.

Consequently, Figure 9.21 shows the LCOE values for all three plant types of the current study. The change in LCOE with total capacity for each plant type is fitted with a polynomial equation. The cost of electricity for CCGT and ISCC systems has a negative gradient, indicating a decrease in the cost of electricity with an increase in plant capacity. For CSP systems, there is an almost constant cost of electricity from 50 to 200 MW capacities. The cost of generating electricity from CSP systems increases from 250 to 600 MW. The increase in the LCOE can be explained by the inconsistency of the LCOE values of CSP plants in USA (see Appendix B). Furthermore, the increase of the LCOE with CSP plant capacity could be due to solar multiple²⁴ values of models not being optimized for each case. Solar multiple of the plant should be large enough to ensure a certain range in the nominal operation of the solar thermal system. Montes et al. explain that optimum solar multiple depends not only on the solar field size, but also on the plant location, the design point and the power cycle parameters at nominal operating conditions [224]. Large solar arrays without heat storage waste more solar thermal energy than normal, resulting in lower profit margins [224]. So, from results in Figure 9.21, CSP plants investigated in study should not exceed 200 MW. Also, Authors advise that at most a 10 % solar share must be utilized by ISCC plants because additional solar share results in losses [101] [224].

The most economical LCOE values for each of the CSP without TES, CSP with TES, CCGT_ISCC (see Appendix A why CCGT_ISCC is chosen over a standalone CCGT), and ISCC_81.4 are 0.1727 \$/kWh, 0.1191 \$/kWh, 0.0529 \$/kWh, and 0.0495 \$/kWh, respectively. To obtain a single value that represents the cost of generating electricity from a technology, current study takes an arithmetic average of 12 different capacities from 50 MW to 600 MW (Figure 9.21). The arithmetic average cost of electricity from CSP without TES, CSP with TES, CCGT_ISCC, and ISCC_81.07 is 0.1777 \$/kWh, 0.1278 \$/kWh, 0.0635 \$/kWh, and 0.0581 \$/kWh, respectively.

Considering all capacities in Figure 9.20, the ISCC system is more economical than CCGT and CSP systems. The cost of generating electricity from CSP without TES systems is 2.80 and 3.06 times the cost of generating electricity from CCGT and ISCC systems, respectively.

²⁴ Solar multiple: The ratio of the heat output produced by the solar field at the design point to the heat output required by the power block under nominal conditions.

However, the inclusion of a TES facility reduces the LCOE to almost the retail cost of electricity in Zimbabwe. The average cost of electricity in Zimbabwe is [225] [216]:

- 0.095 \$/kWh for generation
- 0.12 \$/kWh for retail (sale to customer)

The numbers above dismiss the feasibility of generating electricity from a standalone CSP PP without TES. Though the LCOE from CSP without TES is the highest, integrating a 50 MW solar into a CCGT (i.e., ISCC_{50MW}) reduces the LCOE to 0.0518 \$/kWh from \$0.1727 \$/kWh (average cost of electricity for CSP) for a standalone 50 MW CSP PP. Also, the CSP with TES is not far away from retail cost of electricity. From the 12 capacities of the CSP with TES, CSP_{50MW} and CSP_{100MW} generate electricity at 0.1191 \$/kWh and 0.1199 \$/kWh, respectively, which is barely less than the retail cost.

All ISCC PP and CCGT PP capacities generate electricity at costs less than 0.12 \$/kWh. For economic considerations, the ISCC and CCGT technologies can be adopted in Zimbabwe for electricity generation. Figure 9.22 shows the payback period (PBP) of ISCC and CCGT systems. Overall, the CCGT systems pay back later than the ISCC systems.

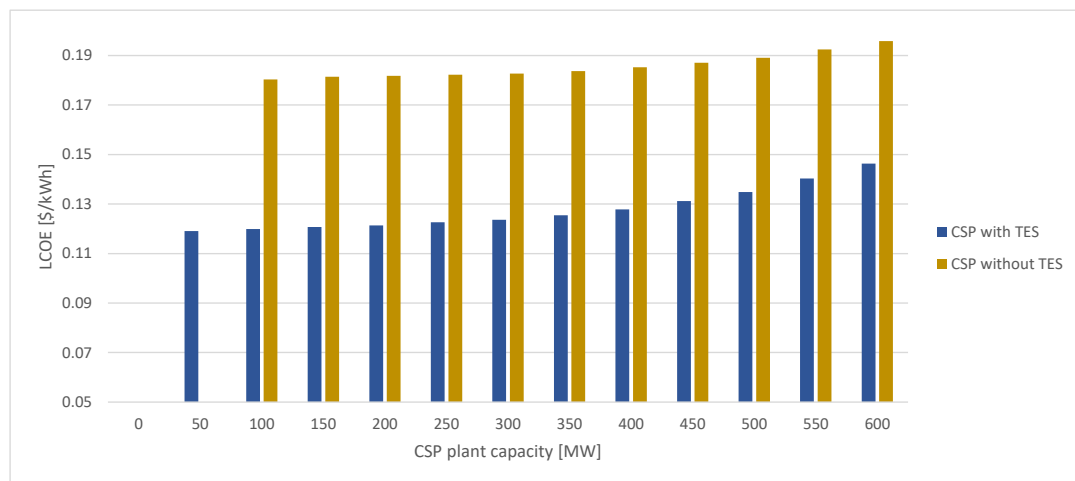


Figure 9.19. LCOE from SAM



Figure 9.20. ISCC_87 and ISCC_81.09 LCOE difference

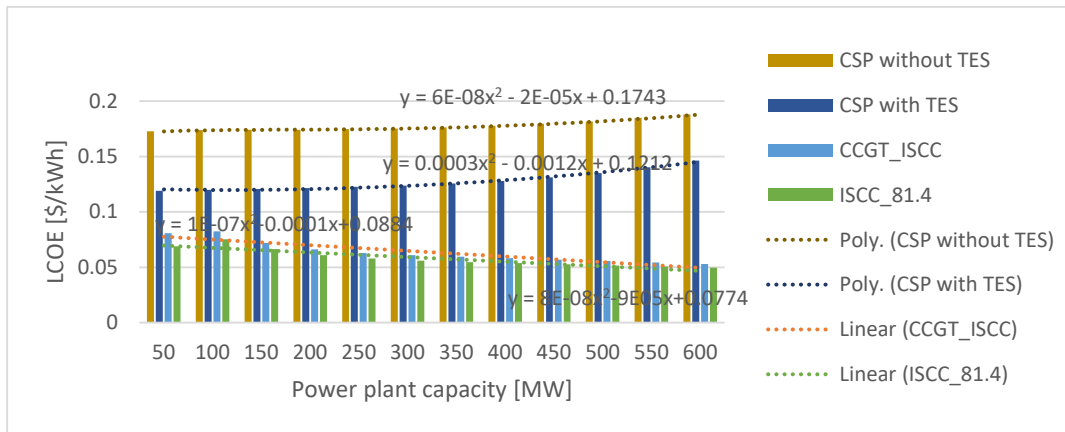


Figure 9.21. Levelized cost of electricity for different technologies

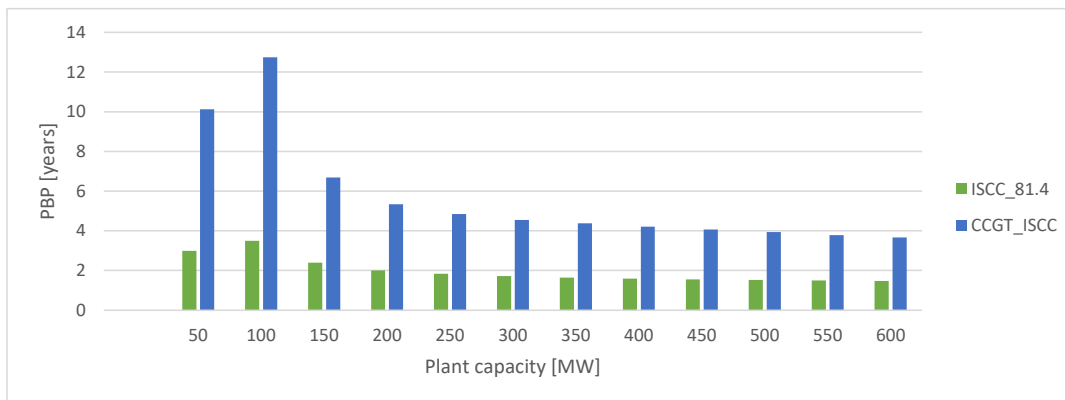


Figure 9.22. Payback period

9.6 Environmental Analysis

Solar energy produces 48 gCO₂eq/kWh during the early years of operation, and Figure 9.23 shows the kgCO₂eq produced by different capacities of the CSP PP. A CSP_{600MW} produces 78 and 75 times less CO₂eq/kWh than a CCGT_{600MW} and ISCC_{600MW} system, respectively (Figure 9.23 and Figure 9.24).

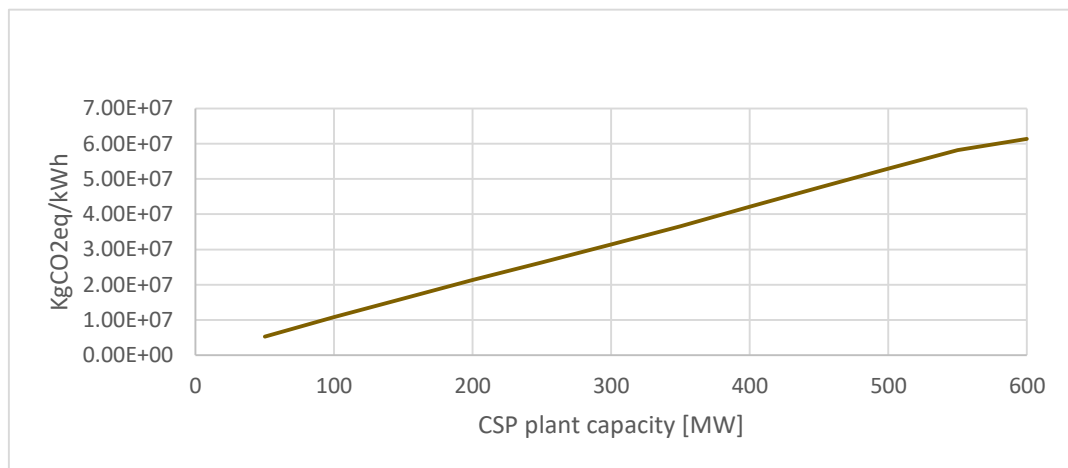


Figure 9.23. KgCO₂eq from CSP capacities

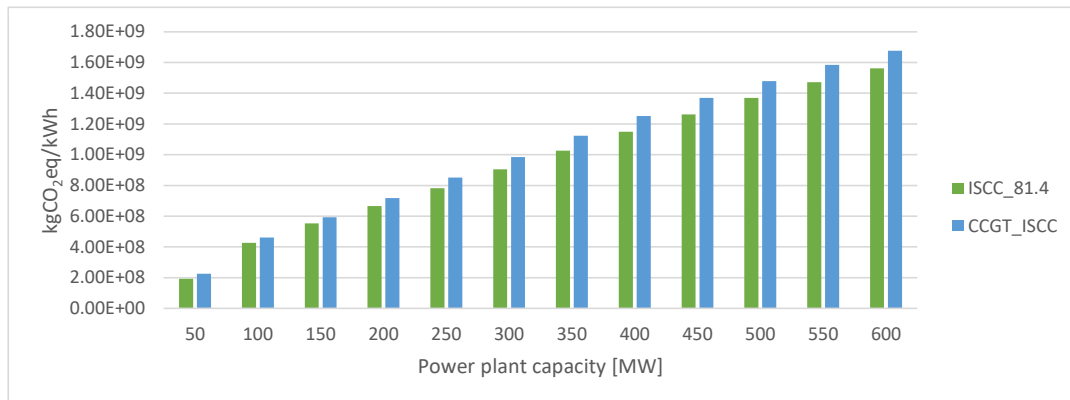


Figure 9.24. KgCO₂eq from different capacities of CCGT and ISCC processes

Currently, Zimbabwe has a total capacity of 1 190 MW for coal fueled power plants. Considering the information in Table 1.2, coal emits 0.82 kgCO₂eq/kWh. If the coal PPs operate at a capacity factor of 80 %, then they generate 8.34E+09 kWh/yr. (Equation 2.11)

releasing 6.84E+09 kgCO₂eq. The kgCO₂eq from the coal power plants in Zimbabwe would generate 4 times more kgCO₂eq released by the CCGT_{600MW} (Figure9.24). Overall, the ISCC system is more environmentally friendly than the coal and the CCGT power plants.

9.7 Economic Analysis - Updated

Considering EIA’s proposed carbon fee²⁵ of 0.015 \$/kg for CO₂ emissions [226], LCOE is given by Equation 2.9, the simplified version with the inclusion of the carbon fee is given by:

$$LCOE = \frac{Col \times Fcr + O\&M + Fc + Cf}{EG} \quad (9.1)$$

Where, *Col* is the cost of investment [\$], *Fcr* is the fixed charge ratio, *O&M* operation and maintenance cost [\$], *Fc* is the fuel cost [\$] (*considering that fuel is normally sold above the breakeven point, inclusive of drilling costs, cost of wells, O & M, pipeline infrastructure, etc., there was no need to estimate the individual entities of producing CBM from coal seams*), *Cf* is the carbon fee [\$], and *EG* is the electricity generation [kWh]. The updated LCOE values are provided in Figure 9.25.

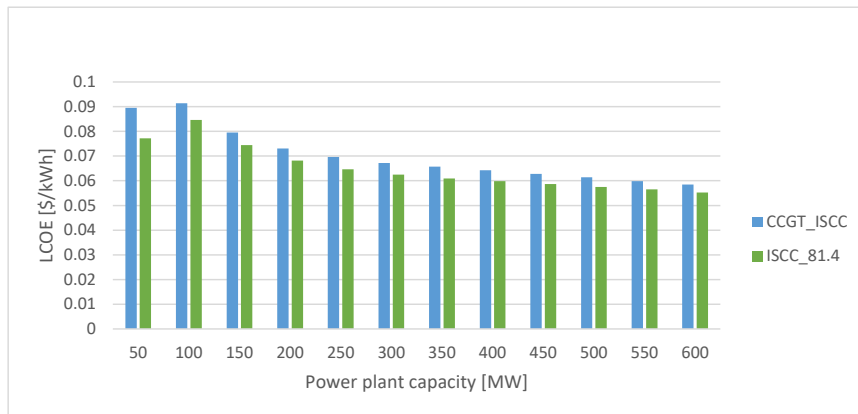


Figure 9.25. LCOE considering cost of CO₂ emissions

²⁵ Carbon fee: Proposed charges for the cost of burning fossil fuels.

The ISCC system generates electricity at the lowest prices and is preferable, even with the inclusion of CO₂ cost. The LCOE results for CCGT and ISCC systems range within the fossil fuel-fired power generation costs for the G20 countries, which range from 0.054 to 0.167 \$/kWh [227].

The LCOE calculations for the ISCC plant (Figs. 9.20 and 9.21) assumed a constant 10 % solar share of the plant's total capacity. However, the following estimations are performed to validate the best ISCC (CCGT+CSP) combination. A constant ISCC_{600MW} capacity (e.g. CCGT_{50MW} + CSP_{550MW}) is maintained, while changing the CCGT and CSP shares. Considering an example where the solar cycle contributes 550 MW while the CCGT cycle contributes 50 MW, the use of a constant capacity factor overestimates the ISCC plant's power output, thereby, underestimating the LCOE. This is because for example, Lupane has only an average of 8.3 daily solar hours, so, for 15.7 hours the ISCC plant's power output is from the CCGT_{50MW} cycle *only*. To eliminate those errors, current study adopts the use of the polynomial equations for the CCGT and CSP with TES plants from Figure 9.21:

From Figure 9.21 the LCOE equation for the CCGT plant is given by:

$$LCOE = 1E - 07 \times CCGT_{X_{MW}}^2 - 0.0001 \times CSP_{X_{MW}} + 0.0884 \quad (9.2)$$

Where, $CCGT_{X_{MW}}$ is the capacity of the CCGT cycle.

While, the LCOE equation for the CSP plant is given by:

$$LCOE = 6E - 08 \times CSP_{X_{MW}}^2 - 2E - 05 \times CSP_{X_{MW}} + 0.1743 \quad (9.3)$$

Where, $CSP_{X_{MW}}$ is the capacity of the CSP cycle.

The LCOE for the ISCC (CCGT+CSP) is the combination of Equations 9.2 and 9.3, such that when the ISCC combination is CSP_{0MW} + CCGT_{600MW}, the calculated LCOE is the cost of generating electricity from a CCGT_{600MW} as in Figure 9.21 and vice versa. The weighted average of Equations 9.1 and 9.2 is the LCOE for the CCGT+CSP capacity. Accordingly, Table 9.15 shows the ISCC combinations and the estimated LCOE values. The CCGT_{550MW} and CSP_{50MW} combination has the lowest LCOE value of 0.0728 \$/kWh. The solar share is 8.33 % of the PP capacity, validating the Breeze (2016) [101] assumption of less than 10 % solar share. Table 9.15 shows an increase in the LCOE with an increase in the solar cycle's

share, which suggests why it is important to validate the nominal operating conditions for solar thermal systems.

Table 9.15. LCOE for an ISCC system for different CCGT + CSP combinations

Power plant	CCGT cycle [MW]	Solar cycle [MW]	LCOE [\$/kWh]
CCGT	600	0	0.0644
ISCC	550	50	0.0728
ISCC	500	100	0.0817
ISCC	450	150	0.0909
ISCC	400	200	0.1005
ISCC	350	250	0.1104
ISCC	300	300	0.1206
ISCC	250	350	0.1309
ISCC	200	400	0.1414
ISCC	150	450	0.1520
ISCC	100	500	0.1627
ISCC	50	550	0.1733
CSP	0	600	0.1839

9.8 Finalized CBM-ISCC PP Evaluation

According to updated economic analysis, ISCC PP choice is settled on a 600 MW facility of CCGT_{550MW} and CSP_{50MW} combination. Table 9.16 shows PP properties as determined by EBSILON software. The gross aperture area needed for the CSP_{50MW} system is 0.2376 km², which is merely 0.0063 % of the land area found suitable for concentrating solar power in Lupane area (Section 9.3).

Table 9.16 The ISCC_{600MW} power plant properties determined by EBSILON

ISCC plant property	Value
GT capacity	376 MW
ST capacity (without solar input)	174.44 MW
Total ST capacity	224 MW
Solar thermal input	143.3 MW
Plant capacity	600 MW
Heat rate	8 150 BTUs/kWh
Capacity factor	81.4 %
Gross aperture area for CSP	0.2376 km ²
DNI	850 W/m ²
Number of PTCs	275
LCOE	0.0728 \$/kWh

From Table 9.16, the GT capacity of 376 MW has a heat rate of 8 150 BTUs/kWh. If the GT generates electricity at the ISCC plant's capacity factor of 81.4 %, then it generates 2.68E+09 kWh/year. Considering the 8 150 BTUs/kWh, the GT requires 2.19E+13 BTUs to generate 2.68E+09 kWh/year. If: 1 m³ = 35 915 BTUs, then the GT requires 6.08E+08 m³ of CBM per year (18.3 Bm³ for 30 years).

The CBM reserves estimated in Table 9.12 shows that the P90 reserves in Lupane are 125 Bm³, compared against the 18.3 Bm³ needed for 30 years lifespan of the proposed ISCC_{600MW}. Thus, there appears to be enough CBM to provide for the plant.

To estimate the number of wells supplying gas to the PP and their production rate at any given time, two scenarios are considered:

1. Production from coal seams without enhancement.
2. Production from hydraulically fractured beds (Section 5.11).

Table 9.17 shows the parameters used to estimate the decline curves for the two scenarios mentioned above.

Table 9.17. CBM production rate and well count parameters

Hwange-Lupane		Reference
coal seam property	Value	
Coal rank, CRk	CRk > High volatile A bituminous CRk < Subbituminous C	
q_i (no HF)	162.36 MSCFd	[150]
q_i with HF	600 MSCFd	[150]
Average depth	550 m [1 804 ft.]	[180] [198]
Decline rate	0.00029 %/day	[228]
b1	0	[148]
b2	0.4	[148]
b3	0.6	[152]

For unconventional resources such as CBM, to predict the flow rate of a well (with respect to time) in the decline stage (Sec. 5.9, Figs. 5.7 and 5.9), and to avoid extreme over prediction of reserves, typically Modified Arps equation is utilized. However, the limit after which the decline rate turns from hyperbolic to exponential is often based on experience or best guess [229]. Okuszko et al. (2007) [148] highlights that there is not much difference between CBM and conventional well decline behavior, such that CBM decline can be adequately modelled using the original Arps equation (Equations 5.12 and 5.13). Since decline stage is the predominant stage in a wells life, anticipated production rates, cumulative production, and number of wells needed by the proposed plant is estimated using Arps Equation in this study. Due to geological heterogeneity, we expect well initial rates and decline parameters to vary over the geographical area. To account for the uncertainty brought by geological heterogeneity we use three decline b values which represent the P10-50-90 of parameters for the field, values of which are obtained Table 9.17.

9.8.1 Well Count and Production Rates without HF Application

Results for a hypothetical CBM development in the Lupane region, without HF application in the wells, is given in Figure 9.26. Table 9.18 shows the tabulated results. From Table 9.18

b=0, b= 0.4 and b= 0.6 wells needed a total of 1 190, 968 and 899 wells, respectively, to meet the demand of 1.83E+10 m³ for 30 years.

Table 9.18. Arps CBM results for Lupane without HF

	$q(30\text{ years})$ [m ³ /d]	N_p (30years) [m ³]	Total number of wells
b=0	197.1 (6.96 MSCF/d)	1.53E+07	1 190
b=0.4	598.9 (21.15 MSCF/d)	1.88E+07	968
b=0.6	784 (27.69 MSCF/d)	2.03E+07	899

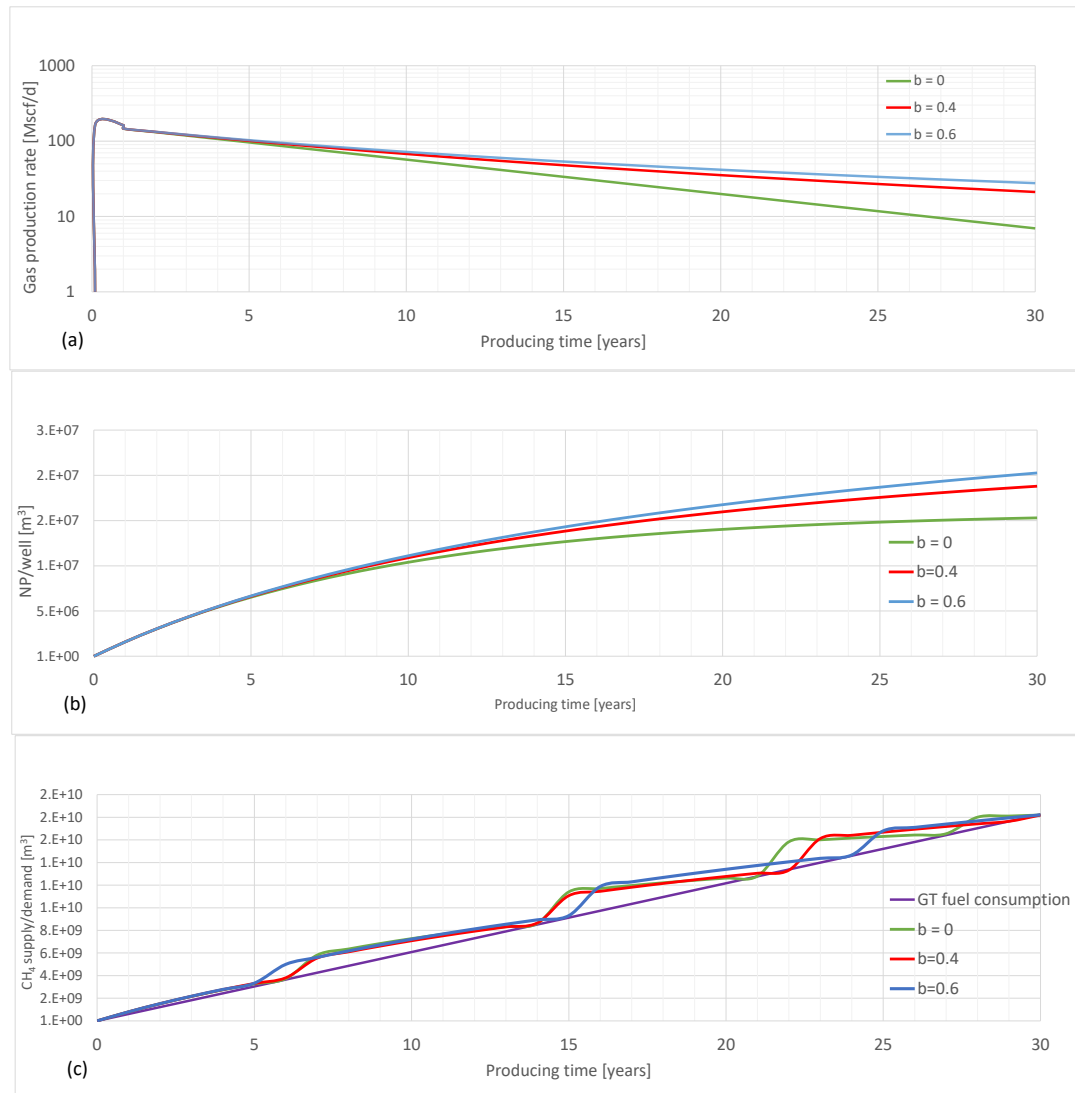


Figure 9.26. (a) Well's production rate with time, (b) A well's cumulative production, (c) Demand from GT vs. supply from the wells

9.8.2 Well Count and Production Rates with HF Application

If hydraulic fracturing is applied to the CBM wells, the initial production rate can be as high as 600 MSCFd [150]. Results for a hypothetical CBM development in the Lupane region, with HF application in the wells, is given in Figure 9.27. Table 9.19 shows the tabulated results. From Table 9.19 $b=0$, $b=0.4$ and $b=0.6$ wells needed a total of 322, 262 and 243 wells respectively, to meet the demand of $1.83E+10 \text{ m}^3$ for 30 years.

Table 9.19. Arps CBM results for Lupane with HF

	$q(30 \text{ years}) [\text{m}^3/\text{d}]$	$Np (30 \text{ years}) [\text{m}^3]$	Total number of wells
$b=0$	728.0 (25.71 MSCF/d)	$5.65E+07$	322
$b=0.4$	2 212.7 (78.14 MSCF/d)	$6.95E+07$	262
$b=0.6$	2 897.7 (102.33 MSCF/d)	$7.49E+07$	243

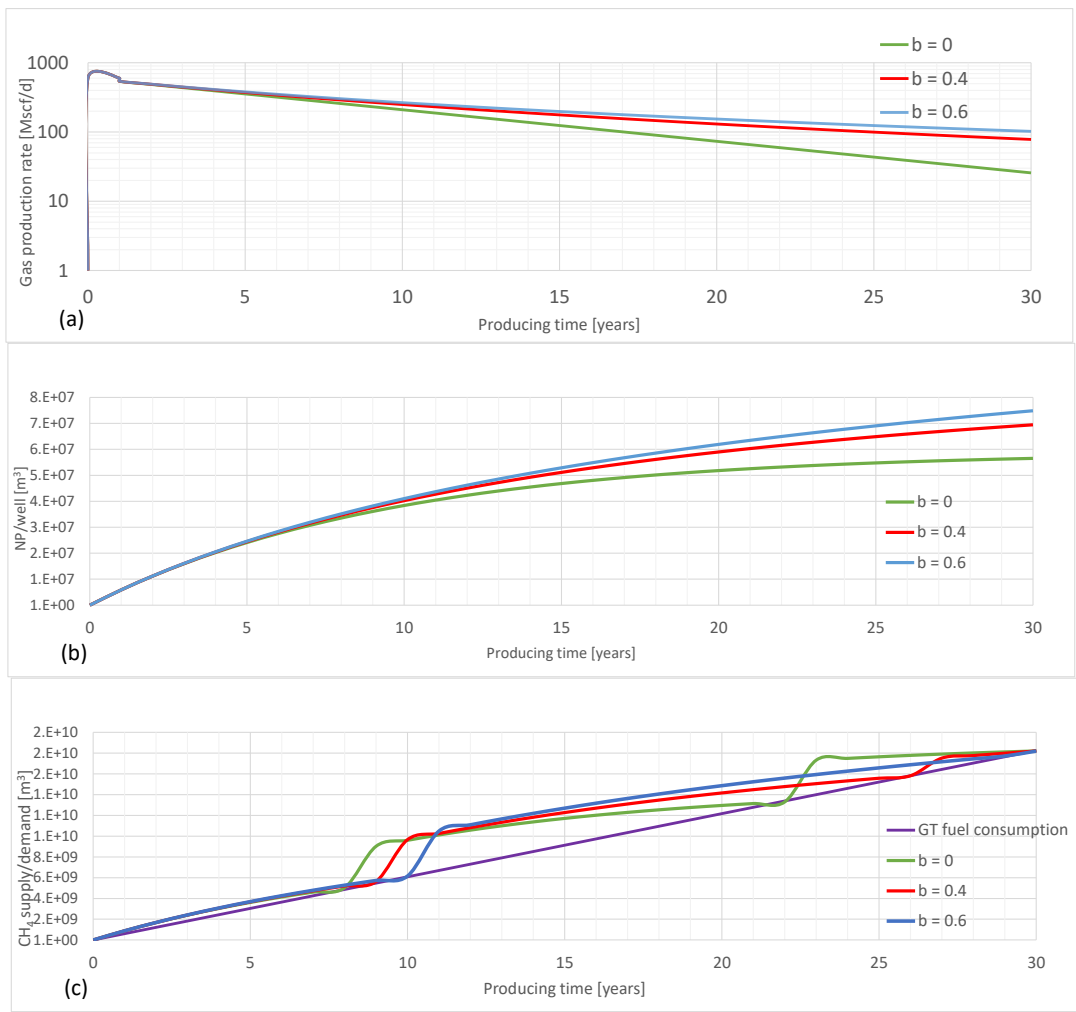


Figure 9.27. Well's production rate with time, (b) A well's cumulative production, (c) Demand from GT vs. supply from the wells

CHAPTER 10

CONCLUSIONS

This study was motivated by the increase of anthropogenic GHGs, consequent global climate change issue, power poverty in some parts of the world, and the pursuit of providing sustainable energy (as part of SDG7).

The North-Western region of landlocked South African country Zimbabwe is chosen as the area of focus, considering that the nation has suffered a fair share of climate change effects, receives adequate sun light for generating power, has a significant population with no access to electricity, and has mostly unsustainable power plants fueled by coal.

Various findings from this study are summarized as follows:

- 1) The OGIP of the North-Western region is estimated using the MCS. The coal bed methane resources range from 706 Bm³ to 5 699 Bm³.
- 2) A CBM site evaluation was conducted. Within the North-Western region of Zimbabwe, the Hwange-Lupane area was established as the zone with the most preferred parameters for CBM development.
- 3) Within the Hwange-Lupane area, a GIS-AHP analysis was conducted to determine the most preferred location for concentrating solar power. The theoretical CSP potential for the suitable area in Hwange (792 km² available for CSP) ranges from 529 to 696 TWh/year, and in Lupane (3 771 km² available for CSP) ranges from 1 207 to 1 613 TWh/year, respectively.
- 4) The CSP potential uncovered in this study proves that Zimbabwe has enough solar resources to shift to clean energy, considering application of solar technologies with heat and energy storage systems.
- 5) From this GIS-AHP analysis, it was determined that the Lupane region (the study area) was the best location for the ISCC system.

- 6) Accordingly, the CBM resources specific for Lupane is found to range from 250 to 1 400 Bm³. As expected the OGIP decreases going from full study area (North-Western region of Zimbabwe) to the specific Lupane area established to be suitable for both CSP & CBM, as the area becomes smaller.
- 7) A techno-economic-environmental analysis for CSP, CCGT, and ISCC systems was performed for the study area.
- 8) A 600 MW ISCC PP is proposed to generate electricity for the chosen study area.
- 9) The ISCC PP is compared with a standalone CSP PP, and standalone CCGT PP, and the coal-fired power plants in Zimbabwe.
- 10) Proposed ISCC PP only technically competes with the CCGT PP, where the latter generates 7 % more electricity than the former. ISCC proves to be more sustainable than the use of standalone CCGT, CSP or coal-fueled PP.
- 11) The CCGT generated the most power, followed by the ISCC system. The CSP system without TES and with TES generated 3 times and 2 times, respectively, less power output than the CCGT system. The low CSP power output is due to the short solar hours (averaging at 8.3 hours), low solar cycle efficiency (of approximately 35 %) and low capacity factors (ranging from 28 % to 47 % for CSP both with and without TES).
- 12) The best LCOE values for CSP, CCGT, and ISCC are found to be 0.1727 \$/kWh, 0.0529 \$/kWh, and 0.0495 \$/kWh, respectively. The arithmetic average cost of electricity from CSP, CCGT, and ISCC is 0.178 \$/kWh, 0.063 \$/kWh, and 0.0581 \$/kWh, respectively.
- 13) The LCOE range for the ISCC hybrid (0.050 \$/kWh – 0.069 \$/kWh) is less than that one of CCGT systems (0.053 \$/kWh – 0.081\$/kWh), indicating and supporting the sustainable use of the hybrid technology over CCGT.
- 14) The feasibility of ISCC PP was established by the resultant LCOE at 0.0728 \$/kWh, which is less than Zimbabwe's retail cost of electricity (0.12 \$/kWh).
- 15) The CCGT_{600MW} and ISCC_{600MW} investigated in this study respectively produce 48.6 % and 45.3 % more power than the 600 MW coal fired PP currently under construction in Hwange.

16) The kgCO₂eq from the coal power plants in Zimbabwe (Hwange, Munyati, Harare, and Bulawayo) would generate 4 times more kgCO₂eq released by the CCGT_{600MW}. Thus, overall, the ISCC system is more environmentally friendly than the coal and the CCGT power plants.

17) ISCC PP is proposed for the following reasons:

- It produces electricity at a more favorable price.
- The ISCC system introduces a better energy mix (introduces the adoption of CSP and CCGT systems in one facility)
- The ISCC system emits fewer GHGs than the CCGT and coal thermal systems.

18) Predicted CBM reserves are enough to replace coal in all thermal plants in Zimbabwe. Using both CBM and solar resources presents Zimbabwe with many advantages, including meeting all the objectives of SDG7 for a sustainable environment.

10.1 Recommendations

The estimation of the original gas in place was performed by taking parameters from Zimbabwe's neighboring countries because there was not enough available data in the study area. So, additional petrophysical studies are needed for improved estimations.

The results from the current study proved the feasibility of concentrating solar power in the Hwange-Lupane region of Zimbabwe. However, the current study integrated only 8.33 % solar share because of the uneconomical cost of electricity values obtained by increasing the solar capacity. Accordingly, additional feasibility studies on concentrated solar power with heat and energy storage could improve solar share in the ISCC.

The environmental results suggest that the CCGT and ISCC systems are preferred over coal thermal power plants. However, the two systems still emit considerable amounts of GHGs. Taking advantage of the storage capacities of coal seams and their potential to store CO₂, carbon capture and storage studies should be conducted to explore CO₂ storage potential in the region.

REFERENCES

- [1] P. Friedlingstein *et al.*, ‘Global Carbon Budget 2020’, *Earth Syst. Sci. Data*, vol. 12, no. 4, pp. 3269–3340, Dec. 2020, doi: 10.5194/essd-12-3269-2020.
- [2] I. V. Muralikrishna and V. Manickam, ‘Chapter Five - Life Cycle Assessment’, in *Environmental Management*, I. V. Muralikrishna and V. Manickam, Eds. Butterworth-Heinemann, 2017, pp. 57–75. doi: 10.1016/B978-0-12-811989-1.00005-1.
- [3] C. Le Quéré *et al.*, ‘The global carbon budget 1959–2011’, *Earth Syst. Sci. Data*, vol. 5, no. 1, pp. 165–185, May 2013, doi: 10.5194/essd-5-165-2013.
- [4] G. d’experts intergouvernemental sur l’évolution du climat W. G. II and I. P. on C. Change, *Climate Change 2007 - Impacts, Adaptation and Vulnerability: Working Group II Contribution to the Fourth Assessment Report of the IPCC*. Cambridge University Press, 2007.
- [5] K. Lambeck, A. Purcell, and A. Dutton, ‘The anatomy of interglacial sea levels: The relationship between sea levels and ice volumes during the Last Interglacial’, *Earth Planet. Sci. Lett.*, vol. 315–316, pp. 4–11, Jan. 2012, doi: 10.1016/j.epsl.2011.08.026.
- [6] H. Ritchie, M. Roser, and P. Rosado, ‘CO₂ and Greenhouse Gas Emissions’, *Our World Data*, May 2020, Accessed: Dec. 26, 2022. [Online]. Available: <https://ourworldindata.org/co2-emissions>
- [7] O. US EPA, ‘Sources of Greenhouse Gas Emissions’, Dec. 29, 2015. <https://www.epa.gov/ghgemissions/sources-greenhouse-gas-emissions> (accessed Dec. 26, 2022).
- [8] ‘Goal 7: Ensure access to affordable, reliable, sustainable and modern energy for all — SDG Indicators’. <https://unstats.un.org/sdgs/report/2016/goal-07/> (accessed Dec. 26, 2022).
- [9] ‘2022-forum-report.pdf’. Accessed: Dec. 26, 2022. [Online]. Available: <https://mo.ibrahim.foundation/sites/default/files/2022-07/2022-forum-report.pdf>
- [10] D. Eckstein, M.-L. Hutfils, and M. Wings, ‘GLOBAL CLIMATE RISK INDEX 2019’, 2019.
- [11] D. Jones, ‘Global Electricity Review 2022’, *Ember*, Mar. 29, 2022. <https://ember-climate.org/insights/research/global-electricity-review-2022/> (accessed Dec. 26, 2022).
- [12] A. Liebman and R. Gawler, ‘Baffled by baseload? Dumbfounded by dispatchables? Here’s a glossary of the energy debate’, *The Conversation*. <http://theconversation.com/baffled-by-baseload-dumbfounded-by-dispatchables-heres-a-glossary-of-the-energy-debate-84212> (accessed Dec. 26, 2022).
- [13] O. US EPA, ‘Centralized Generation of Electricity and its Impacts on the Environment’, Aug. 04, 2015. <https://www.epa.gov/energy/centralized-generation-electricity-and-its-impacts-environment> (accessed Dec. 26, 2022).
- [14] POWER, ‘History of Power: The Evolution of the Electric Generation Industry’, *POWER Magazine*, Oct. 01, 2022. <https://www.powermag.com/history-of-power-the-evolution-of-the-electric-generation-industry/> (accessed Dec. 29, 2022).
- [15] ‘Radiyozh’, *Medium*. <https://radiyozh.medium.com> (accessed Dec. 26, 2022).
- [16] O. Edenhofer *et al.*, Eds., *Climate Change 2014: Mitigation of Climate Change; Summary for Policymakers Technical Summary; Part of the Working Group III Contribution to the Fifth Assessment Report of the Intergovernmental Panel on Climate Change*. Geneva, Switzerland: Intergovernmental Panel on Climate Change, 2015.

- [17] ‘National Renewable Energy Laboratory (NREL) Home Page’. <https://www.nrel.gov/index.html> (accessed Dec. 26, 2022).
- [18] H. Ritchie, M. Roser, and P. Rosado, ‘Energy’, *Our World Data*, Oct. 2022, Accessed: Dec. 26, 2022. [Online]. Available: <https://ourworldindata.org/energy-access>
- [19] L. S. Langston, ‘Turbines, Gas☆’, in *Reference Module in Earth Systems and Environmental Sciences*, Elsevier, 2014. doi: 10.1016/B978-0-12-409548-9.09044-8.
- [20] A. Faghri and Y. Zhang, *Transport Phenomena in Multiphase Systems*. Elsevier, 2006.
- [21] ‘Comprehensive Renewable Energy’, *ScienceDirect*. <http://www.sciencedirect.com:5070/referencework/9780080878737/comprehensive-renewable-energy> (accessed Dec. 26, 2022).
- [22] ‘The Shift Data Portal’. <https://www.theshiftdataportal.org/> (accessed Dec. 26, 2022).
- [23] R. J. Bass, W. Malalasekera, P. Willmot, and H. K. Versteeg, ‘The impact of variable demand upon the performance of a combined cycle gas turbine (CCGT) power plant’, *Energy*, vol. 36, no. 4, pp. 1956–1965, Apr. 2011, doi: 10.1016/j.energy.2010.09.020.
- [24] K. Ijagbemi, *Sustainable Power Technology: A Viable Sustainable Energy Solution*. IntechOpen, 2017. doi: 10.5772/intechopen.70306.
- [25] ‘List of natural gas power stations’, *Wikipedia*. Aug. 22, 2022. Accessed: Dec. 29, 2022. [Online]. Available: https://en.wikipedia.org/w/index.php?title=List_of_natural_gas_power_stations&ol did=1105998965
- [26] ‘SGT5-8000H | H-class Gas Turbine | Gas Turbines | Manufacturer | Siemens Energy Global’, *siemens-energy.com Global Website*. <https://www.siemens-energy.com/global/en/offerings/power-generation/gas-turbines/sgt5-8000h.html> (accessed Dec. 26, 2022).
- [27] E.-E. E. Portal and vinod ramireddy, ‘An Overview of Combined Cycle Power Plant’, *EEP - Electrical Engineering Portal*, Aug. 25, 2012. <https://electrical-engineering-portal.com/an-overview-of-combined-cycle-power-plant> (accessed Dec. 26, 2022).
- [28] A. Behbahani-nia, S. Sayadi, and M. Soleymani, ‘Thermoeconomic optimization of the pinch point and gas-side velocity in heat recovery steam generators’, *Proc. Inst. Mech. Eng. Part J. Power Energy*, vol. 224, no. 6, pp. 761–771, Sep. 2010, doi: 10.1243/09576509JPE953.
- [29] P. Aref, ‘Development of a framework for thermoeconomic optimization of simple and combined gas-turbine cycles’, Nov. 2012, Accessed: Dec. 26, 2022. [Online]. Available: <https://dspace.lib.cranfield.ac.uk/handle/1826/7892>
- [30] V. Ganapathy, : *Design, Applications, and Calculations*. Boca Raton: CRC Press, 2002. doi: 10.1201/9780203910221.
- [31] A. Pasha and S. Jolly, ‘Combined cycle heat recovery steam generators optimum capabilities and selection criteria’, *Heat Recovery Syst. CHP*, vol. 15, no. 2, pp. 147–154, Feb. 1995, doi: 10.1016/0890-4332(95)90021-7.
- [32] ‘Modular HRSG Series Generator Boiler | Cleaver-Brooks’. <https://cleaverbrooks.com/Product/modular-hrsg> (accessed Dec. 26, 2022).
- [33] A. Abdollahian and M. Ameri, ‘Effect of supplementary firing on the performance of a combined cycle power plant’, *Appl. Therm. Eng.*, vol. 193, p. 117049, Jul. 2021, doi: 10.1016/j.applthermaleng.2021.117049.

- [34] R. Kehlhofer, ‘Combined-cycle gas and steam turbine power plants’, Jan. 1991, Accessed: Dec. 26, 2022. [Online]. Available: <https://www.osti.gov/biblio/5646323>
- [35] A. Larson, ‘Benefits of Single-Shaft Combined Cycle Power Plants’, 2018. <https://www.powermag.com/benefits-of-single-shaft-combined-cycle-power-plants/> (accessed Dec. 26, 2022).
- [36] O. US EPA, ‘EPA - TTN EMC - Spectral Database - Reports - Combine Cycle Gas-Fired Gas Turbine Emissions Test’. <https://www3.epa.gov/ttn/emc/ftir/reports/r08.html> (accessed Dec. 26, 2022).
- [37] ‘Frequently Asked Questions (FAQs) - U.S. Energy Information Administration (EIA)’. <https://www.eia.gov/tools/faqs/faq.php> (accessed Dec. 26, 2022).
- [38] ‘Frequently Asked Questions (FAQs) - U.S. Energy Information Administration (EIA)’. <https://www.eia.gov/tools/faqs/faq.php> (accessed Dec. 26, 2022).
- [39] ‘Power Plants - Performance Efficiencies’. https://www.engineeringtoolbox.com/power-plant-efficiency-d_960.html (accessed Dec. 26, 2022).
- [40] ‘ML120960701.pdf’. Accessed: Dec. 26, 2022. [Online]. Available: <https://www.nrc.gov/docs/ML1209/ML120960701.pdf>
- [41] ‘Levelized Costs of New Generation Resources in the Annual Energy Outlook 2022’, 2022.
- [42] D. Ray, ‘Lazard’s Levelized Cost of Energy Analysis—Version 15.0’, 2021.
- [43] G. J. Suppes and T. S. Storvick, Eds., ‘CHAPTER 7 - Production of Electricity’, in *Sustainable Nuclear Power*, Burlington: Academic Press, 2007, pp. 185–200. doi: 10.1016/B978-012370602-7/50024-7.
- [44] ‘Chapter 7 – Selecting the Power Plant | Elsevier Enhanced Reader’. <https://reader.elsevier.com/reader/sd/pii/B9780123973085000076?token=9E717A65ED73DD026485E113DD68C6020E7CC4B51A57F0312985455FC1AF52122E906B29224C4A5733AF81A62C559123&originRegion=eu-west-1&originCreation=20221226215722> (accessed Dec. 26, 2022).
- [45] V. Sarhosis, A. A. Jaya, and H. R. Thomas, ‘Economic modelling for coal bed methane production and electricity generation from deep virgin coal seams’, *Energy*, vol. 107, pp. 580–594, Jul. 2016, doi: 10.1016/j.energy.2016.04.056.
- [46] R. E. Hebner *et al.*, ‘Dynamic Load and Storage Integration’, *Proc. IEEE*, vol. 103, no. 12, pp. 2344–2354, Dec. 2015, doi: 10.1109/JPROC.2015.2457772.
- [47] H. Ruf *et al.*, *Analysis of physical coupling nodes of Hybrid Energy Grids*. 2015. doi: 10.13140/RG.2.1.3067.4647.
- [48] J. D. Wojcik and J. Wang, ‘Feasibility study of Combined Cycle Gas Turbine (CCGT) power plant integration with Adiabatic Compressed Air Energy Storage (ACAES)’, *Appl. Energy*, vol. 221, pp. 477–489, Jul. 2018, doi: 10.1016/j.apenergy.2018.03.089.
- [49] J. A. Duffie (Deceased), W. A. Beckman, and N. Blair, *Solar Engineering of Thermal Processes, Photovoltaics and Wind*, 1st ed. Wiley, 2020. doi: 10.1002/9781119540328.
- [50] J. E. Frederick, ‘OZONE DEPLETION AND RELATED TOPICS | Ozone as a UV Filter’, in *Encyclopedia of Atmospheric Sciences (Second Edition)*, G. R. North, J. Pyle, and F. Zhang, Eds. Oxford: Academic Press, 2015, pp. 359–363. doi: 10.1016/B978-0-12-382225-3.00296-6.
- [51] ‘Renewable Energy Resources | John Twidell, Tony Weir | Taylor & Francis’. <https://www.taylorfrancis.com/books/mono/10.4324/9781315766416/renewable-energy-resources-john-twidell-tony-weir> (accessed Dec. 27, 2022).

- [52] S. Vashishtha, ‘Differentiate between the DNI, DHI and GHI?’, Apr. 26, 2012. <https://firstgreenconsulting.wordpress.com/2012/04/26/differentiate-between-the-dni-dhi-and-ghi/> (accessed Dec. 27, 2022).
- [53] J. Spelling, ‘Hybrid Solar Gas-Turbine Power Plants : A Thermoeconomic Analysis’, 2013, Accessed: Dec. 27, 2022. [Online]. Available: <http://urn.kb.se/resolve?urn=urn:nbn:se:kth:diva-121315>
- [54] B. E, ‘On Electric Effects under the Influence of Solar Radiation’, *Compt Rend*, vol. 9, p. 561, 1839.
- [55] G. Abbe and H. Smith, ‘Technological development trends in Solar-powered Aircraft Systems’, *Renew. Sustain. Energy Rev.*, vol. 60, pp. 770–783, Jul. 2016, doi: 10.1016/j.rser.2016.01.053.
- [56] D. Lincot, ‘The new paradigm of photovoltaics: From powering satellites to powering humanity’, *Comptes Rendus Phys.*, vol. 18, no. 7, pp. 381–390, Sep. 2017, doi: 10.1016/j.crhy.2017.09.003.
- [57] W. G. Adams and R. E. Day, ‘V. The action of light on selenium’, *Proc. R. Soc. Lond.*, vol. 25, no. 171–178, pp. 113–117, Jan. 1877, doi: 10.1098/rspl.1876.0024.
- [58] C. E. Fritts, ‘On a new form of selenium cell, and some electrical discoveries made by its use’, *Am. J. Sci.*, vol. s3-26, no. 156, pp. 465–472, Dec. 1883, doi: 10.2475/ajs.s3-26.156.465.
- [59] W. Siemens, ‘On the electro motive action of illuminated selenium, discovered by Mr. Fritts, of New York’, *J. Frankl. Inst.*, vol. 119, no. 6, pp. 453-IN6, Jun. 1885, doi: 10.1016/0016-0032(85)90176-0.
- [60] E. F. Kingsbury and R. S. Ohl, ‘Photoelectric properties of ionically bombarded silicon’, *Bell Syst. Tech. J.*, vol. 31, no. 4, pp. 802–815, Jul. 1952, doi: 10.1002/j.1538-7305.1952.tb01407.x.
- [61] ‘Principle of Solar Cell | About Solar Energy | Our Solar Power Spirit | Solar Energy | Products | KYOCERA’, May 20, 2008. https://global.kyocera.com/prdct/solar/spirit/about_solar/cell.html (accessed Dec. 27, 2022).
- [62] SunPower, ‘How Much Energy Does a Solar Panel Produce?’, *SunPower - United States*, Jun. 24, 2019. <https://us.sunpower.com/solar-resources/how-much-energy-does-solar-panel-produce> (accessed Dec. 27, 2022).
- [63] O. M. Ai-Habahbeh, B. A. Ai-Hrout, E. M. Al-Hiary, and S. A. Ai-Fraihat, ‘Reliability investigation of photovoltaic cell using finite element modeling’, in *2013 9th International Symposium on Mechatronics and its Applications (ISMA)*, Apr. 2013, pp. 1–5. doi: 10.1109/ISMA.2013.6547391.
- [64] P. Sanjay, ‘With 2,245 MW of Commissioned Solar Projects, World’s Largest Solar Park is Now at Bhadla’, *Mercom India*, Mar. 19, 2020. <https://mercomindia.com/world-largest-solar-park-bhadla/> (accessed Dec. 27, 2022).
- [65] ‘Bhadla Solar Park, Jodhpur District, Rajasthan, India’. <https://www.nsenergybusiness.com/projects/bhadla-solar-park-rajasthan/> (accessed Dec. 27, 2022).
- [66] J. Zachary, ‘10 - Integrated solar combined cycle (ISCC) systems’, in *Combined Cycle Systems for Near-Zero Emission Power Generation*, A. D. Rao, Ed. Woodhead Publishing, 2012, pp. 283–305. doi: 10.1533/9780857096180.283.
- [67] J. Mbabazi Moyo, R. Krueger, and A. Von Wachenfelt, ‘Concentrated Solar Power (CSP) and Photovoltaic (PV): Has time come for solar energy in Africa?’, France, 2017.

- [68] A. Berrada, K. Loudiyi, and R. El Mrabet, 'Chapter 1 - Introduction to hybrid energy systems', in *Hybrid Energy System Models*, A. Berrada and R. El Mrabet, Eds. Academic Press, 2021, pp. 1–43. doi: 10.1016/B978-0-12-821403-9.00001-9.
- [69] A. Aktaş and Y. Kirçiçek, 'Chapter 3 - Why Solar Hybrid System?', in *Solar Hybrid Systems*, A. Aktaş and Y. Kirçiçek, Eds. Academic Press, 2021, pp. 47–68. doi: 10.1016/B978-0-323-88499-0.00003-3.
- [70] International Energy Agency, *Technology Roadmap: Concentrating Solar Power*. OECD Publishing, 2010. doi: 10.1787/9789264088139-en.
- [71] Z. Rao, C. Peng, Y. Wang, Y. Wang, G. Liu, and S. Liao, 'Response behaviors of CO₂ transcritical Rankine cycle based parabolic trough solar power plant to cloud disturbance', *Appl. Therm. Eng.*, vol. 189, p. 116722, May 2021, doi: 10.1016/j.applthermaleng.2021.116722.
- [72] M. T. Islam, N. Huda, A. B. Abdullah, and R. Saidur, 'A comprehensive review of state-of-the-art concentrating solar power (CSP) technologies: Current status and research trends', *Renew. Sustain. Energy Rev.*, vol. 91, pp. 987–1018, Aug. 2018, doi: 10.1016/j.rser.2018.04.097.
- [73] A. Poullikkas, I. Hadjipaschalis, and G. Kourtis, 'A comparative overview of wet and dry cooling systems for Rankine cycle based CSP plants'.
- [74] H. Akbari *et al.*, 'Efficient energy storage technologies for photovoltaic systems', *Sol. Energy*, vol. 192, pp. 144–168, Nov. 2019, doi: 10.1016/j.solener.2018.03.052.
- [75] H. Ibrahim, R. Beguenane, and A. Merabet, 'Technical and financial benefits of electrical energy storage', in *2012 IEEE Electrical Power and Energy Conference*, Oct. 2012, pp. 86–91. doi: 10.1109/EPEC.2012.6474985.
- [76] A. Maronga, K. J. Nyoni, P. G. Tuohy, and A. Shane, 'Evaluation of PV and CSP Systems to Supply Power in the Zimbabwe Mining Sector', *Energies*, vol. 14, no. 13, Art. no. 13, Jan. 2021, doi: 10.3390/en14133740.
- [77] A. Boretti and S. Castelletto, 'Cost and performance of CSP and PV plants of capacity above 100 MW operating in the United States of America', *Renew. Energy Focus*, vol. 39, pp. 90–98, Dec. 2021, doi: 10.1016/j.ref.2021.07.006.
- [78] G. Ghasemi, Y. Noorollahi, H. Alavi, M. Marzband, and M. Shahbazi, 'Theoretical and technical potential evaluation of solar power generation in Iran', *Renew. Energy*, vol. 138, pp. 1250–1261, Aug. 2019, doi: 10.1016/j.renene.2019.02.068.
- [79] L. Sun *et al.*, 'A GIS-based multi-criteria decision making method for the potential assessment and suitable sites selection of PV and CSP plants', *Resour. Conserv. Recycl.*, vol. 168, p. 105306, May 2021, doi: 10.1016/j.resconrec.2020.105306.
- [80] M. B. Alqaderi, W. Emar, and O. A., 'Concentrated Solar Power Site Suitability using GIS-MCDM Technique taken UAE as a Case Study', *Int. J. Adv. Comput. Sci. Appl.*, vol. 9, no. 4, 2018, doi: 10.14569/IJACSA.2018.090440.
- [81] B. Haddad, P. Díaz-Cuevas, P. Ferreira, A. Djebli, and J. P. Pérez, 'Mapping concentrated solar power site suitability in Algeria', *Renew. Energy*, vol. 168, pp. 838–853, May 2021, doi: 10.1016/j.renene.2020.12.081.
- [82] A. Alami Merrouni, F. Elwali Elalaoui, A. Ghennioui, A. Mezrhab, and A. Mezrhab, 'A GIS-AHP combination for the sites assessment of large-scale CSP plants with dry and wet cooling systems. Case study: Eastern Morocco', *Sol. Energy*, vol. 166, pp. 2–12, May 2018, doi: 10.1016/j.solener.2018.03.038.
- [83] 'Estimating the Renewable Energy Potential in Morocco: solar energy as a case study - IOPscience'. <https://iopscience.iop.org/article/10.1088/1755-1315/161/1/012015/meta> (accessed Dec. 27, 2022).

- [84] A. Aly, S. S. Jensen, and A. B. Pedersen, ‘Solar power potential of Tanzania: Identifying CSP and PV hot spots through a GIS multicriteria decision making analysis’, *Renew. Energy*, vol. 113, pp. 159–175, Dec. 2017, doi: 10.1016/j.renene.2017.05.077.
- [85] M. Giamalaki and T. Tsoutsos, ‘Sustainable siting of solar power installations in Mediterranean using a GIS/AHP approach’, *Renew. Energy*, vol. 141, pp. 64–75, Oct. 2019, doi: 10.1016/j.renene.2019.03.100.
- [86] T. L. Saaty and L. G. Vargas, ‘Estimating technological coefficients by the analytic hierarchy process’, *Socioecon. Plann. Sci.*, vol. 13, no. 6, pp. 333–336, 1979.
- [87] ‘saaty1.pdf’. Accessed: Dec. 27, 2022. [Online]. Available: <http://www.cashflow88.com/decisiones/saaty1.pdf>
- [88] H. do N. Camelo, P. S. Lucio, J. B. V. Leal Junior, P. C. M. de Carvalho, and D. von G. dos Santos, ‘Innovative hybrid models for forecasting time series applied in wind generation based on the combination of time series models with artificial neural networks’, *Energy*, vol. 151, pp. 347–357, May 2018, doi: 10.1016/j.energy.2018.03.077.
- [89] K. Dykes *et al.*, ‘Opportunities for Research and Development of Hybrid Power Plants’, National Renewable Energy Lab. (NREL), Golden, CO (United States), NREL/TP-5000-75026, May 2020. doi: 10.2172/1659803.
- [90] Z. Wang and L. Duan, ‘Study on integrated solar combined cycle system with a new operation strategy of changeable integration mode under different Direct Normal Irradiance (DNI) conditions’, *Energy Sci. Eng.*, vol. 8, no. 8, pp. 2907–2921, 2020, doi: 10.1002/ese3.711.
- [91] ‘Egypt’s First Solar Thermal Power Plant - Ambassador report - Our Actions - Tunza Eco Generation’. <https://tunza.eco-generation.org/ambassadorReportView.jsp?viewID=42610> (accessed Dec. 27, 2022).
- [92] A. Rovira *et al.*, ‘Comparison of Different Technologies for Integrated Solar Combined Cycles: Analysis of Concentrating Technology and Solar Integration’, *Energies*, vol. 11, no. 5, Art. no. 5, May 2018, doi: 10.3390/en11051064.
- [93] L. Duan, Z. Wang, and Y. Guo, ‘Off-design performance characteristics study on ISCC system with solar direct steam generation system’, *Energy*, vol. 205, p. 118044, Aug. 2020, doi: 10.1016/j.energy.2020.118044.
- [94] A. Z. Abass and D. A. Pavlyuchenko, ‘Turning Iraq into a country of energy exporter through the exploitation of solar energy and vast desert land’, *E3S Web Conf.*, vol. 114, p. 05009, 2019, doi: 10.1051/e3sconf/201911405009.
- [95] A. Z. Abass and D. A. Pavlyuchenko, ‘Southern Iraq gas station conversation to integrated solar combined cycle’, *E3S Web Conf.*, vol. 114, p. 05008, 2019, doi: 10.1051/e3sconf/201911405008.
- [96] G. C. Bakos and D. Parsa, ‘Technoeconomic assessment of an integrated solar combined cycle power plant in Greece using line-focus parabolic trough collectors’, *Renew. Energy*, vol. 60, pp. 598–603, Dec. 2013, doi: 10.1016/j.renene.2013.05.025.
- [97] Z. Zhang, L. Duan, Z. Wang, and Y. Ren, ‘General performance evaluation method of integrated solar combined cycle (ISCC) system’, *Energy*, vol. 240, p. 122472, Feb. 2022, doi: 10.1016/j.energy.2021.122472.
- [98] H. Nezammahalleh, F. Farhadi, and M. Tanhaemami, ‘Conceptual design and techno-economic assessment of integrated solar combined cycle system with DSG technology’, *Sol. Energy*, vol. 84, no. 9, pp. 1696–1705, Sep. 2010, doi: 10.1016/j.solener.2010.05.007.

- [99] N. Abdelhafidi, N. E. I. Bachari, Z. Abdelhafidi, A. Cheknane, A. Mokhnache, and L. Castro, 'Modeling of integrated solar combined cycle power plant (ISCC) of Hassi R'mel, Algeria', *Int. J. Energy Sect. Manag.*, vol. 14, no. 3, pp. 505–526, Jan. 2020, doi: 10.1108/IJESM-08-2018-0013.
- [100] Y. Li and Y. Xiong, 'Thermo-economic analysis of a novel cascade integrated solar combined cycle system', *Energy*, vol. 145, pp. 116–127, Feb. 2018, doi: 10.1016/j.energy.2017.12.128.
- [101] P. Breeze, 'Chapter 7 - Combined Cycle Power Plants', in *Gas-Turbine Power Generation*, P. Breeze, Ed. Academic Press, 2016, pp. 65–75. doi: 10.1016/B978-0-12-804005-8.00007-0.
- [102] B. Kelly, U. Herrmann, and M. J. Hale, 'Optimization Studies for Integrated Solar Combined Cycle Systems', presented at the ASME 2001 Solar Engineering: International Solar Energy Conference (FORUM 2001: Solar Energy — The Power to Choose), Mar. 2020, pp. 393–398. doi: 10.1115/SED2001-150.
- [103] Y. Li, N. Zhang, and N. Lior, 'Performance comparison of two low-CO₂ emission solar/methanol hybrid combined cycle power systems', *Appl. Energy*, vol. 155, pp. 740–752, Oct. 2015, doi: 10.1016/j.apenergy.2015.06.052.
- [104] S. Adibhatla and S. C. Kaushik, 'Energy, exergy and economic (3E) analysis of integrated solar direct steam generation combined cycle power plant', *Sustain. Energy Technol. Assess.*, vol. 20, pp. 88–97, Apr. 2017, doi: 10.1016/j.seta.2017.01.002.
- [105] S. Wang, Z. Fu, G. Zhang, and T. Zhang, 'Advanced Thermodynamic Analysis Applied to an Integrated Solar Combined Cycle System', *Energies*, vol. 11, no. 6, Art. no. 6, Jun. 2018, doi: 10.3390/en11061574.
- [106] M. J. Economides and D. A. Wood, 'The state of natural gas', *J. Nat. Gas Sci. Eng.*, vol. 1, no. 1, pp. 1–13, Jul. 2009, doi: 10.1016/j.jngse.2009.03.005.
- [107] T. A. Moore, 'Coalbed methane: A review', *Int. J. Coal Geol.*, vol. 101, pp. 36–81, Nov. 2012, doi: 10.1016/j.coal.2012.05.011.
- [108] 'Coal Bed Methane Market Size | Industry Report, 2020-2027'. <https://www.grandviewresearch.com/industry-analysis/coal-bed-methane-industry> (accessed Dec. 27, 2022).
- [109] '218EWGEffective-Coalbed-Methane-CBM-Recovery-Technologies-for-APEC-Developing-Economies.pdf'. Accessed: Dec. 27, 2022. [Online]. Available: <https://www.apec.org/docs/default-source/Publications/2018/9/Effective-Coalbed-Methane-Recovery-Technologies-for-APEC-Developing-Economies/218EWGEffective-Coalbed-Methane-CBM-Recovery-Technologies-for-APEC-Developing-Economies.pdf>
- [110] 'Coal explained - U.S. Energy Information Administration (EIA)'. <https://www.eia.gov/energyexplained/coal/> (accessed Dec. 27, 2022).
- [111] D. D. Rice, 'AAPG Studies in Geology #38'.
- [112] R. M. Flores, 'Coalbed methane: From hazard to resource', *Int. J. Coal Geol.*, vol. 35, no. 1, pp. 3–26, Feb. 1998, doi: 10.1016/S0166-5162(97)00043-8.
- [113] A. G. Kim and L. J. Douglas, *Hydrocarbon Gases Produced in a Simulated Swamp Environment*. U.S. Department of Interior, Bureau of Mines, 1972.
- [114] J. Ayoub, L. Colson, J. Hinkel, D. Johnston, and J. Levine, 'Learning to produce coalbed methane', *Oilfield Rev. Neth.*, vol. 3:1, Jan. 1991, Accessed: Dec. 27, 2022. [Online]. Available: <https://www.osti.gov/etdeweb/biblio/5913462>
- [115] D. L. Gautier, G. L. Dolton, K. I. Takahashi, and K. L. Varnes, '1995 National Assessment of United States oil and gas resources: Results, methodology, and

- supporting data', U.S. Geological Survey, USGS Numbered Series 30, 1996. doi: 10.3133/ds30.
- [116] Q. Hu, Y. Xie, C. Feng, and Z. Zhang, 'Fractal-like kinetics of adsorption on heterogeneous surfaces in the fixed-bed column', *Chem. Eng. J.*, vol. 358, pp. 1471–1478, Feb. 2019, doi: 10.1016/j.cej.2018.10.165.
- [117] K. Srinivasan, B. B. Saha, K. C. Ng, P. Dutta, and M. Prasad, 'A method for the calculation of the adsorbed phase volume and pseudo-saturation pressure from adsorption isotherm data on activated carbon', *Phys. Chem. Chem. Phys.*, vol. 13, no. 27, pp. 12559–12570, Jun. 2011, doi: 10.1039/C1CP20383E.
- [118] S. Mokhtab, W. A. Poe, and J. Y. Mak, 'Natural Gas Dehydration and Mercaptans Removal', pp. 307–348, 2019, doi: 10.1016/B978-0-12-815817-3.00009-5.
- [119] Y. Cai, D. Liu, Y. Yao, J. Li, and Y. Qiu, 'Geological controls on prediction of coalbed methane of No. 3 coal seam in Southern Qinshui Basin, North China', *Int. J. Coal Geol.*, vol. 88, no. 2, pp. 101–112, Nov. 2011, doi: 10.1016/j.coal.2011.08.009.
- [120] I. Langmuir, 'THE ADSORPTION OF GASES ON PLANE SURFACES OF GLASS, MICA AND PLATINUM.', *ACS Publications*, May 01, 2002. <https://pubs.acs.org/doi/pdf/10.1021/ja02242a004> (accessed Dec. 27, 2022).
- [121] K. Aminian and G. Rodvelt, 'Chapter 4 - Evaluation of Coalbed Methane Reservoirs', in *Coal Bed Methane*, P. Thakur, S. Schatzel, and K. Aminian, Eds. Oxford: Elsevier, 2014, pp. 63–91. doi: 10.1016/B978-0-12-800880-5.00004-8.
- [122] 'G4-Gippsland-gas-prospectivity-report-June-2015.pdf'. Accessed: Dec. 27, 2022. [Online]. Available: https://earthresources.vic.gov.au/__data/assets/pdf_file/0006/456738/G4-Gippsland-gas-prospectivity-report-June-2015.pdf
- [123] C. Xu, L. Qin, K. Wang, H. Sun, and M. Cao, 'Gas seepage laws based on dual porosity and dual permeability: Numerical simulation and coalbed methane extraction practice', *Energy Sci. Eng.*, vol. 9, no. 4, pp. 509–519, 2021, doi: 10.1002/ese3.871.
- [124] SPE, 'petroleum-resources-classification-system-definitions', 2003. <https://www.spe.org/en/industry/petroleum-resources-classification-system-definitions/> (accessed Dec. 27, 2022).
- [125] J. Richardson and W. Yu, 'Calculation of Estimated Ultimate Recovery and Recovery Factors of Shale-Gas Wells Using a Probabilistic Model of Original Gas in Place', *SPE Reserv. Eval. Eng.*, vol. 21, no. 03, pp. 638–653, Feb. 2018, doi: 10.2118/189461-PA.
- [126] I. O. Obielum, P. U. Giegbefumwen, and P. O. Ogbeide, 'A P/Z Plot For Estimating Original Gas in Place in a Geo-pressured Gas Reservoir By The Use of A Modified Material Balance Equation', presented at the SPE Nigeria Annual International Conference and Exhibition, Aug. 2015. doi: 10.2118/178354-MS.
- [127] M. B. Haq and M. K. Rahman, 'A Comparative Study of Three Methods for Estimating Initial Gas-in-place in Gas Fields in Bangladesh', *Pet. Sci. Technol.*, vol. 26, no. 5, pp. 532–544, Mar. 2008, doi: 10.1080/10916460600809865.
- [128] A. Haris, M. Novriyani, S. Suparno, R. Hidayat, and A. Riyanto, 'Integrated seismic stochastic inversion and multi-attributes to delineate reservoir distribution: Case study MZ fields, Central Sumatra Basin', *AIP Conf. Proc.*, vol. 1862, no. 1, p. 030180, Jul. 2017, doi: 10.1063/1.4991284.
- [129] A. Haris, H. A. Almunawwar, A. Riyanto, and A. Bachtiar, 'Shale Hydrocarbon Potential of Brown Shale, Central Sumatra Basin Based on Seismic and Well Data

- Analysis', *IOP Conf. Ser. Earth Environ. Sci.*, vol. 62, no. 1, p. 012018, Apr. 2017, doi: 10.1088/1755-1315/62/1/012018.
- [130] A. Altowilib, A. AlSaihati, H. Alhamood, S. Alafnan, and S. Alarifi, 'Reserves Estimation for Coalbed Methane Reservoirs: A Review', *Sustainability*, vol. 12, no. 24, Art. no. 24, Jan. 2020, doi: 10.3390/su122410621.
- [131] Z. Wang and X. Tang, 'New Insights from Supercritical Methane Adsorption in Coal: Gas Resource Estimation, Thermodynamics, and Engineering Application', *Energy Fuels*, vol. 32, no. 4, pp. 5001–5009, Apr. 2018, doi: 10.1021/acs.energyfuels.8b00477.
- [132] 'Petroleum-Resources-Management-System-2007.pdf'. Accessed: Dec. 27, 2022. [Online]. Available: <https://www.spe.org/industry/docs/Petroleum-Resources-Management-System-2007.pdf>
- [133] Z. Komlosi, 'How to Measure Exploration-Production Efficiency', presented at the SPE Annual Technical Conference and Exhibition, Oct. 1999. doi: 10.2118/56458-MS.
- [134] B. Thander, A. Sircar, and G. P. Karmakar, 'Hydrocarbon Resource Estimation: Application of Monte Carlo Simulation', 2014.
- [135] M. K. Verma, 'Fundamentals of Carbon Dioxide-Enhanced Oil Recovery (CO₂-EOR)—A Supporting Document of the Assessment Methodology for Hydrocarbon Recovery Using CO₂-EOR Associated with Carbon Sequestration', Open-File Report, 2015. [Online]. Available: <https://pubs.usgs.gov/of/2015/1071/pdf/ofr2015-1071.pdf>
- [136] P. C. Thakur, H. G. Little, and W. G. Karis, 'Global coalbed methane recovery and use', *Energy Convers. Manag.*, vol. 37, no. 6, pp. 789–794, Jun. 1996, doi: 10.1016/0196-8904(95)00257-X.
- [137] M. Mazzotti, R. Pini, and G. Storti, 'Enhanced coalbed methane recovery', *J. Supercrit. Fluids*, vol. 47, no. 3, pp. 619–627, Jan. 2009, doi: 10.1016/j.supflu.2008.08.013.
- [138] Y. Qin, T. A. Moore, J. Shen, Z. Yang, Y. Shen, and G. Wang, 'Resources and geology of coalbed methane in China: a review', *Int. Geol. Rev.*, vol. 60, no. 5–6, pp. 777–812, Apr. 2018, doi: 10.1080/00206814.2017.1408034.
- [139] 'Potential for Enhanced coalbed methane recovery -ccc252.pdf'. Accessed: Dec. 27, 2022. [Online]. Available: <https://usea.org/sites/default/files/media/Potential%20for%20Enhanced%20coalbed%20methane%20recovery%20-ccc252.pdf>
- [140] X. G. Zhang, P. G. Ranjith, M. S. A. Perera, A. S. Ranathunga, and A. Haque, 'Gas Transportation and Enhanced Coalbed Methane Recovery Processes in Deep Coal Seams: A Review', *Energy Fuels*, vol. 30, no. 11, pp. 8832–8849, Nov. 2016, doi: 10.1021/acs.energyfuels.6b01720.
- [141] N. S. Goraya, N. Rajpoot, and B. Marriyappan Sivagnanam, 'Coal Bed Methane Enhancement Techniques: A Review', *ChemistrySelect*, vol. 4, no. 12, pp. 3585–3601, 2019, doi: 10.1002/slct.201803633.
- [142] A. Wahid, F. A. Putra, M. T. Hidayat, and M. Yusuf, 'Enhanced coal bed methane (ECBM) recovery: optimization of CBM production using different injected gas composition and rate for south sumatra CBM field, Indonesia', *E3S Web Conf.*, vol. 67, p. 03015, 2018, doi: 10.1051/e3sconf/20186703015.
- [143] V. Prabhakaran, '(8) Cone Meters - Coalbed Methane Measurement | LinkedIn'. <https://www.linkedin.com/pulse/cone-meters-coalbed-methane-measurement-vaisak-prabhakaran/> (accessed Dec. 27, 2022).

- [144] ‘Black Diamond Energy Coalbed Methane’. <https://www.blackdiamondenergy.com/coalbed2.html> (accessed Dec. 27, 2022).
- [145] ‘KGS Pub. Inf. Circ. 19--Part 1 of 3’. https://www.kgs.ku.edu/Publications/pic19/pic19_1.html (accessed Dec. 27, 2022).
- [146] T. Cai, Z. Feng, Y. Jiang, and D. Zhao, ‘Thermodynamic Characteristics of Methane Adsorption of Coal with Different Initial Gas Pressures at Different Temperatures’, *Adv. Mater. Sci. Eng.*, vol. 2019, p. e4751209, Mar. 2019, doi: 10.1155/2019/4751209.
- [147] H. Wang, H. Merry, G. Amorer, and B. Kong, ‘Enhance Hydraulic Fractured Coalbed Methane Recovery by Thermal Stimulation’, presented at the SPE/CSUR Unconventional Resources Conference, Oct. 2015. doi: 10.2118/175927-MS.
- [148] K. E. Okuszko, B. W. Gault, and L. Mattar, ‘Production Decline Performance of CBM Wells’, presented at the Canadian International Petroleum Conference, Jun. 2007. doi: 10.2118/2007-078.
- [149] P. Thakur, ‘14 - Gas production and decline from vertical wells’, in *Coal Bed Methane (Second Edition)*, P. Thakur, S. J. Schatzel, K. Aminian, G. Rodvelt, M. H. Mosser, and J. S. D’Amico, Eds. Elsevier, 2020, pp. 255–266. doi: 10.1016/B978-0-12-815997-2.00014-7.
- [150] P. Thakur, S. J. Schatzel, K. Aminian, G. Rodvelt, M. H. Mosser, and J. S. D’Amico, *Coal Bed Methane: Theory and Applications*. Elsevier, 2020.
- [151] J. J. Arps, ‘Analysis of Decline Curves’, *Trans. AIME*, vol. 160, no. 01, pp. 228–247, Dec. 1945, doi: 10.2118/945228-G.
- [152] S. Yang, Y. Kang, Q. Zhao, H. Wang, and J. Li, ‘Method for predicting economic peak yield for a single well of coalbed methane’, *J. China Univ. Min. Technol.*, vol. 18, no. 4, pp. 521–526, Dec. 2008, doi: 10.1016/S1006-1266(08)60287-4.
- [153] C. H. Sondergeld, K. E. Newsham, J. T. Comisky, M. C. Rice, and C. S. Rai, ‘Petrophysical Considerations in Evaluating and Producing Shale Gas Resources’, presented at the SPE Unconventional Gas Conference, Feb. 2010. doi: 10.2118/131768-MS.
- [154] ‘Zimbabwe CO2 Emissions - Worldometer’. <https://www.worldometers.info/co2-emissions/zimbabwe-co2-emissions/> (accessed Dec. 27, 2022).
- [155] A. Maviza and F. Ahmed, ‘Climate change/variability and hydrological modelling studies in Zimbabwe: a review of progress and knowledge gaps’, *SN Appl. Sci.*, vol. 3, no. 5, p. 549, Apr. 2021, doi: 10.1007/s42452-021-04512-9.
- [156] A. Brazier, *Climate change in Zimbabwe: facts for planners and decision makers*. Harare: Konrad-Adenauer-Stiftung, 2015.
- [157] ‘National_Renewable_Energy_Policy_Final.pdf’. Accessed: Dec. 27, 2022. [Online]. Available: https://www.zera.co.zw/National_Renewable_Energy_Policy_Final.pdf
- [158] ‘Zimbabwe CO2 Emissions - Worldometer’. <https://www.worldometers.info/co2-emissions/zimbabwe-co2-emissions/> (accessed Dec. 27, 2022).
- [159] N. Louis and T. H. Mathew, ‘COVID-19 Pandemic: A Threat Towards Achieving the Sustainable Development Goal on Combating Climate Change and Its Impacts in Zimbabwe’s Rural Communities’, in *Sustainable Development in Africa: Fostering Sustainability in one of the World’s Most Promising Continents*, W. Leal Filho, R. Pretorius, and L. O. de Sousa, Eds. Cham: Springer International Publishing, 2021, pp. 507–522. doi: 10.1007/978-3-030-74693-3_28.

- [160] 'Access to electricity (% of population) - Zimbabwe | Data'. <https://data.worldbank.org/indicator/EG.ELC.ACCS.ZS?locations=ZW> (accessed Dec. 27, 2022).
- [161] E. F. Chipango, 'Constructing, understanding and interpreting energy poverty in Zimbabwe: A postmodern perspective', *Energy Res. Soc. Sci.*, vol. 75, p. 102026, May 2021, doi: 10.1016/j.erss.2021.102026.
- [162] Vizzuality, 'Zimbabwe Deforestation Rates & Statistics | GFW'. <https://www.globalforestwatch.org/dashboards/country/ZWE> (accessed Dec. 27, 2022).
- [163] 'Zimbabwe Power Company - Powering Zimbabwe into the future'. <https://www.zpc.co.zw/> (accessed Dec. 27, 2022).
- [164] P. Hulsman, H. H. G. Savenije, and M. Hrachowitz, 'Satellite-based drought analysis in the Zambezi River Basin: Was the 2019 drought the most extreme in several decades as locally perceived?', *J. Hydrol. Reg. Stud.*, vol. 34, p. 100789, Apr. 2021, doi: 10.1016/j.ejrh.2021.100789.
- [165] J. H. J. Potgieter, 'An evaluation of the coal bed methane potential of the Mid-Zambezi and North Eastern Kalahari Karoo basins', 2017, Accessed: Dec. 27, 2022. [Online]. Available: <http://scholar.ufs.ac.za/xmlui/handle/11660/6484>
- [166] 'Solar resource maps of Zimbabwe'. <https://solargis.com/maps-and-gis-data/download/zimbabwe> (accessed Dec. 27, 2022).
- [167] T. Houser and S. Mohan, *Fueling Up: The Economic Implications of America's Oil and Gas Boom*. Columbia University Press, 2013.
- [168] N. Mukwakwami, 'Coal bed methane Investment Guide for Zimbabwe', Accessed: Dec. 27, 2022. [Online]. Available: https://www.academia.edu/5772544/Coal_bed_methane_Investment_Guide_for_Zimbabwe
- [169] 'Inflation rates in Zimbabwe', *Worlddata.info*. <https://www.worlddata.info/africa/zimbabwe/inflation-rates.php> (accessed Dec. 27, 2022).
- [170] 'News - Zimbabwe Power Company'. <https://www.zpc.co.zw/articles> (accessed Dec. 27, 2022).
- [171] E. Chabuka, 'Intensive load shedding is imminent as Kariba lake levels are too low to generate electricity', *Techzim*, Nov. 27, 2022. <https://www.techzim.co.zw/2022/11/intensive-load-shedding-is-imminent-as-kariba-lake-levels-are-too-low-to-generate-electricity/> (accessed Dec. 27, 2022).
- [172] S. Ziuku, L. Seyitini, B. Mapurisa, D. Chikodzi, and K. van Kuijk, 'Potential of Concentrated Solar Power (CSP) in Zimbabwe', *Energy Sustain. Dev.*, vol. 23, pp. 220–227, Dec. 2014, doi: 10.1016/j.esd.2014.07.006.
- [173] N. Kaseke, 'A COMPARATIVE COST ASSESSMENT OF ELECTRICITY OUTAGES AND GENERATION EXPANSION IN ZIMBABWE', vol. 3, no. 4, 2014.
- [174] T. Makonese, 'Renewable energy in Zimbabwe', in *2016 International Conference on the Domestic Use of Energy (DUE)*, Mar. 2016, pp. 1–9. doi: 10.1109/DUE.2016.7466713.
- [175] L. Al-Ghussain, R. Samu, O. Taylan, and M. Fahrioglu, 'Techno-Economic Comparative Analysis of Renewable Energy Systems: Case Study in Zimbabwe', *Inventions*, vol. 5, no. 3, Art. no. 3, Sep. 2020, doi: 10.3390/inventions5030027.

- [176] R. Samu, M. Fahrioglu, and C. Ozansoy, ‘The potential and economic viability of wind farms in Zimbabwe’, *Int. J. Green Energy*, vol. 16, no. 15, pp. 1539–1546, Dec. 2019, doi: 10.1080/15435075.2019.1671424.
- [177] A. B. Maqhuzu, K. Yoshikawa, and F. Takahashi, ‘The effect of coal alternative fuel from municipal solid wastes employing hydrothermal carbonization on atmospheric pollutant emissions in Zimbabwe’, *Sci. Total Environ.*, vol. 668, pp. 743–759, Jun. 2019, doi: 10.1016/j.scitotenv.2019.03.050.
- [178] ‘Zimbabwe Coal Reserves and Consumption Statistics - Worldometer’. <https://www.worldometers.info/coal/zimbabwe-coal/> (accessed Dec. 27, 2022).
- [179] C. R. Fielding, ‘Coal depositional models for deltaic and alluvial plain sequences’, *Geology*, vol. 15, no. 7, pp. 661–664, Jul. 1987, doi: 10.1130/0091-7613(1987)15<661:CDMFDA>2.0.CO;2.
- [180] P. M. Oesterlen and J. Lepper, ‘The Lower Karoo coal (k2–3) of the Mid-Zambezi basin, Zimbabwe: depositional analysis, coal genesis and palaeogeographic implications’, *Int. J. Coal Geol.*, vol. 61, no. 1, pp. 97–118, Jan. 2005, doi: 10.1016/j.coal.2004.07.002.
- [181] ‘Fred-Moyo-Oliver-Maponga.pdf’. Accessed: Dec. 27, 2022. [Online]. Available: <https://fffcarbon.co.za/wp-content/uploads/2013/04/Fred-Moyo-Oliver-Maponga.pdf>
- [182] ‘harare.pdf’. Accessed: Dec. 27, 2022. [Online]. Available: <https://eoi.gov.in/harare/?pdf7472?000>
- [183] ‘COALBED METHANE WELLS PRODUCING IN ZIMBABWE’, *Oil & Gas Journal*, Mar. 20, 1995. <https://www.ogj.com/general-interest/companies/article/17216355/coalbed-methane-wells-producing-in-zimbabwe> (accessed Dec. 27, 2022).
- [184] O. J. Maponga, ‘ZIMBABWE’S COAL-BED METHANE POTENTIAL’.
- [185] R. E. B. M. Sibanda, ‘A solutionist approach to unlocking and monetizing coal-bed methane potential in the new Zimbabwe’, Mini Dissertation, University of Pretoria, 2018. Accessed: Dec. 27, 2022. [Online]. Available: <https://repository.up.ac.za/handle/2263/70006>
- [186] P. M. Barrett *et al.*, ‘The age of the Tashinga Formation (Karoo Supergroup) in the Mid-Zambezi Basin, Zimbabwe and the first phytosaur from mainland sub-Saharan Africa’, *Gondwana Res.*, vol. 81, pp. 445–460, May 2020, doi: 10.1016/j.gr.2019.12.008.
- [187] D. J. Soeder and S. J. Borglum, ‘5 - International shale plays’, in *The Fossil Fuel Revolution: Shale Gas and Tight Oil*, D. J. Soeder and S. J. Borglum, Eds. Elsevier, 2019, pp. 137–171. doi: 10.1016/B978-0-12-815397-0.00006-9.
- [188] O. Catuneanu *et al.*, ‘The Karoo basins of south-central Africa’, *J. Afr. Earth Sci.*, vol. 43, no. 1, pp. 211–253, Oct. 2005, doi: 10.1016/j.jafrearsci.2005.07.007.
- [189] D. M. Bailey, D. Heinrich, and A. Kruczkiewicz, ‘Climate Profiles of Countries in Southern Africa: Zimbabwe’.
- [190] N. Jones, N. Smith, M. Browne, D. Creedy, K. Garner, and S. Durucan, ‘UK coal resource for new exploitation technologies’, Nov. 2004, Accessed: Dec. 27, 2022. [Online]. Available: <https://www.osti.gov/etdweb/biblio/20567957>
- [191] F. Meißner and D. Naumenko, ‘Non-Conventional Gas Regulation in Europe: Implications for Ukraine’.
- [192] Z. Zhang, Y. Qin, J. Bai, X. Fu, and D. Liu, ‘Evaluation of favorable regions for multi-seam coalbed methane joint exploitation based on a fuzzy model: A case study

- in southern Qinshui Basin, China’, *Energy Explor. Exploit.*, vol. 34, no. 3, pp. 400–417, May 2016, doi: 10.1177/0144598716631660.
- [193] ‘ECBM_Feasibility.pdf’. Accessed: Dec. 27, 2022. [Online]. Available: https://minasyenergia.upm.es/investigacion/co2/doc/ECBM_Feasibility.pdf
- [194] R. E. Bevins, S. C. White, and D. Robinson, ‘The South Wales Coalfield: low grade metamorphism in a foreland basin setting?’, *Geol. Mag.*, vol. 133, no. 6, pp. 739–749, Nov. 1996, doi: 10.1017/S0016756800024584.
- [195] D. K. Murray, ‘Coalbed methane in the USA: analogues for worldwide development | Geological Society, London, Special Publications’. <https://www.lyellcollection.org/doi/abs/10.1144/gsl.sp.1996.109.01.01> (accessed Dec. 27, 2022).
- [196] J. Siemek and S. Nagy, ‘Estimation of Uncertainles in Gas-Condensate Systems Reserves by Monte Carlo Simulation’, 2004.
- [197] B. Zahner, ‘Application of Material Balance to Determine Ultimate Recovery of a San Juan Fruitland Coal Well’, presented at the SPE Annual Technical Conference and Exhibition, Oct. 1997. doi: 10.2118/38858-MS.
- [198] H.-H. Palloks, *An Assessment of Some of the Coal Deposits in North-west Zimbabwe*. Zimbabwe Geological Survey, 1984.
- [199] O. Barker, ‘CBM IN THE SPRINGBOK FLATS COALFIELD: A MAJOR UNTAPPED SOURCE OF ENERGY’.
- [200] ‘4232h8215tz28j.pdf’. Accessed: Dec. 27, 2022. [Online]. Available: <https://www.asx.com.au/asxpdf/20111205/pdf/4232h8215tz28j.pdf>
- [201] ‘Africa Groundwater’. <https://www2.bgs.ac.uk/africagroundwateratlas/index.html> (accessed Dec. 27, 2022).
- [202] M. S. Mabitje, ‘Determination of Total Organic Carbon content using Passey’s ΔLogR method in coals of the Central Kalahari Karoo Basin, Botswana.’.
- [203] Padcoal (Pvt) Ltd, ‘Gokwe Coal Field - A Rich Resource; Coal Special Grant SG152/10 - Nyagare Hills’, 2011.
- [204] ‘USGS.gov | Science for a changing world’. <https://www.usgs.gov/> (accessed Dec. 27, 2022).
- [205] ‘World Bank Group - International Development, Poverty, & Sustainability’, *World Bank*. <https://www.worldbank.org/en/home> (accessed Dec. 27, 2022).
- [206] ‘MapCruzin Data Research & GIS Project Specialist’. <https://mapcruzin.com/> (accessed Dec. 27, 2022).
- [207] ‘Africa Groundwater Atlas’, *British Geological Survey*. <https://www.bgs.ac.uk/geology-projects/africa-groundwater-atlas/> (accessed Dec. 27, 2022).
- [208] Z. Wang, ‘Chapter 7 - Site Selection, Power Load, and Power Generation Procedures’, in *Design of Solar Thermal Power Plants*, Z. Wang, Ed. Academic Press, 2019, pp. 417–424. doi: 10.1016/B978-0-12-815613-1.00007-9.
- [209] G. Tazi, O. Jbaihi, A. Ghennioui, A. A. Merrouni, and M. Bakkali, ‘Estimating the Renewable Energy Potential in Morocco: solar energy as a case study’, *IOP Conf. Ser. Earth Environ. Sci.*, vol. 161, no. 1, p. 012015, Jun. 2018, doi: 10.1088/1755-1315/161/1/012015.
- [210] L. Qoaider and A. Liqreina, ‘Optimization of dry cooled parabolic trough (CSP) plants for the desert regions of the Middle East and North Africa (MENA)’, *Sol. Energy*, vol. 122, pp. 976–985, Dec. 2015, doi: 10.1016/j.solener.2015.10.021.
- [211] ‘Home - System Advisor Model - SAM.’ <https://sam.nrel.gov/> (accessed Dec. 27, 2022).

- [212] M. J. Montes, A. Abánades, and J. M. Martínez-Val, 'Performance of a direct steam generation solar thermal power plant for electricity production as a function of the solar multiple', *Sol. Energy*, vol. 83, no. 5, pp. 679–689, May 2009, doi: 10.1016/j.solener.2008.10.015.
- [213] 'Natural Gas Weekly Update'. <https://www.eia.gov/naturalgas/weekly/> (accessed Dec. 29, 2022).
- [214] K. van Kuijk, 'SOLAR PV POTENTIAL IN RURAL ZIMBABWE'.
- [215] B. J. Alqahtani and D. Patiño-Echeverri, 'Integrated Solar Combined Cycle Power Plants: Paving the way for thermal solar', *Appl. Energy*, vol. 169, pp. 927–936, May 2016, doi: 10.1016/j.apenergy.2016.02.083.
- [216] G. Dzoma, 'ZESA increases tariffs starting 6 October 2022', *Zimpricecheck*, Oct. 08, 2022. <https://zimpricecheck.com/market-intelligence/zesa-increases-tariffs-starting-6-october-2022/> (accessed Dec. 28, 2022).
- [217] 'STEAG EBSILON', *STEAG Ebsilon*. <https://www.ebsilon.com/en/> (accessed Dec. 27, 2022).
- [218] S. Simske, 'Sensitivity analysis and big system engineering', 2019, pp. 187–201. doi: 10.1016/B978-0-12-814623-1.00005-8.
- [219] A. Fawthrop, 'Top six largest natural gas producing countries in 2019'. <https://www.nsenergybusiness.com/features/natural-gas-producing-countries/> (accessed Dec. 27, 2022).
- [220] 'western.pdf'. Accessed: Dec. 27, 2022. [Online]. Available: <http://pttc.mines.edu/CBM/western%20canada/western.pdf>
- [221] S. T. Inc, 'Download Statgraphics Centurion 18'. <https://www.statgraphics.com/download18> (accessed Dec. 28, 2022).
- [222] '2D, 3D & 4D GIS Mapping Software | ArcGIS Pro'. <https://www.esri.com/en-us/arcgis/products/arcgis-pro/overview> (accessed Dec. 28, 2022).
- [223] '61646_Levelised-Cost-of-Electricity-Peer-Review-Paper-FINAL.pdf'. Accessed: Dec. 28, 2022. [Online]. Available: https://assets.publishing.service.gov.uk/media/57a08991e5274a31e0000154/61646_Levelised-Cost-of-Electricity-Peer-Review-Paper-FINAL.pdf
- [224] M. J. Montes, A. Abánades, J. M. Martínez-Val, and M. Valdés, 'Solar multiple optimization for a solar-only thermal power plant, using oil as heat transfer fluid in the parabolic trough collectors', *Sol. Energy*, vol. 83, no. 12, pp. 2165–2176, Dec. 2009, doi: 10.1016/j.solener.2009.08.010.
- [225] 'ZESA Increases Electricity Tariffs Effective 15 May 2022 | Energy Central'. <https://energycentral.com/news/zesa-increases-electricity-tariffs-effective-15-may-2022> (accessed Dec. 28, 2022).
- [226] 'EIA Annual Energy Outlook 2021 - Issue in Focus - U.S. Energy Information Administration (EIA)'. https://www.eia.gov/outlooks/aeo/emissions/carbon_fee/index.php (accessed Dec. 28, 2022).
- [227] 'GSR2022_Full_Report.pdf'. Accessed: Dec. 28, 2022. [Online]. Available: https://www.ren21.net/wp-content/uploads/2019/05/GSR2022_Full_Report.pdf
- [228] 'KKO20201119-Research-Report-final.pdf'. Accessed: Dec. 28, 2022. [Online]. Available: <https://www.kinetiko.com.au/wp-content/uploads/2020/11/KKO20201119-Research-Report-final.pdf>
- [229] J. Seshadri and L. Mattar, 'Comparison of Power Law and Modified Hyperbolic Decline Methods', presented at the Canadian Unconventional Resources and International Petroleum Conference, Oct. 2010. doi: 10.2118/137320-MS.

- [230] INVESTOPEDIA, 'Diseconomies of Scale Definition: Causes and Types Explained', *Investopedia*. <https://www.investopedia.com/terms/d/diseconomiesofscale.asp> (accessed Feb. 06, 2023).

APPENDICES

A. Standalone CCGT vs. CCGT derived from ISCC

As mentioned in Section 8.4.1, 50 to 600 MW range of heat rates for a CCGT operating at an ISCC facility (Figure 8.6) and a standalone CCGT (Figure 8.7) is modeled in EBSILON to estimate the LCOE. Figure 9.18 shows LCOE values for CCGT PPs, and the difference could have been caused by the optimization of either of the systems.

Figure 9.18 shows that the LCOE difference is less than 5 % for plant capacity from 100 MW to 600 MW, while the LCOE difference between the CCGT_ISCC50MW and CCGT50MW is 8.82 %. The difference in the cost of electricity is less than 10 %. Because the difference in LCOE between a standalone model and the model reduced from the ISCC hybrid is practically negligible, main economic analysis is carried out with the CCGT_ISCC.

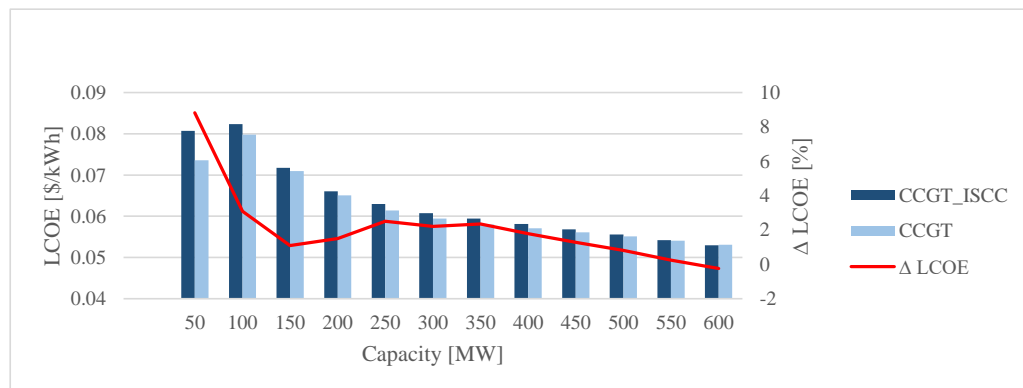


Figure 10.1. CCGT_ISCC and CCGT LCOE difference

B. CSP LCOE vs. Plant Capacity

Figure 10.2 shows different capacities of CSP plants located in the USA. Typically, economies of scale suggests that smaller plants have higher average cost for power generation, whereas increasing the plant capacity should reduce the cost. However, the continual increase of capacity may result in diseconomies of scale which may be caused by several reasons [230]. From Figure 10.2, it should have been that the CSP_{75MW} of Martin Next Generation is less costly than the CSP_{30MW} of Nevada Solar One, however, due to many factors the cost of electricity does not follow the economies of scale.

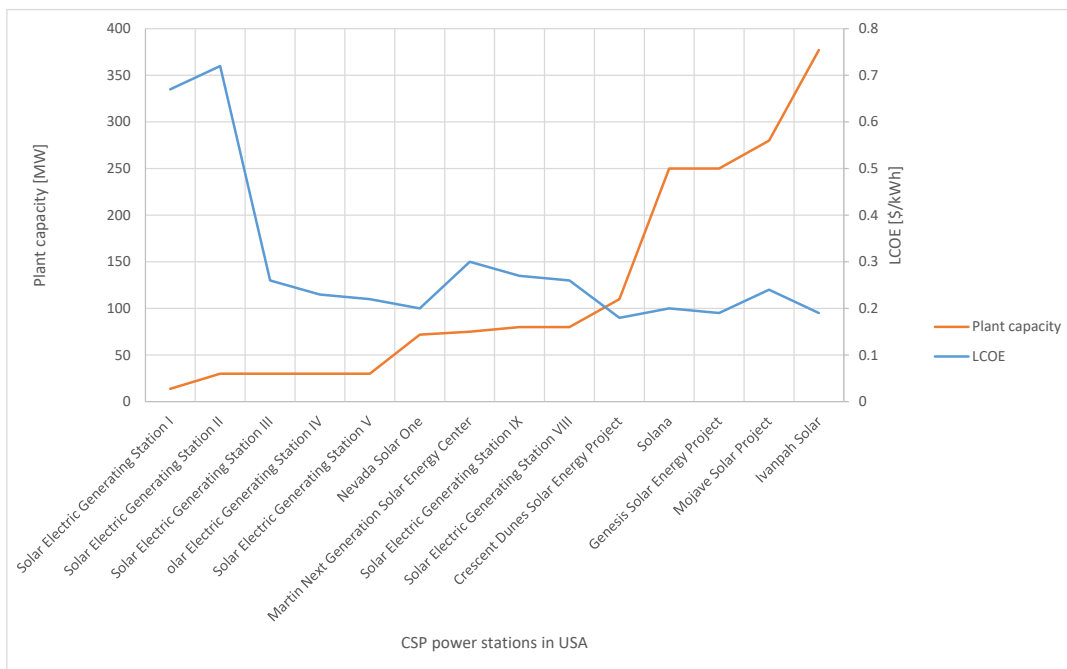


Figure 10.2. CSP plants in USA [211]

For CSP systems, the nominal operating range must be determined as suggested by Figure 10.3. The solar multiple must be large enough to ensure a certain range where the solar thermal plant is operating at nominal conditions, but it should not be very great. Huge sizes of solar fields without thermal storage would achieve a worse return on their investment, as solar thermal energy above nominal level would be wasted [224]. Figure 10.3 shows the relationship between the solar multiple and the LCOE.

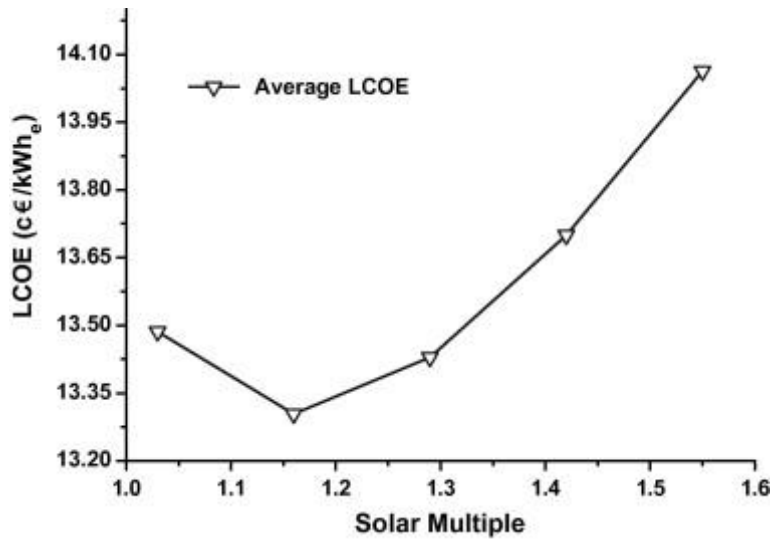


Figure 10.3. Effect of solar multiple on LCOE [224]

TEZ İZİN FORMU / THESIS PERMISSION FORM

PROGRAM / PROGRAM

Sürdürülebilir Çevre ve Enerji Sistemleri / Sustainable Environment and Energy Systems

Siyaset Bilimi ve Uluslararası İlişkiler / Political Science and International Relations

İngilizce Öğretmenliği / English Language Teaching

Elektrik Elektronik Mühendisliği / Electrical and Electronics Engineering

Bilgisayar Mühendisliği / Computer Engineering

Makina Mühendisliği / Mechanical Engineering

YAZARIN / AUTHOR

Soyadı / Surname : Mutume

Adı / Name : Bruce

Programı / Program : Sustainable Environment and Energy Systems

TEZİN ADI / TITLE OF THE THESIS (İngilizce / English) :

Coal bed methane-Concentrated Solar Power Hybrid System Potential in Zimbabwe

TEZİN TÜRÜ / DEGREE: Yüksek Lisans / Master Doktora / PhD


1. Tezin tamamı dünya çapında erişime açılacaktır. / Release the entire work immediately for access worldwide.

2. Tez iki yıl süreyle erişime kapalı olacaktır. / Secure the entire work for patent and/or proprietary purposes for a period of two years. *


3. Tez altı ay süreyle erişime kapalı olacaktır. / Secure the entire work for period of six months. *

Yazarın imzası / Author Signature  Tarih / Date 01/03/2023.

Tez Danışmanı / Thesis Advisor Full Name: Asst. Prof. Dr. Doruk Alp

Tez Danışmanı İmzası / Thesis Advisor Signature: 

Eş Danışmanı / Co-Advisor Full Name: Prof. Dr. Murat Fahrioglu

Eş Danışmanı İmzası / Co-Advisor Signature: 

Program Koordinatörü / Program Coordinator Full Name: Prof. Dr. Ceren Ince

Program Koordinatörü İmzası / Program Coordinator Signature: 